Dissertations, Master's Theses and Master's Reports

2020

# REAL-TIME PREDICTIVE CONTROL OF CONNECTED VEHICLE POWERTRAINS FOR IMPROVED ENERGY EFFICIENCY

Joseph Oncken
*Michigan Technological University*, jeoncken@mtu.edu

REAL-TIME PREDICTIVE CONTROL OF CONNECTED VEHICLE

POWERTRAINS FOR IMPROVED ENERGY EFFICIENCY

By

Joseph E. Oncken

A DISSERTATION

Submitted in partial fulfillment of the requirements for the degree of

DOCTOR OF PHILOSOPHY

In Mechanical Engineering – Engineering Mechanics

MICHIGAN TECHNOLOGICAL UNIVERSITY

2020

This dissertation has been approved in partial fulfillment of the requirements for the Degree of DOCTOR OF PHILOSOPHY in Mechanical Engineering – Engineering Mechanics.

Department of Mechanical Engineering – Engineering Mechanics

Dissertation Advisor: *Dr. Bo Chen*

Committee Member: *Dr. Darrell Robinette*

Committee Member: *Dr. Jeff Naber*

Committee Member: *Dr. Jeff Burl*

Department Chair: *Dr. William W. Predebon*

# Table of Contents

iv

# List of figures

# List of tables

# Preface

Included in Chapter 3 is a journal article reproduced in its entirety. I have written the publication as the lead author and lead contributor. As co-author, my advisor Dr. Bo Chen has provided important guidance and advice. The content of Chapter 4 has been submitted for publication as a journal article and is currently in the review process. I have written the publication as the lead author and lead contributor. My co-author Kovid Sachdeva provided the initial development and supporting MATLAB code of the optimal mode path planning algorithm. Co-authors Kovid Sachdeva and Huanqing Wang provided optimal operating point tables used in the article. As co-author, my advisor Dr. Bo Chen has provided important guidance and advice.

# Acknowledgements

I would like to thank my advisor, Dr. Bo Chen, for guiding me through my graduate studies. I truly appreciate the amount of time and effort she puts into her graduate students. Her help in all aspects of graduate work, whether it be the technical research itself, the journal article process, or presenting to project sponsors and other researchers, were all invaluable both in the development of myself as researcher and in obtaining my Ph.D.

I would like to thank my committee members, Dr. Jeff Burl, Dr. Jeff Naber, and Dr. Darrell Robinette, for their time spent evaluating my work. I need to give Dr. Darrell Robinette special thanks for acting, at times, as an informal advisor, especially when it came to understanding vehicle systems and vehicle testing.

Special thanks to Dr. Djedje-Kossu Zahui for his role in my development as an engineer and setting me on the path towards a Ph.D.

Thank you to all my IMES lab colleagues, Pradeep, Chong, Xin, Luting, Kovid, Huanqing, and others, for all the assistance you offered along the path to my Ph.D. Also thank you to all my NEXTCAR colleagues, Chris, Brandon, and especially Josh.

I would like to thank all my friends that have helped me along the way. John and Jasmine for being an unwavering wall of support in all aspects of life. Josh as we navigated the world of grad school together. Jon and Miles for bringing me into the clan and all the adventures and shenanigans that followed. Jess for your friendship and your constant support. Chris and Luke for keeping things entertaining whenever we get to see each other.

Thanks to all the other friends I have met from my time in Houghton, Eric, Will, Ben, Stas, Joe, and many others, for making my time at MTU a wonderful experience.

Most importantly, I need to thank my parents and family. My parents have always fully supported me in any endeavor I undertook, and graduate school was no exception. Without their love and support, I never would have achieved this milestone.

Finally, I need to acknowledge my time spent in the Keweenaw and on the shores of Lake Superior. The natural beauty of the area is unparalleled and has provided an essential escape during difficult times along the path to my PhD. For anyone who reads this, I highly advise spending a night on the shores of Superior. The power of the waves crashing and the vastness of the stars does make one feel small, but they instill in oneself a deep appreciation for the natural world in which we are a part of.

*Those who have never seen Superior get an inadequate, even inaccurate, idea, by hearing it spoken of as a "lake", and to those who have sailed over its vast extent the word sounds ludicrous. Though its waters are fresh and crystal, Superior is a Sea.*

The Reverend George Grant, 1872

# List of abbreviations

| | |
|---|---|
| $\alpha_{Out}$ | Drive Unit Output Acceleration |
| $a_{Profile}$ | Reference Acceleration Profile |
| $\alpha, \beta, \gamma$ | Cost Function Weight Factors |
| $\beta_{MA,MB}$ | Motor-Generator Power Direction Boolean |
| $C$ | Cumulative Cost |
| $E_{CD,CS}$ | Energy Consumed |
| $\varepsilon$ | Output Torque Constraint Variable |
| $\eta$ | Component Efficiency |
| $F_0, F_1, F_2$ | Road load Coefficients |
| $FDR$ | Final Drive Ratio |
| $GR$ | Motor Reduction Gear |
| $H$ | Residing Cost |
| $I_{MA,MB,Engine,Out}$ | Component Inertia |
| $J$ | Path Cost |
| $\lambda$ | Cost Function Normalizing Factor |
| $m$ | Vehicle Mass |
| $m_f$ | Fuel Consumed |
| $mode$ | Powertrain Mode |
| $P$ | Mode with Lowest Cost |
| $P_{Battery}$ | Battery Power |
| $Q_{Battery}$ | Battery Capacity |
| $R_{1,2}$ | Planetary Gear Ring Tooth Count |
| $R_{Battery}$ | Battery Internal Resistance |
| $R_{Tire}$ | Tire Radius |
| $S_{1,2}$ | Planetary Gear Sun Tooth Count |
| $SOC$ | State of Charge |
| $T_{MA,MB,Engine,Out}$ | Component Torques |
| $\theta_{Grade}$ | Road Grade |
| $\omega_{MA,MB,Engine,Out}$ | Component Speeds |
| $V_{OC}$ | Open Circuit Battery Voltage |
| $v_{Profile}$ | Reference Velocity Profile |
| $\omega_{MA,MB,Engine,Out}$ | Component Speeds |
| $X, U, V$ | State, Control, and Disturbance Vectors |

# Abstract

The continued push for the reduction of energy consumption across the automotive vehicle fleet has led to widespread adoption of hybrid and plug-in hybrid electric vehicles (PHEV) by auto manufacturers. In addition, connected and automated vehicle (CAV) technologies have seen rapid development in recent years and bring with them the potential to significantly impact vehicle energy consumption. This dissertation studies predictive control methods for PHEV powertrains that are enabled by CAV technologies with the goal of reducing vehicle energy consumption.

First, a real-time predictive powertrain controller for PHEV energy management is developed. This controller utilizes predictions of future vehicle velocity and power demand in order to optimize powersplit decisions of the vehicle. This predictive powertrain controller utilizes nonlinear model predictive control (NMPC) to perform this optimization while being cognizant of future vehicle behavior.

Second, the developed NMPC powertrain controller is thoroughly evaluated both in simulation and real-time testing. The controller is assessed over a large number of standardized and real-world drive cycles in simulation in order to properly quantify the energy savings benefits of the controller. In addition, the NMPC powertrain controller is deployed onto a real-time rapid prototyping embedded controller installed in a test vehicle. Using this real-time testing setup, the developed NMPC powertrain controller is evaluated using on-road testing for both energy savings performance and real-time performance.

Third, a real-time integrated predictive powertrain controller (IPPC) for a multi-mode PHEV is presented. Utilizing predictions of future vehicle behavior, an optimal mode path plan is computed in order to determine a mode command best suited to the future conditions. In addition, this optimal mode path planning controller is integrated with the NMPC powertrain controller to create a real-time integrated predictive powertrain controller that is capable of full supervisory control for a multi-mode PHEV.

Fourth, the IPPC is evaluated in simulation testing across a range of standard and real-world drive cycles in order to quantify the energy savings of the controller. This analysis is comprised of the combined benefit of the NMPC powertrain controller and the optimal mode path planning controller. The IPPC is deployed onto a rapid prototyping embedded controller for real-time evaluation. Using the real-time implementation of the IPPC, on-road testing was performed to assess both energy benefits and real-time performance of the IPPC.

Finally, as the controllers developed in this research were evaluated for a single vehicle platform, the applicability of these controllers to other platforms is discussed. Multiple cases are discussed on how both the NMPC powertrain controller and the optimal mode path planning controller can be applied to other vehicle platforms in order to broaden the scope of this research.

# 1  Introduction

## 1.1  Background

In response to regulatory, environmental, and market forces, automotive manufactures have focused on two technology domains in the search for ways to reduce the energy consumption of their vehicles and increase overall vehicle fleet efficiency. These two technology areas, vehicle electrification and connected and automated vehicle (CAV) technologies have seen significant developments in recent years. Hybrid electric vehicles (HEV) and plug-in hybrid electric vehicles (PHEV) have been popular electrification options amongst automakers for many years. As a result, the design and control of these hybridized powertrain is well understood and have been thoroughly researched. However, the advent of CAV technology and the information it can provide has led to new control possibilities for HEVs and PHEVs, specifically predictive powertrain control, that require further study.

According to [1] and [2], a research priority in the realm of CAV technology is to further quantify exactly the energy impact these technologies provide. As predictive powertrain control methods are directly enabled by CAV technology [3], this dissertation will focus on providing a thorough assessment of the reduction in energy consumption that predictive powertrain methods can have on a PHEV. Additionally, there exists limited research into predictive control methods for HEV and PHEV energy management that demonstrate real-time capability. This dissertation will also aim to develop predictive powertrain control

methods that not only reduce energy consumption relative to existing control methods, but also demonstrate that the developed control methods are capable of operating in a real-time environment.

## 1.2 Literature Review

Research in three particular categories will be reviewed in order to contextualize the research presented in this dissertation. Section 1.2.1 focuses specifically on non-predictive methods of electrified vehicle (xEV) control methods. Section 1.2.2 will review previous work in predictive control methodologies for xEV vehicles. Finally, the advent of CAV technologies has opened a window of opportunity to integrate vehicle level functions, like powertrain control, with CAV technology. Section 1.2.3 examines the potential applications and impact that CAV technologies can have on powertrain level control.

### 1.2.1 xHEV Powertrain Control Methods

A multitude of methods have been studied for the control and energy management of HEV and PHEV powertrains [4]. These methods can fall into several categories, including heuristic methods, instantaneous optimization methods, local optimization methods, and globally optimal methods [5-7]. Heuristic methods like rules-based control, such as in [8, 9], were studied early in the development of HEVs. While easy to implement and fast performing in real-time control, the complexity of HEV systems and the variability of operating conditions that HEVs encounter often result in sub-optimal energy management of the HEV powertrain when using rules-based methods. Instantaneous optimization

2

energy management strategies for HEVs optimize a cost function at each execution step of the controller allowing for the consideration of the current state of the vehicle in the choosing of a most optimal control action for the given moment. Strategies that fall in under the instantaneous optimization method umbrella include the equivalent consumption management strategy (ECMS). The ECMS, which is capable of real time control, utilizes a cost function with a predetermined equivalence factor between the cost of fuel and electrical energy consumption [6, 10-12]. Improvements to the ECMS method include adaptive ECMS, or A-ECMES. This strategy was able to improve upon ECMS by adapting the equivalence factor to changing driving conditions [13]. However, even with this adapting factor, the A-ECMS method does not include a mechanism to account for future conditions of the vehicle, which can lead to suboptimal control decisions over the course of an entire drive cycle.

Global optimal control methods can serve a useful purpose in determining a true optimal control strategy for a vehicle over a drive cycle [14, 15]. Denis et al. [16] examined the use of DP and the genetic algorithm (GA) as methods for powersplit control in a parallel hybrid finding that, while slower to solve, the DP-based method provided greater energy savings. However, as both the DP and GA implementations required full cycle knowledge, neither were suitable for real-time control. Pei and Leamy [17] use DP to generate global optimal energy management strategy for a parallel and powersplit HEV. This global optimal strategy was then used to evaluate an ECMS-based strategy.

There are several common methods used for local optimal control of PHEV powertrains. DP is one of methods used in this application, but instead of optimizing an energy management strategy for the entire drive cycle, short segments are used. For example, papers [18], [19], and [20] utilize a DP-based controller with a short horizon look-ahead for energy management in a parallel HEV. However, the implementation was only in simulation and has no real-time capability demonstrated. Model predictive control (MPC) is another popular local optimal method for xEV powertrain energy management and will be discussed in depth in the subsequent section.

### 1.2.2 Model Predictive Control xEV Applications

The use of model predictive control for energy management in xEVs has been a well-researched topic over the past decade and has been shown to be an effective control method for optimizing the energy management of xEV powertrains [21]. Through the capability of considering predicted future vehicle behavior in the determination of a current control action, the use of MPC for xEV powertrain energy management can be an effective tool for reducing energy consumption. A number of past studies have been conducted on the use of MPC in xEVs. Ripaccioli et al. in [22] proposed an MPC controller for a parallel HEV and was shown in simulation to reduce fuel consumption relative to a conventionally controlled vehicle. The same author presented an MPC controller for a series HEV in [23]. An MPC torque-split control strategy was presented for a parallel HEV in [24]. This work incorporated engine transient characteristics into the MPC formulation finding that this addition reduced fuel consumption when compared to the steady-state implementation. A

similar study was conducted in [25], once again finding that the incorporation of engine dynamics into an MPC formulation for a parallel HEV can reduce fuel consumption compared to the steady-state implementation. The authors of [26] presented a stochastic MPC for powersplit control of a parallel HEV. In this implementation, future road grade is incorporated into the MPC using a Markov chain. This method reduced fuel consumption when compared to an ECMS strategy that does not contain the road grade preview. The authors of [27] developed both a linear and non-linear MPC control for a powersplit HEV finding that, in simulation testing, that the NMPC implementation offered higher fuel economy than that of the linear MPC implementation. In [28] and [29], the authors developed an NMPC controller for a powersplit HEV powertrain that was incorporated with an electrochemical battery model that was considerate of battery aging. An NMPC controller for a single mode, powersplit HEV was also proposed in [30] where testing was expanded to real time in a benchtop embedded controller and simulator. While for a conventional vehicle with a CVT, paper [31] demonstrated that real-time MPC for powertrain control is possible in a production-level embedded controller thus providing validity to the goal of achieving real-time MPC control for a xEV powertrain.

### 1.2.3  Powertrain Applications of Connected and Automated Vehicle Technologies

For at least the last decade, the mobility industry has seen CAV technologies as a key enabler to the success of electrified vehicles [32]. During the course of this decade, significant progress has been made in making this view a reality. Not only does the integration of CAV technology offer promise in terms of safety, comfort, and convenience,

the use of CAV tech offers significant promise as a tool to reduce energy consumption [33]. CAV technologies can impact a vehicle, those that alter interaction of a vehicle with its surroundings and those that alter the behavior of a vehicle within itself. Inter-vehicle technologies such as Eco-Routing, Eco Approach and Departure, Platooning and Speed Harmonization, have the potential to offer significant energy savings benefits [34-37]. However, the focus of this work is on how CAV technologies can impact intra-vehicle behavior, specifically on how the information provided by CAV technologies can improve powertrain operation.

Predictive control strategies for xEV powertrains can produce energy savings when compared to non-predictive strategies, especially when integrated with CAV technology [3]. Using reliable forecasts obtained through CAV technology can improve the performance of predictive energy management strategies when compared to predictions developed using historical data as presented in [23, 38, 39]. However, a requirement for the successful implementation of predictive control methods is the ability to obtain a prediction of future driving conditions, such as vehicle speed, road grade, and light timing [4]. As commercial development of CAV technology continues, it is becoming feasible to obtain these future predictions through V2X communication [40]. Because of this, the integration of CAV technology and powertrain control has becoming a popular research topic. For example, paper [41] examines on how future route knowledge can impact 48V mild hybrid control as well as engine control. In [42], Hu et al. present a controller that uses Pontryagin's Minimum Principal to optimize vehicle acceleration and automatic transmission gear state given forecasted vehicle speed and road grade. However, this work

was performed in simulation only and was limited to a conventional vehicle. Papers [43] and [44] present a method for utilizing a full route preview to optimize where along the route charge depleting and charge sustaining powertrain operation should be used for the minimal energy consumption.

## 1.3   Research Objective and Contributions

The research objective of this dissertation is to investigate predictive control methods for PHEV powertrain control that leverage vehicle connectivity for energy savings and are both capable and practical for real-time control. Control methods for HEVs and PHEVs have been well studied; however, a control strategy that is predictive in nature, utilizes vehicle connectivity, and capable of real-time control on an embedded control has yet to be developed. This dissertation presents an Integrated Predictive Powertrain Controller (IPPC) for the 2$^{nd}$ generation Chevrolet Volt, a multi-mode PHEV. The IPPC consists of two layers of control. The lower layer, detailed in Chapter 3, presents a non-linear model predictive controller designed for optimal energy management of the Chevrolet Volt. This layer of control utilizes predictions of future vehicle speed and road conditions to produce an optimized powersplit for the vehicle. The energy savings benefits of this controller were demonstrated in simulation. In addition, the controller was implemented in a real-time environment and the performance observed in simulation was validated in real-time. The upper layer of control, detailed in Chapter 4, presents a method in which predictions of future vehicle behavior are used to plan an optimal path of vehicle powertrain modes that

minimizes energy consumption. The energy savings benefit of this control level was evaluated in simulation testing as well as validated through real-time testing.

## 1.4 Outline of the Dissertation

The dissertation is organized as follows. Chapter 2 presents details of the vehicle used as a research platform in this dissertation. This chapter will also discuss the simulation model utilized in this research. Chapter 3 introduces a real-time predictive powertrain controller for a connected PHEV that utilizes non-linear model predictive control to optimize powersplit for reduced energy consumption. Chapter 4 presents an Integrated Predictive Powertrain Controller for a multi-mode PHEV. This includes the integration of an Optimal Mode Path Planning algorithm and the NMPC Powertrain Controller presented in Chapter 3 into one real-time integrated controller for multi-mode PHEV powertrain control. Chapter 5 provides further performance analysis into the controllers presented in Chapters 3 and 4. Chapter 6 examines the applicability of the controllers developed in Chapters 3 and 4 to other vehicle platforms. Finally, Chapter 7 provides conclusions along with potential future work possibilities.

# 2 Research Environment: Vehicle Model and Test Setup

This chapter will provide an overview of the platforms on which this research was conducted. Two main sections are contained within this chapter. First, the vehicle utilized in this work, specifically the powertrain of said vehicle, will be detailed in order to provide appropriate context for the control algorithms presented in later chapters. Secondly, a general overview of the model used for simulation testing of the developed control algorithms is provided. For details of the real-time model and test vehicle used for real-time evaluation of the developed control algorithms, please refer to Chapter 3.4.

## 2.1 2$^{nd}$ Generation Chevrolet Volt

This dissertation investigates predictive control methods for PHEV powertrain control. Therefore, a vehicle platform is required on which to perform this investigation. The vehicle platform used in this research is the 2$^{nd}$ generation Chevrolet Volt, a multi-mode PHEV manufactured by General Motors capable of both electric-only and hybrid operation.

### 2.1.1 Vehicle Specifications

The Volt's powertrain components consist of a 1.5L 4-cylinder engine paired with two electric machines. BSFC and efficiency maps of these components are provided in Section 3.2. These components are integrated into the vehicle's drive unit which produces five distinct operating modes through the use of two planetary gear sets, two actuated clutches

and a one-way clutch. Two of the modes are electric-only modes, while the remaining three are hybrid operating modes. The battery pack on the 2nd generation Volt is an 18.4 kWh unit allowing for a 50-mile EV range.

A simplified lever representation of this drive unit is provided in Figure 2-1 while major parameters of the vehicle are given in Table 2-1. Full details and specifications of the Volt powertrain components can be found in [45-49], and a breakdown of the vehicle's performance is provided in [50, 51].
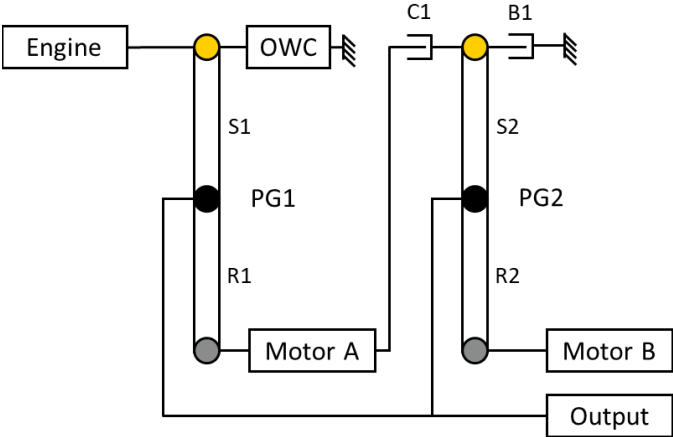


Figure 2-1: 2nd Generation Chevrolet Volt drive unit lever diagram representation.

Table 2-1: Major parameters of the 2nd generation Chevrolet Volt [47].

| Parameter | Value | Units |
|-----------|-------|-------|
| Max Engine Power | 75 | kW |
| Max Torque Engine | 140 | Nm |

| | | |
|---|---|---|
| Max Power MGA | 48 | kW |
| Max Torque MGA | 118 | Nm |
| Max Power MGB | 87 | kW |
| Max Torque MGB | 280 | Nm |
| Battery Capacity | 18.4 | kW-hr |
| Battery Max Discharge Power | 120 | kW |
| Curb Weight | 1607 | kg |

### 2.1.2 Drive Unit Mode Breakdown

These five drive unit modes are broken down into two electric-only, or charge depleting (CD), modes and three hybrid, or charge sustaining (CS), modes. CD operation is default for the vehicle. This strategy is utilized by the vehicle until one of two events occurs at which point CS operating will begin. The first event is that battery SOC reaches its lower limit, approximately 16%. The second event is in the case that the driver commands CS mode through an in-vehicle setting. CS operation utilizes the three hybrid modes to maintain battery SOC within ~±1% of either ~16% in the case of a fully depleted battery or, in the case of a non-depleted battery, the SOC of the battery at the time of the in-vehicle CS command.

The electric-only modes consist of one motor operation, 1-EV, and two motor operation, 2-EV. In EV operation, as shown in Figure 2-2, clutch C1 is open, clutch B1 is closed which allows Motor B to provide power directly to the output, and the one-way clutch is loaded which allows Motor A to provide power directly to the output in 2-EV mode. 1-EV uses Motor B only to provide power to the wheels. Due to the ability of Motor B to provide sufficient tractive effort in most driving conditions, 1-EV mode is used for the majority of electric-only operation. In high torque demand situations, such as vehicle launch and high acceleration events, 2-EV mode will be utilized in which case Motor A supplies the additional torque required to meet demand [47]. The governing torque and speed equations, derived using the lever analogy of planetary gear sets [52], of the drive unit in EV mode are provided in (2-1).

$$
\begin{cases}
T_{Out,EV} = \left(\dfrac{R_1 + S_1}{S_1}\right) * T_{MA} + \left(\dfrac{R_2 + S_2}{S_2}\right) * T_{MB} \\
\qquad \omega_{MA,EV} = \left(\dfrac{R_1 + S_1}{S_1}\right) * \omega_{Out} \\
\qquad \omega_{MB,EV} = \left(\dfrac{R_2 + S_2}{S_2}\right) * \omega_{Out}
\end{cases}
\qquad (2\text{-}1)
$$
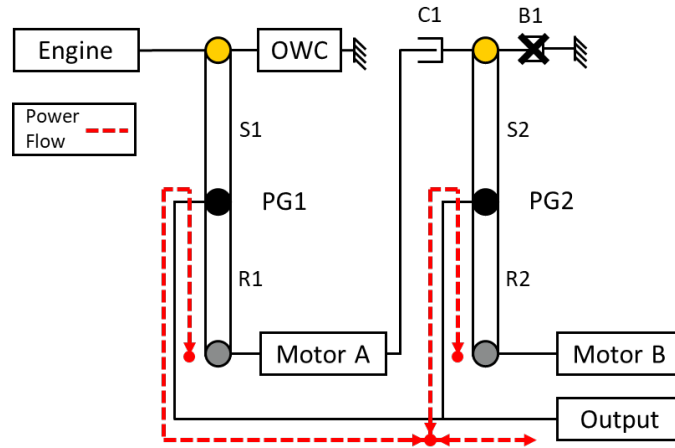
Figure 2-2: EV Mode Clutch State and Power Flow.

Low extended range (LER) is the first of three hybrid modes produced by the drive unit. LER is an input powersplit hybrid arrangement. In this mode, the engine speed is decoupled from the wheels. The engine's power is split on PG1 between the carrier, which serves as the output, and Motor A, which acts as a generator and speed controller for the engine. Depending on the amount of power produced by Motor A, power is sent to Motor B, which also provides power to the output, and, in the case of the power produced by Motor A being in excess of that required by Motor B, to the battery. Clutch C1 is open in this arrangement and clutch B1 is closed as shown in Figure 2-3. LER mode is most efficient during high torque, low speed events. LER use is very prominent in scenarios such as city driving where frequent stop and starts occur and overall vehicle speeds are relatively low [47]. The governing torque and speed equations of the drive unit in LER mode are provided in (2-2).

$$\begin{cases} T_{Out,LER} = \left(\dfrac{R_1 + S_1}{R_1}\right) * T_{Engine} + \left(\dfrac{R_2 + S_2}{S_2}\right) * T_{MB} \\[2ex] T_{MA,LER} = \left(\dfrac{S_1}{R_1}\right) * T_{Engine} \\[2ex] \omega_{MA,LER} = -\left(\dfrac{R_1}{S_1}\right) * \omega_{Engine} + \left(\dfrac{R_1 + S_1}{S_1}\right) * \omega_{Out} \\[2ex] \omega_{MB,LER} = \left(\dfrac{R_2 + S_2}{S_2}\right) * \omega_{Out} \end{cases} \qquad (2\text{-}2)$$
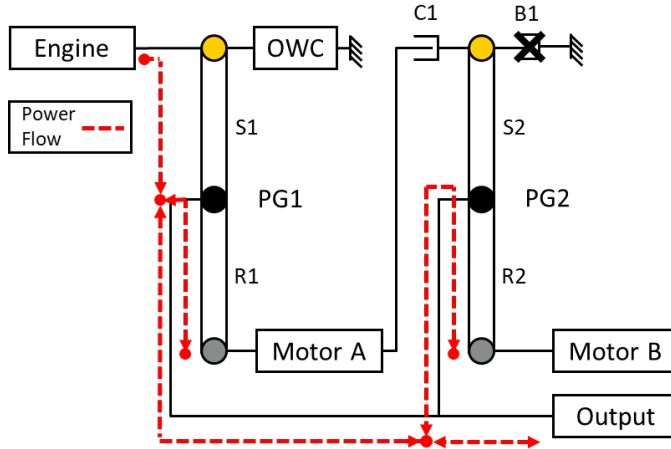


Figure 2-3: LER Mode Clutch State and Power Flow.

Fixed ratio extended range (FER) mode is a parallel hybrid arrangement. Shown in Figure 2-4, clutch B1 and C1 are both closed which results in both Motor A and the ring of PG2 being grounded and the engine speed being directly coupled to wheel speed. This allows the engine deliver power directly to the output carrier while Motor B is able to either provide or absorb power from the output carrier depending on the current output power demand. FER is very efficient during acceleration events and can provide efficient charging of the battery when overall output power demand is low [47]. The governing torque and speed equations of the drive unit in FER mode are provided in (2-3).

14

$$\begin{cases} T_{Out,FER} = \left(\frac{R_1 + S_1}{R_1}\right) * T_{Engine} + \left(\frac{R_2 + S_2}{S_2}\right) * T_{MB} \\ \omega_{MB,FER} = \left(\frac{R_2 + S_2}{S_2}\right) * \omega_{Out} \\ \omega_{Engine,FER} = \left(\frac{R_1 + S_1}{R_1}\right) * \omega_{Out} \end{cases} \tag{2-3}$$
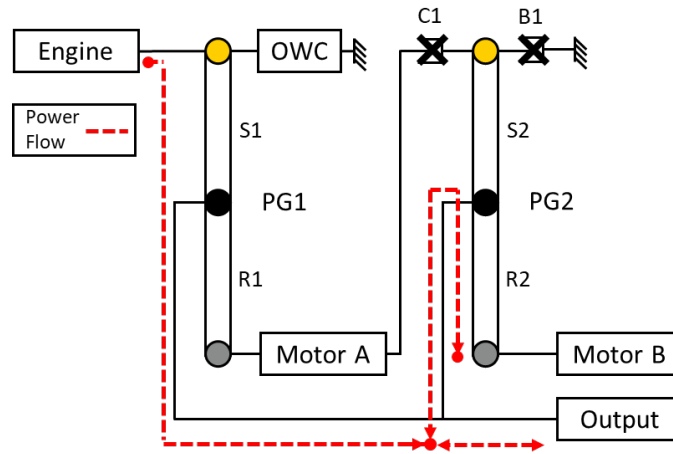


Figure 2-4: FER Mode Clutch State and Power Flow.

The final hybrid mode is high extended range, or HER. HER mode is a compound powersplit hybrid arrangement where clutch C1 is closed and B1 is open as shown in Figure 2-5. As with LER mode, the engine speed is decoupled from wheel speed and must be controlled by the electric machines. Because this clutch arrangement allows the engine to be ran at low speeds with high drive unit output speeds, this mode is most efficient when used in low-torque demand situations such as highway driving [47]. The governing torque and speed equations of the drive unit in HER mode are provided in (2-4).

$$
\begin{cases}
T_{Out,HER} = \left(\dfrac{R_1 + S_1}{R_1}\right) * T_{Engine} + \left(\dfrac{R_2 + S_2}{S_2}\right) * T_{MB} \\[2mm]
T_{MA,HER} = -\left(\left(\dfrac{S_1}{R_1}\right) * T_{Engine} + \left(\dfrac{R_2}{S_2}\right) * T_{MB}\right) \\[2mm]
\omega_{MA,HER} = -\left(\dfrac{R_1}{S_1}\right) * \omega_{Engine} + \left(\dfrac{R_1 + S_1}{S_1}\right) * \omega_{Out} \\[2mm]
\omega_{MB,HER} = \left(\dfrac{R_1 R_2}{S_1 S_2}\right) * \omega_{Engine} + \left(\dfrac{S_1 S_2 - R_1 R_2}{S_1 S_2}\right) * \omega_{out}
\end{cases}
\tag{2-4}
$$
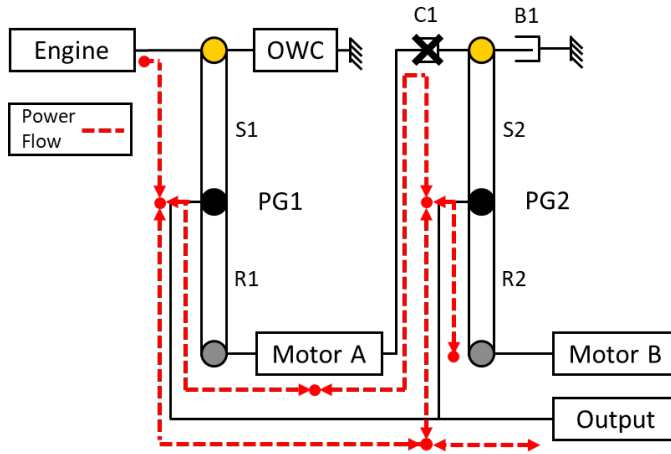


Figure 2-5: HER Mode Clutch State and Power Flow.

## 2.2 Simulation Model

All simulations conducted in this research were completed using MATLAB Simulink. A simplified overview of the Simulink model used for analysis is presented in Figure 2-6. The model is divided into three main sections. The first section, show in red, is the Trajectory Generator. This portion of the model is responsible for creating the reference trajectories used by the predictive controller. In simulation testing, these trajectories are generated from vehicle data collected in both dynamometers and simulation testing. At each timestep in the simulation of the drive cycle, this portion of the model extracts the

projected velocity for the length of the prediction horizon from the logged vehicle data.
From this velocity trajectory, a torque trajectory is also calculated for the length of the
prediction horizon. The mathematical details of this process are covered in the subsequent
chapters.
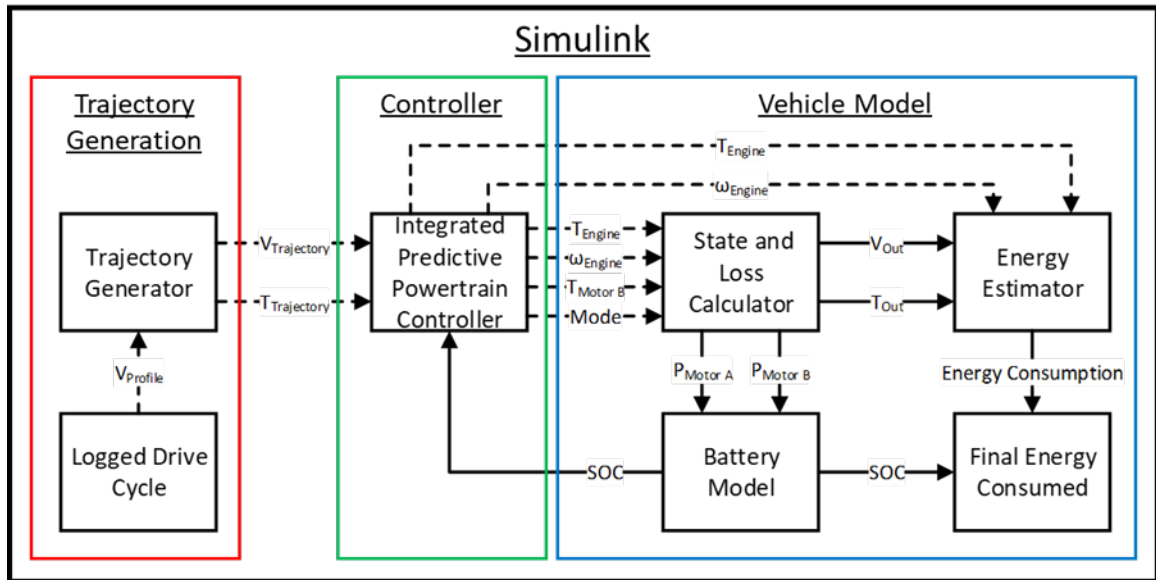


Figure 2-6: Simulation Implementation

The second portion of the model, shown in green, is the Control section of the model. This
contains both the NMPC Powertrain Controller (NMPC PTC) which will be detailed in
Chapter 3 and the Optimal Mode Path Planning (OMPP) Algorithm which will be covered
in Chapter 4. In terms of implementation in the model, the NMPC PTC is C-based, which
is integrated into the model as a Simulink S-function. The OMPP is implemented in
Simulink as a MATLAB function block. Each of these two controllers receive the
prediction horizon trajectories from the Trajectory Generation portion of the model as well

as feedback from the Vehicle portion of the model. Control actions containing engine and motor torques, as well as drive unit mode, are sent to the Vehicle portion of the model.

The final subunit of the model is that of the vehicle powertrain. This subunit contains three main subsystems. The first subsystem, the state and loss calculator, utilizes the speed and torque equations, given in equations (2-1)-(2-4), in order to compute the remaining component torques and speeds within the drive unit that are not control actions. With every component speed and torque now know, the e-motor torques and speeds are passed through manufacturer-provided detailed efficiency maps of both the motors and power electronics in order to compute the total power draw from each motor. These motor powers are then passed to the second vehicle subsystem, the battery model. The battery is modeled as an RC equivalent circuit and was developed by the MTU NEXTCAR program utilizing manufacturer provided parameters. Details of this model are given in [53]. Once SOC is computed, it is provided as feedback to the control section of the model. The third subsystem of the vehicle portion of the model is the energy estimator. The energy consumption model, developed as part of the MTU NEXTCAR program, uses over 200 hours of vehicle data collected in both on-road and dynamometer testing in order to train a response surface model that outputs the both fuel and electrical energy consumed by the vehicle in megajoules. Full details of this model are given in [54].

# 3 Real-Time Model Predictive Powertrain Control for a Connected Plug-In Hybrid Electric Vehicle[1] [55]

The continued development of connected and automated vehicle technologies presents the opportunity to utilize these technologies for vehicle energy management. Leveraging this connectivity among vehicles and infrastructure allows a powertrain controller to be predictive and forward-looking. This paper presents a real-time predictive powertrain control strategy for a Plug-in Hybrid Electric Vehicle (PHEV) in a connected vehicle environment. This work focuses on the optimal energy management of a multi-mode PHEV based on predicted future velocity, power demand, and road conditions. The powertrain control system in the vehicle utilizes vehicle connectivity to a cloud-based server in order to obtain future driving conditions. For predictive powertrain control, a Nonlinear Model Predictive Controller (NMPC) is developed to make torque-split decisions within each operating mode of the vehicle. The torque-split among two electric machines and one combustion engine is determined such that fuel consumption is minimized while battery SOC and vehicle velocity targets are met. The controller has been extensively tested in simulation across multiple real-world driving cycles where energy savings in the range of 1 to 4% have been demonstrated. The developed controller has also been deployed and tested in real-time on a test vehicle equipped with a rapid prototyping

embedded controller. Real-time in-vehicle testing confirmed the energy savings observed in simulation and demonstrated the ability of the developed controller to be effective in a real-time environment.

## 3.1 Introduction

The ongoing push in the automotive sector to reduce vehicle energy consumption requires the development and adoption of new technologies. One major technology that the automotive industry has turned to over the past two decades has been the development and utilization of hybrid electric vehicles (HEV) and, more recently, plug-in hybrid electric vehicles (PHEV). While HEVs and PHEVs have been able to reduce energy consumption relative to their conventional counterparts, the opportunity exits to further reduce HEV and PHEV energy consumption through the integration of vehicle powertrain control with connected and automated vehicle (CAV) technologies. The incorporation of CAV technologies into HEV and PHEV energy management strategies has the potential to have significant energy savings benefits [35, 41]. [33] has shown that regardless of powertrain type, conventional, HEV, or battery electric vehicle (BEV), the integration of vehicle connectivity reduces energy consumption. [1] shows that not only the benefits that the integration of CAV technologies provides at the vehicle level, but also those at the transportation system and urban system levels. While there has been significant research into HEV and PHEV energy management, research into practical PHEV energy management strategies that incorporate the potential benefits of CAV technology is lacking. This paper will detail a PHEV energy management strategy that is not only capable

of interfacing with CAV technologies, but is capable of doing so in a real-time environment.

Multiple solutions to HEV and PHEV energy management have been well studied [4] for non-CAVs. Early strategies included the equivalent consumption management strategy (ECMS), and adaptive ECMS (A-ECMS). ECMS is an instantaneous optimization strategy that utilizes an equivalent factor between the cost of fuel and SOC variation [6, 10, 11]. The A-ECMS strategy improves upon the ECMS strategy by adapting the equivalence factor to changing driving conditions [13]. However, while these methods are capable of real-time control, the lack of a mechanism to consider future driving conditions sacrifices overall optimality. Dynamic programming (DP) has been well studied as a method to achieve a global optimal control strategy for the entire drive cycle [14, 15, 18]. However, due to DP's requirement for knowledge of the entire drive cycle, it is an impractical method for real-time PHEV control.

Model predictive control (MPC) and nonlinear model predictive control (NMPC) are options for predictive HEV control while maintaining the capability for real-time implementation. By utilizing a short horizon look ahead of driving conditions, the ability to allow future events to influence the current control is maintained while reducing the amount of predictive information required when compared to the whole-cycle knowledge requirement of DP. In [26], the authors implemented stochastic MPC for powersplit control of a parallel HEV where the future road grade is modeled as a Markov chain and incorporated into the MPC. The authors were able to reduce fuel consumption relative to

an ECMS strategy that lacks the road grade preview. The authors of [38] also implemented stochastic MPC but with a Markov chain-based driver model that predicts the future power demand for the prediction horizon. Using the proposed method, the authors were able to approach the fuel consumption levels resulting from MPC control with full power demand knowledge of the prediction horizon. In [27] and [29], the authors were able to implement NMPC for single mode HEVs to further reduce energy consumption over MPC; however, validation work was completed in simulation only and not expanded to real-time testing. Paper [30] also proposed an NMPC controller for a single mode HEV, but in this case, testing was expanded to real time where the controller was simulated on an embedded controller.

One major challenge in the implementation of predictive energy management strategies is obtaining an accurate real-time prediction of future conditions such as vehicle speed and road grade. The ongoing commercial development of CAV technologies is now making it possible to obtain static future information such as road conditions through V2V and V2I communication [40]. According to [3], this information can be utilized to make accurate predictions of future vehicle behavior that can serve as an input to real-time, in-vehicle predictive PHEV control. Using reliable forecasts obtained through CAV technology, the effectiveness of predictive energy management strategies can be improved when compared to estimated forecasts developed using historical data as is done in [23, 38]. With these CAV technologies becoming commercially available, it is appropriate to develop and implement methods for PHEV energy management that leverage this predictive information.

The purpose of this work is to investigate the effectiveness and real-time feasibility of predictive powertrain energy management using NMPC for a connected multi-mode PHEV, specifically the 2nd generation Chevrolet Volt. In order to satisfy this objective, an NMPC powertrain controller (NMPC PTC) was developed for the 2nd generation Chevrolet Volt. This controller was extensively tested across many standard and real-world drive cycles in order to quantify its performance. In addition to simulation validation, the developed controller was deployed and tested in real-time on a test vehicle. This work is one component of a holistic CAV controls and optimization system for a PHEV developed under the Michigan Technological University NEXTCAR program [56]. In addition to the powertrain controller presented in this paper, components of this system, which is outlined in Figure 3-1, include technologies such as eco-routing, eco approach and departure, PHEV charge depleting/charge sustaining mode blending, optimal velocity profiling and optimal powertrain mode selection. These technologies cover a range of time horizons from full trip consideration used in eco-routing to a seconds-scale forward look-ahead used in this paper. Further information on these technologies can be found in [43, 57-59]. The outputs of other components serve as crucial inputs to the NMPC PTC such as providing a future predicted velocity trajectory for the NMPC PTC to follow.
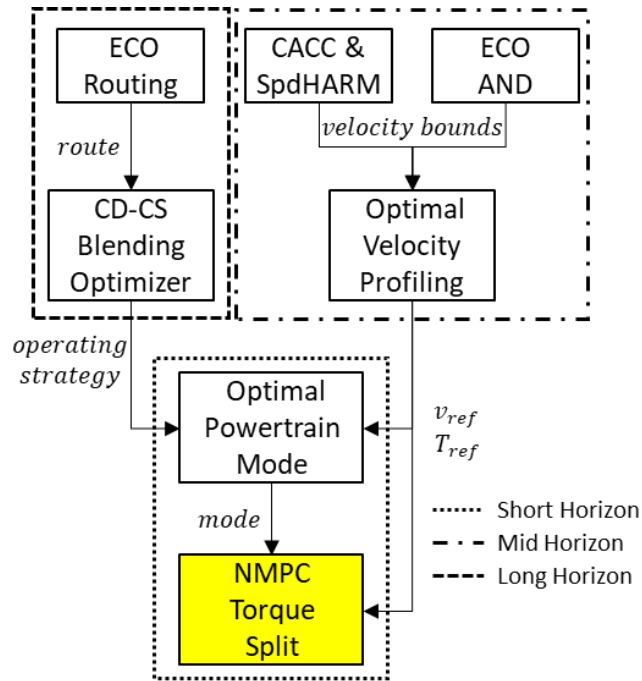
Figure 3-1. MTU NEXTCAR CAV Technology System.

The main contributions of this paper are as follows: (1)     A predictive real-time capable energy management strategy integrated with vehicle dynamics, road grade, and real-time vehicle operating conditions, has been developed for a multi-mode PHEV. This strategy utilizes NMPC to perform online optimization of the powertrain torque split and engine speed in order to minimize fuel consumption while maintaining SOC targets. (2)   The impact of drive cycle variation on the energy savings using developed optimal controller is quantified. First, the developed controller is evaluated over the three EPA standard cycles. Next, a distribution of controller performance has been generated using repeated real-world drive cycles recorded over the same route in order to not only assess the performance of the developed NMPC PTC, but to also quantify the variation of controller performance that results from drive cycle variation when repeating the same route in real-

world conditions. Finally, the controller is evaluated over two real world routes to demonstrate controller effectiveness in non-cycle scenarios. (3) The developed NMPC PTC is demonstrated in real-time on an in-vehicle hardware-in-loop test platform. This test platform is able to run the developed NMPC PTC in real-time in parallel to the vehicle's stock controller while interfacing with hardware such as on-board sensors, the vehicle's CAN bus and control modules, and a cloud-based server that provides future driving information such as future road grade and predicted vehicle velocity. Results of this testing validate that the developed controller is capable of running in a real-time, hardware integrated control system while still achieving the energy savings demonstrated in the extensive simulation testing.

The rest of the paper is organized as follows. Section 3.2 introduces the powertrain and plant model of the 2nd generation Chevrolet Volt. Section 3.3 presents the architecture of the developed NMPC powertrain controller. Section 3.4 provides a description of the instrumented vehicles used for real-time testing as well as the real-time implementation of the NMPC PTC. Section 3.5 assesses the energy savings of the NMPC PTC across multiple standard and real-world drive-cycles in simulation testing. Finally, Section 3.6 presents the energy savings and real-time performance of the NMPC PTC when tested in-vehicle on a rapid-prototyping embedded controller.

## 3.2 Chevrolet Volt Powertrain Plant Model

### 3.2.1 Drive Unit Dynamics

The platform upon which this research is based is the 2nd generation Chevrolet Volt, a multi-mode PHEV. Specifications of this vehicle such as engine size, motor-generator size, battery capacity, etc., can be found in [45-49, 60]. At the heart of this vehicle is the Voltec hybrid drive unit. The architecture of this drive unit is shown in Figure 3-2. This drive unit is designed to operate in five distinct powertrain operating modes sorted into two categories, charge depletion (CD) operation and charge sustaining (CS) operation. CD operation is the default operating strategy and is utilized by the vehicle until the battery is fully depleted or the driver elects to enter into CS mode through an in-vehicle command. The CS strategy uses the three hybrid modes to most efficiently meet the drivers demand while maintaining SOC within a narrow band. This SOC band is a ~±1% region around a reference SOC. In a fully depleted state, this reference SOC is ~16% SOC [47].
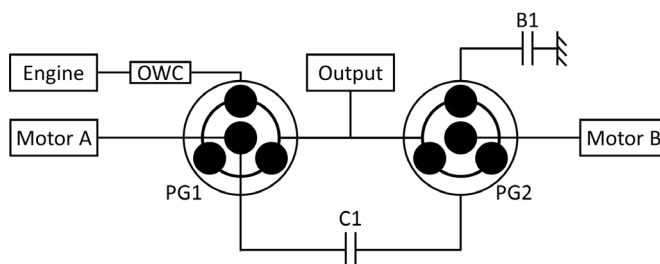


Figure 3-2. Second Generation Chevrolet Volt Drive Unit Architecture

CD operation utilizes two modes, single motor (1-EV) and dual motor (2-EV) operation. 1-EV mode is utilized for the majority of time spent in CD operation. Motor B provides all

tractive power in 1-EV mode and is capable of sufficiently propelling the vehicle in most operating cases. 2-EV mode utilizes Motor A operating in parallel with Motor B. 2-EV mode is active in high torqued demand situations such as vehicle launch from stop and intense accelerations while at speed [47]. Equation (3-1) governs the speed and torque relationships in electric-only mode.

$$
\begin{bmatrix}
I_{Out} & 0 & 0 & R_1+S_1 & R_2+S_2 \\
0 & I_{MA} & 0 & -S_1 & 0 \\
0 & 0 & I_{MB} & 0 & -S_2 \\
R_1+S_1 & -S_1 & 0 & 0 & 0 \\
R_2+S_2 & 0 & -S_2 & 0 & 0
\end{bmatrix}
\times
\begin{bmatrix}
\dot{\omega}_{Out} \\
\dot{\omega}_{MA} \\
\dot{\omega}_{MB} \\
F_{PG1} \\
F_{PG2}
\end{bmatrix}
=
\begin{bmatrix}
-T_{Out} \\
T_{MA} \\
T_{MB} \\
0 \\
0
\end{bmatrix}
\tag{3-1}
$$

CS operation is comprised of three distinct hybrid operating modes. The first hybrid mode is Low Extended Range (LER). LER is an input power split configuration designed for efficient operation at low vehicle speeds and also for high torque demand situations [47]. Equation (3-2) represents the torque and speed of LER operating mode. In LER, clutch B1 is closed which grounds the ring of the second planetary gear set. This leads to a direct relationship between output speed and Motor B speed.

$$
\begin{bmatrix}
I_{Engine} & 0 & 0 & 0 & -R_1 & 0 \\
0 & I_{Out} & 0 & 0 & R_1+S_1 & R_2+S_2 \\
0 & 0 & I_{MA} & 0 & -S_1 & 0 \\
0 & 0 & 0 & I_{MB} & 0 & -S_2 \\
-R_1 & R_1+S_1 & -S_1 & 0 & 0 & 0 \\
0 & R_2+S_2 & 0 & -S_2 & 0 & 0
\end{bmatrix}
\times
\begin{bmatrix}
\dot{\omega}_{Engine} \\
\dot{\omega}_{Out} \\
\dot{\omega}_{MA} \\
\dot{\omega}_{MB} \\
F_{PG1} \\
F_{PG2}
\end{bmatrix}
=
\begin{bmatrix}
T_{Engine} \\
-T_{Out} \\
T_{MA} \\
T_{MB} \\
0 \\
0
\end{bmatrix}
\tag{3-2}
$$

The second hybrid mode is Fixed Ratio Extended Range (FER). FER is a parallel configuration designed for efficient operation in acceleration situations at medium and high vehicle speeds, cruising at medium speeds, and battery charging in low output torque demand situations [47]. Equation (3-3) represents the torque and speed of FER mode.

Motor A is off and grounded through closed clutches C1 and B1 so Motor A torque and speed are constrained to zero.

$$
\begin{bmatrix}
I_{Engine} & 0 & 0 & -R_1 & 0 \\
0 & I_{Out} & 0 & R_1 + S_1 & R_2 + S_2 \\
0 & 0 & I_{MB} & 0 & -S_2 \\
-R_1 & R_1 + S_1 & 0 & 0 & 0 \\
0 & R_2 + S_2 & -S_2 & 0 & 0
\end{bmatrix}
\times
\begin{bmatrix}
\dot{\omega}_{Engine} \\
\dot{\omega}_{Out} \\
\dot{\omega}_{MB} \\
F_{PG1} \\
F_{PG2}
\end{bmatrix}
=
\begin{bmatrix}
T_{Engine} \\
-T_{Out} \\
T_{MB} \\
0 \\
0
\end{bmatrix}
\tag{3-3}
$$

High Extended Range (HER), the third hybrid mode, is a compound power split designed for high vehicle speed, low torque demand situations such as highway cruising [47]. Equation (3-4) represents the torque and speed equations of HER operating mode. Clutch C1 is closed which connects Motor A of the first planetary gear set to the ring of the second planetary gear set.

$$
\begin{bmatrix}
I_{Engine} & 0 & 0 & 0 & -R_1 & 0 \\
0 & I_{Out} & 0 & 0 & R_1 + S_1 & R_2 + S_2 \\
0 & 0 & I_{MA} & 0 & -S_1 & -R_2 \\
0 & 0 & 0 & I_{MB} & 0 & -S_2 \\
-R_1 & R_1 + S_1 & -S_1 & 0 & 0 & 0 \\
0 & R_2 + S_2 & -R_2 & -S_2 & 0 & 0
\end{bmatrix}
\times
\begin{bmatrix}
\dot{\omega}_{Engine} \\
\dot{\omega}_{Out} \\
\dot{\omega}_{MA} \\
\dot{\omega}_{MB} \\
F_{PG1} \\
F_{PG2}
\end{bmatrix}
=
\begin{bmatrix}
T_{Engine} \\
-T_{Out} \\
T_{MA} \\
T_{MB} \\
0 \\
0
\end{bmatrix}
\tag{3-4}
$$

### 3.2.2 Electric Machines

The electric propulsion system of the Chevrolet Volt has four main components. They are the two electric motor-generators contained inside the drive unit as well as a Traction Power Invertor Module (TPIM) for each motor-generator. The efficiency of each of these components is a function of the torque and speed demanded of the motor-generator as shown in (3-5) and Figure 3-3 and Figure 3-4. For simplicity, the efficiency of the motor-generator and TPIM for each motor/TPIM pair is combined into one map which is implemented inside the NMPC PTC.

28

$$\begin{cases} \eta_{MA}\eta_{TPIM\,A} = f(T_{MA}, \omega_{MA}) \\ \eta_{MB}\eta_{TPIM\,B} = f(T_{MB}, \omega_{MB}) \end{cases} \tag{3-5}$$
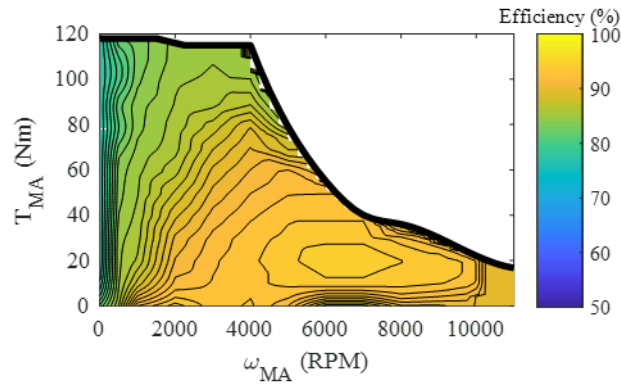


Figure 3-3. Chevrolet Volt Motor-Generator A Efficiency [49].
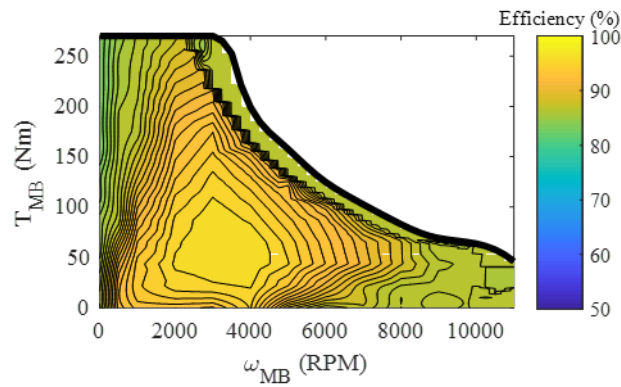


Figure 3-4. Chevrolet Volt Motor-Generator B Efficiency [49].

### 3.2.3   Engine

Engine fuel consumption is modeled through the use of a Brake Specific Fuel Consumption (BSFC) map, represented in (3-6), of the engine as well as a map of approximate fuel consumption due to changing operating point which is represented in (3-7). The development and details of the transient fuel penalty can be found in [53]. The BSFC map,

shown in Figure 3-5, and the transient fuel consumption map, shown in Figure 3-6, are utilized by the NMPC PTC in order to select the most appropriate engine speed and torque that satisfy the objective cost function given the current disturbance.

$$m_{f,static(k)} = \Delta t * T_{Engine(k)} * \omega_{Engine(k)} * BSFC(T_{Engine(k)}, \omega_{Engine(k)}) \qquad (3\text{-}6)$$

$$m_{f,transient(k)} = \Delta t * transient\ penalty(\Delta T_{Engine(k)}, \Delta \omega_{Engine(k)}) \qquad (3\text{-}7)$$
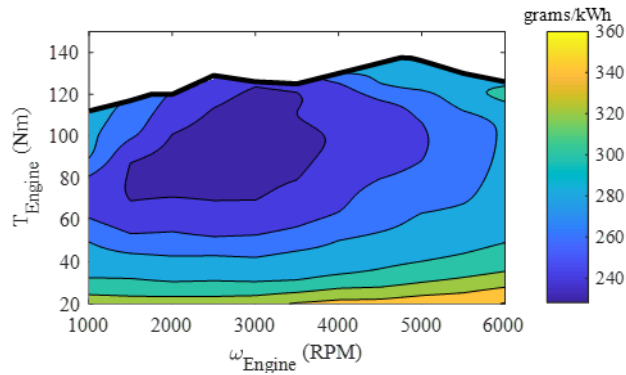


Figure 3-5. Chevrolet Volt Engine BSFC Map [47].
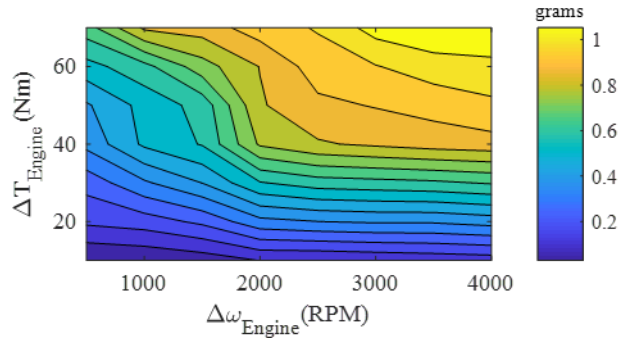


Figure 3-6. Chevrolet Volt Engine Transient Fuel Penalty Map [53].

### 3.2.4 Energy Model

The energy consumption model utilized by this research was developed at MTU as part of the NEXTCAR program. The model is a response fit model trained with more than 200 hours of dynamometer and on-road vehicle data. The model is split into two response surfaces, one for CD mode and one for CS mode. The CD model is a function of vehicle speed and axle torque, while the CS model is a function of vehicle speed, axle torque, and engine speed and torque. Representations of these functions are given in (3-8). The output of this model is energy consumption in megajoules. More information about this model can be found in [54].

$$\begin{cases} E_{CD} = f(T_{Axle}, v_{Veh}) \\ E_{CS} = f(T_{Axle}, v_{Veh}, T_{Engine}, \omega_{Engine}) \end{cases} \tag{3-8}$$

## 3.3 Controller Architecture

The purpose of the NMPC PTC is to make optimal torque-split, and when appropriate, engine speed decisions while within a given operating mode. Due to the differing kinematics and dynamics between the operating modes caused by changing clutch states, each mode has a unique control requirement in terms of relevant control variables and governing plant dynamics. Because of this, each mode has its own NMPC implementations. Four separate controller implementations have been developed, one for EV mode and one for each of the three hybrid modes. The following section will describe the architecture of the NMPC PTC, including control variables, cost functions, and constraints.

Equation (3-9) represents the nonlinear state function of the system where the change in state $\dot{X}$, is a nonlinear function of the current state vector X, the control vector U, and the disturbance vector V. The problem formulation changes for each operating mode due to the differing kinematics between the modes. All four operating modes share a common state vector X and disturbance vector V, but each mode has its own control vector U. Battery SOC is selected as the state variable of NMPC as shown in (3-10).

$$\dot{X} = f(X, U, V) \tag{3-9}$$

$$X = [SOC] \tag{3-10}$$

SOC is estimated as a function of battery power, open circuit voltage, resistance, and battery capacity as shown in (3-11). For this work, open-circuit voltage and resistance were assumed to be constant as battery dynamics are not a main focus of this work. A more thorough investigation of the impact of battery dynamics on HEV powertrain control can be found in [29, 61]. Battery power is a function of both Motor A and B torques and speeds, as well as motor and power invertor efficiencies. The proper efficiency is applied by setting $\beta_{MA}$ and $\beta_{MB}$ to either 1 or -1 depending on if the electric machines are motoring or generating.

$$\dot{SOC}_{(k)} = \frac{\sqrt{V_{OC}^2 - 4P_{Battery(k)}R_{Battery}} - V_{OC}}{2Q_{Battery}R_{Battery}} \tag{3-11}$$

$$P_{Battery} = \left(\eta_{MA}\eta_{TPIM,A}\right)^{\beta_{MA}}T_{MA}\omega_{MA} + \left(\eta_{MB}\eta_{TPIM,B}\right)^{\beta_{MB}}T_{MB}\omega_{MB} \tag{3-12}$$

The control vector, $U$, varies from operating mode to operating mode as shown in (3-13). For EV mode, the two EV modes present in the vehicle have been combined into one NMPC implementation which allows the NMPC PTC to determine the most efficient torque split between the two motor-generators. Therefore, the torque of both Motor A and B need to be controlled. Component speeds are kinematically linked to the output and thus the wheels, so no speed control is required. In LER and HER modes, engine and Motor B torques are selected as control variables. Either engine or Motor A speed also needs to be controlled to fully define the system. Engine speed was chosen as the control variable as the engine operating point is critical to the overall powertrain efficiency. The control vector of FER mode consists of engine torque and Motor B torque. In FER, all component speeds are kinematically linked to the output and Motor A is off and grounded.

$$
\begin{cases}
U_{EV} = \begin{bmatrix} T_{MA} \\ T_{MB} \end{bmatrix} \\[2ex]
U_{LER} = \begin{bmatrix} T_{Engine} \\ T_{MB} \\ \omega_{Engine} \end{bmatrix} \\[3ex]
U_{FER} = \begin{bmatrix} T_{Engine} \\ T_{MB} \end{bmatrix} \\[2ex]
U_{HER} = \begin{bmatrix} T_{Engine} \\ T_{MB} \\ \omega_{Engine} \end{bmatrix}
\end{cases}
\tag{3-13}
$$

The disturbance vector $V$, shown in (3-14), remains the same for each operating mode. This vector brings the predicted drive unit output speed, (3-15), output acceleration, (3-16), and output torque, (3-17), for the length of the prediction into the problem. The data contained in this disturbance vector is provided from two sources. The road grade utilized in the estimation of future required output torque is obtained from map data of a given route. The

reference velocity profile is generated using an optimal velocity prediction algorithm developed as part of the MTU NEXTCAR project, which is presented in [57] and [58].

$$V = \begin{bmatrix} \omega_{Out,Profile} \\ \alpha_{Out,Profile} \\ T_{Out,Profile} \end{bmatrix} \tag{3-14}$$

$$\omega_{Out,Profile} = \frac{FDR}{R_{Tire}} * v_{Profile} \tag{3-15}$$

$$\alpha_{Out,Profile} = \frac{\omega_{Out(k+1)} - \omega_{Out(k)}}{\Delta t} \tag{3-16}$$

$$T_{Out,Profile} = \frac{R_{Tire}}{FDR} * \left( \begin{array}{l} ma_{Profile} + F_0 + F_1 * v_{Profile} \\ + F_2 * v_{Profile}^2 + mgsin(\theta_{Grade}) \end{array} \right) \tag{3-17}$$

Two different cost functions are defined; one for EV mode, (3-18), and one for the hybrid modes, (3-19). In EV mode, the delivery of electrical power in the most efficient manner is a main concern. Therefore, the only objective in EV mode is to minimize overall battery power by choosing the optimal powersplit between the two electric machines. The cost function in the charge sustaining modes includes SOC and fuel consumption terms as shown in (3-20)-(3-22). The objective is to minimize the amount of fuel consumed while maintaining a specific reference SOC level from the beginning of the prediction window until the end of the horizon, $N$. For all testing completed in this work, the reference SOC is held constant to match that of the baseline vehicle as the baseline vehicle aims to track a constant SOC value in CS mode. However, while not shown in this work, the NMPC does have the ability to track a reference SOC trajectory. The transient fuel term is included for the purpose of preventing excessive engine operating point changes that could potentially occur without the penalization of those changes.

$$Cost_{EV} = \sum_{k=1}^{N} \left( P_{Battery(k)} \right) \tag{3-18}$$

$$Cost_{LER,FG,HER} = \sum_{k=1}^{N} \begin{pmatrix} w_1 * \left( SOC_{Reference} - SOC_{(k)} \right)^2 \\ + w_2 * m_{f,static(k)} \\ + w_3 * m_{f,transient(k)} \end{pmatrix} \tag{3-19}$$

$$SOC_{(k+1)} = \dot{SOC}_k * \Delta t + SOC_k \tag{3-20}$$

$$m_{f,static}(N) = l \begin{pmatrix} \left( T_{Engine}, \omega_{Engine} \right)_1, \left( T_{Engine}, \omega_{Engine} \right)_2 \\ , \dots \dots, \left( T_{Engine}, \omega_{Engine} \right)_N \end{pmatrix} \tag{3-21}$$

$$m_{f,transient}(N) = f \begin{pmatrix} \left( \Delta T_{Engine}, \Delta \omega_{Engine} \right)_1, \left( \Delta T_{Engine}, \Delta \omega_{Engine} \right)_2 \\ , \dots \dots, \left( \Delta T_{Engine}, \Delta \omega_{Engine} \right)_N \end{pmatrix} \tag{3-22}$$

The system state and control variables are subject to a set of constraints. Velocity tracking is achieved through the assumption that the application of the predicted output torque will result in the desired velocity trajectory. Therefore, as shown in (3-23), the computed output torque is constrained to the predicted output torque profile within a defined tolerance, $\varepsilon$. To ensure proper velocity tracking, $\varepsilon$ is set to a small value such as 1 Nm. Battery power is constrained to be within the maximum charge and discharge rates of the battery. Maximum engine torque, Motor A torque, and Motor B torque are all defined as a function of the respective component's speed. Finally, engine speed is limited within the minimum and maximum speeds.

$$\begin{cases} -\varepsilon < (T_{Out,Profile} - T_{Out}) < \varepsilon \\ P_{Battery,Charge} < P_{Battrey} < P_{Battery,Discharge} \\ T_{Engine,min}(\omega_{Engine}) < T_{Engine} \\ T_{Engine} < T_{Engine,max}(\omega_{Engine}) \\ T_{MA,min}(\omega_{MA}) < T_{MA} < T_{MA,max}(\omega_{MA}) \\ T_{MB,min}(\omega_{MB}) < T_{MB} < T_{MB,max}(\omega_{MB}) \\ \omega_{Engine,min} < \omega_{Engine} < \omega_{Engine,max} \end{cases} \tag{3-23}$$

Figure 3-7 presents a flow chart of the internal architecture of the NMPC powertrain controller.
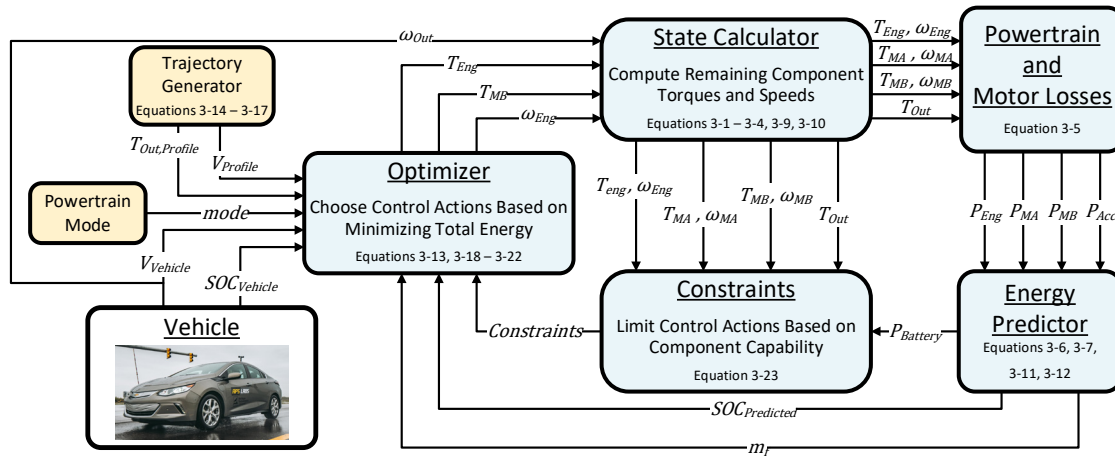


Figure 3-7. NMPC Powertrain Controller Architecture

## 3.4 Real-Time Implementation

### 3.4.1 Test Vehicle Layout

The NMPC PTC was designed to be implemented on any of the four instrumented Chevrolet Volts in MTU's test vehicle fleet. The architecture of the on-board computing unit in test vehicles is shown in Figure 3-8. The vehicles are outfitted with a dSPACE

36

MicroAutoBox II (MAB) that serves as the main processing unit for the vehicle's instrumentation system. The MAB is able to interface with the vehicle's CAN bus to which it has full read access. A host of on-board sensors such as GPS, current and temperature sensors, and accelerometers also interface with the MAB. The MAB is capable of communication with the MTU Mobile Lab computing center as well as other vehicles in the MTU test fleet through a 4G LTE network connection. A human-machine interface (HMI) display is included in order to provide real-time feedback to the driver. The final piece of instrumentation included on the vehicles are Dedicated Short Range Communication (DSRC) units that have the ability to interface with other DSRC-equipped vehicles or infrastructure in order to obtain information such as traffic signal phasing and timing. The in-vehicle installation of this system is shown in Figure 3-9.
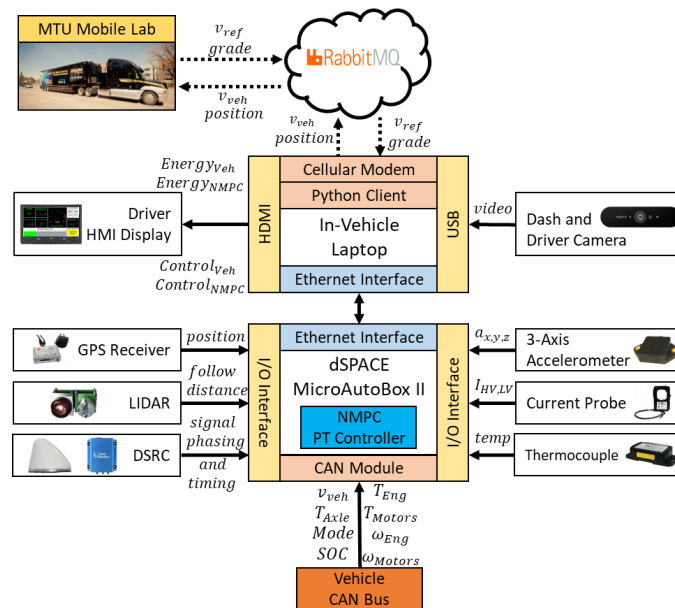


Figure 3-8. MTU Test Vehicle Architecture.
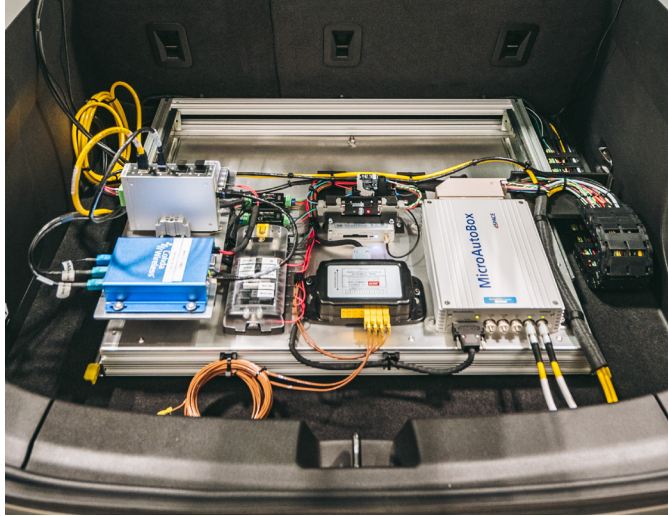
Figure 3-9. MTU Chevrolet Volt vehicle instrumentation package.

### 3.4.2 Implementation of Real-time Predictive Controller

The design goal of this controller was to build a controller that not only reduces energy consumption relative to the stock vehicle's powertrain controller, but is also capable of running in real-time on a prototyping embedded controller as a core element of this CAV control system. The controller was designed and implemented in such a way that the same controller used in simulation can be compiled into executable code. The compiled controller can then be run in a test vehicle in parallel to the vehicle's stock controller in order to assess the performance of the developed NMPC PTC under real-world driving scenarios.

The ACADO, Automatic Control and Dynamic Optimization toolkit was utilized to generate a real-time viable implementation of the NMPC PTC. The ACADO toolkit is an open-source platform designed for the purposes of solving optimal control problems. The

toolkit exports efficient C-code that evaluates NMPC problems with a sequential quadratic programming (SQP)-based solver. This C-code is then able to be deployed onto embedded controller hardware for the purposes of fast optimal control [62-64].

The exported NMPC PTC C-Code is integrated into Simulink through the use of an S-Function. This S-Function can be deployed into the test vehicle model that integrates all on-board sensor, CAN, and communication devices. Inside this model, the controller is interfaced with signals from the vehicle's CAN bus and V2X communication system. This model is then converted to executable code which is deployed onto the in-vehicle MAB. The integration of the NMPC PTC into the test vehicle is shown in Figure 3-8. From this point, the NMPC controller can be run in parallel to the vehicle's stock controller during on-road real-world tests.

## 3.5  Simulation Assessment

In this section, the performance of the NMPC PTC is assessed over three simulation scenarios. Scenario 1 examines the controller's performance across three standard drive cycles, the UDDS, HWFET, and US06. These cycles are also used to determine an appropriate prediction horizon length for all following testing. Scenario 2 examines the controller's performance over a large number of drive cycles driven on the same route in order to obtain a distribution of the controller's performance. Scenario 3 examines two real-world driving routes in order to assess performance of the controller on a non-standard drive cycle.

The process of energy consumption comparison is outlined in Figure 3-10. During on-road or dynamometer vehicle testing, vehicle control actions, such as the speeds and torques of the electric machines and engine, are logged by data logger in the test vehicle. These logged control actions, as well as logged vehicle speed and mode, are then fed through the MTU energy and SOC estimation tools which produce a final energy consumption value and SOC profile to be used as a baseline to compare the NMPC PTC against. In order to achieve an energy consumption value and SOC profile for the NMPC PTC, the following process is used. The logged baseline vehicle velocity, mode, and axle torque are input into the NMPC PTC. The NMPC PTC issues control actions to the MTU energy and SOC estimation tools. SOC is fed back to the NMPC PTC for tracking purposes. The final energy consumption and SOC of the baseline vehicle and NMPC PTC are then compared in order to determine the overall energy savings. In order account for end of cycle differences in SOC between baseline and NMPC results, the SOC difference is converted into an energy value and incorporated into the energy savings calculation as shown in (3-24) and (3-25).

$$Energy\ Savings = \left(\frac{Energy_{Baseline} - Energy_{NMPC} + Energy_{\Delta SOC}}{Energy_{Baseline}}\right) \tag{3-24}$$

$$Energy_{\Delta SOC} = \left(SOC_{End,NMPC} - SOC_{End,Baseline}\right) * Q_{Battery} \tag{3-25}$$
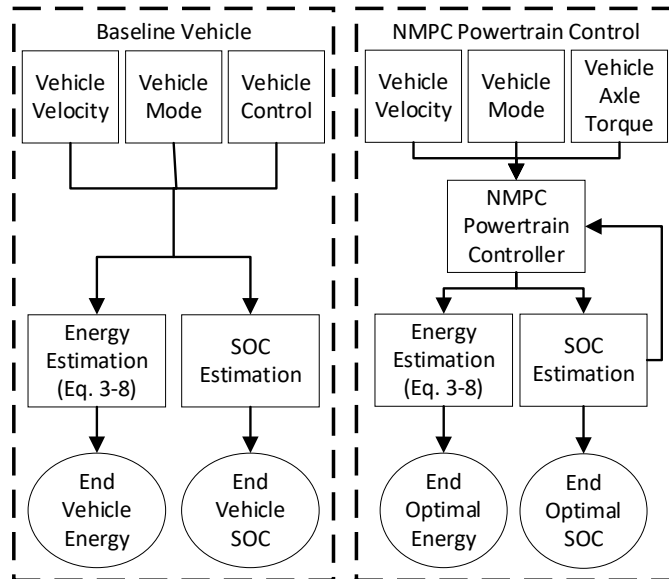
Figure 3-10. Process for energy consumption determination and comparison.

### 3.5.1 Standard Cycle Assessment

Simulation testing was initially completed using standard drive cycles, in this case the UDDS, HWFET, and US06. Baseline control actions for this testing were collected by Argonne National Laboratory (ANL) during their evaluation of the 2nd Generation Chevrolet Volt. Control for these three cycles was simulated using the NMPC PTC. The energy consumption of the NMPC PTC was then compared to that of the baseline vehicle. These cycles were also used to identify an appropriate length of prediction horizon for use in following simulation and real-time testing. Three prediction horizons were examined consisting of 5, 10, and 15 second lengths all using the same cost function weighting factors.

Several trends appeared in the results related to prediction horizon length. Similar levels of energy savings were demonstrated with the 5 and 10 second prediction horizons while the 15 second provided a drop off in energy savings as shown in Figure 3-11. However, with the short 5-second prediction horizon, SOC fluctuates and deviates more from the reference SOC and ultimately results in an end SOC much lower than the reference SOC as shown in Figure 3-12. While this SOC deviation could potentially remedied through cost function weight factor tuning, using the short horizon can result in scenarios where energy savings opportunities are lost that weight factor tuning cannot account for. A scenario from the UDDS cycle that represents start/stop driving is used as an example and is shown in Figure 3-13. Starting at time 389 when the engine turns on, the 5 second horizon is not long enough to capture the future deceleration. This results in an unnecessary higher engine power command, shown in Figure 3-14, relative to the 10 and 15 second horizons. It should be noted that the impact of SOC in this scenario can be neglected as the SOC between the three predictions horizons at the start of this scenario are within 0.03% of each other. For these reasons, the similar levels of energy savings between the 5 and 10 second horizons as well as the extra savings demonstrated in start stop scenarios with the 10 second horizon, all following work utilized a 10-second prediction horizon in order to maximize energy savings while maintaining an acceptable SOC level.
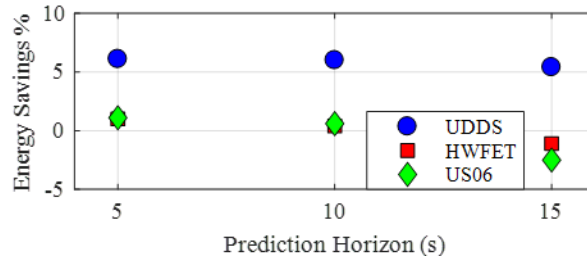
Figure 3-11. Prediction horizon length effect on energy savings relative to the baseline

vehicle.
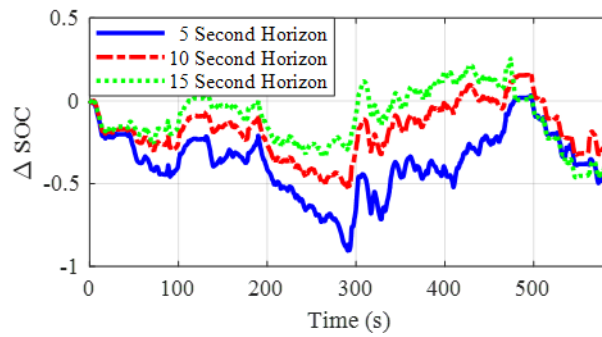


Figure 3-12. Delta SOC from the baseline cycle over the US06 cycle for the three

prediction horizon lengths.
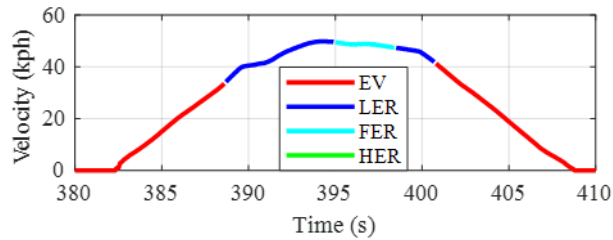


Figure 3-13. Start/Stop segment from the UDDS drive cycle.
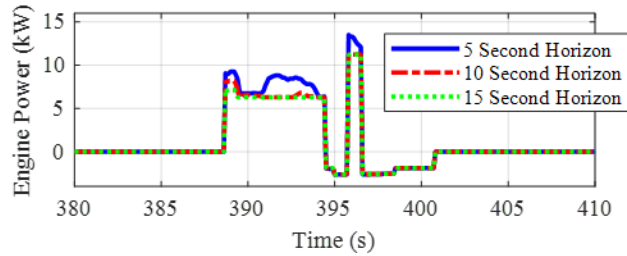
Figure 3-14. Engine power command based on prediction horizon length for a start/stop segment of the UDDS cycle. (Negative engine power is dues to fuel cutoff which puts the engine in a motoring state.)

### 3.5.2 Energy Saving Distribution

An investigation was completed that looked at controller performance over multiple velocity profiles collected on the same route. Controller performance will naturally not be identical between two separate drives of the same route, so a distribution of controller performance was desired to be obtained. In order to achieve this distribution, 30 drive cycles were logged on the Michigan Technological University Drive Cycle (MTUDC), a combined highway and urban cycle ~38 km in length with ~160 m in minimum to maximum elevation change. Shown in Figure 3-15, the MTUDC starts and ends at the Michigan Technological University Advanced Power Systems Laboratory (APS LABS). The direction shown in Figure 3-15 is the forward direction of the MTUDC. Full details of the MTUDC are provided in [51]. 20 of the cycles logged were driven in the forward direction and 10 were driven in the reverse direction.
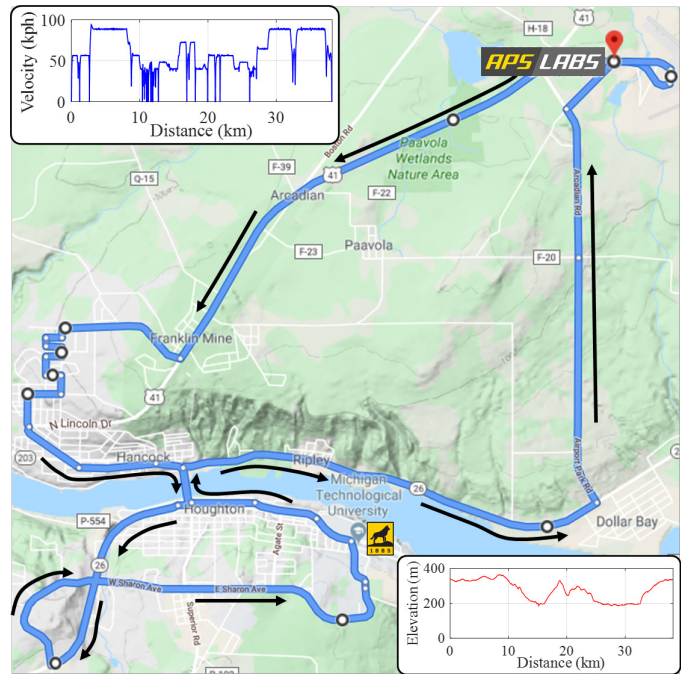
Figure 3-15. Forward MTUDC route as well as velocity and elevation profiles.

Simulations were completed on all 30 logged velocity profiles using the NMPC PTC with the timing parameters shown in Table 3-1. These outputs were then compared to the baseline control actions of the vehicle that were recorded while the velocity profiles were being logged on-road. Upon completion of the simulations, the use of the NMPC PTC resulted in a reduction in energy consumption in both the forward and reverse directions of the MTUDC. A summary of simulation results and the distribution of energy savings are provided in Table 3-2 and Figure 3-16, respectively.

Table 3-1. Simulation Parameters

| NMPC Controller Step Time | 0.1 sec |
|---|---|
| Prediction Horizon | 10 sec |

Table 3-2. MTUDC Cycle Energy Consumption

|  | Number of Cycles | Average Energy Savings | 95% CI |
|---|---|---|---|
| MTUDC | 20 | 1.0% | (0.3%, 1.7%) |
| Reverse MTUDC | 10 | 1.6% | (0.9%, 2.4%) |
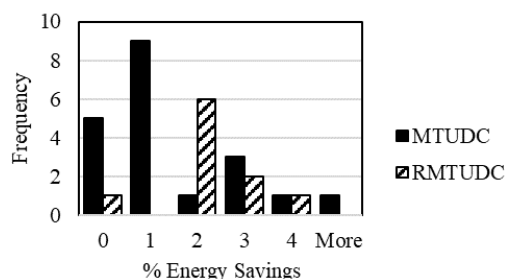


Figure 3-16. MTUDC energy savings distribution using NMPC PTC.

The following analysis more closely examines the energy savings from one of the 20 forward MTUDC cycles. The velocity profile and drive unit modes over this cycle is presented in Figure 3-17. Figure 3-18 presents the energy consumed over this cycle as well as the delta energy consumed between the baseline and NMPC controllers. Delta energy consumed, defined in (3-26), is the difference between baseline and NMPC energy consumed. A downward trend in the plot of this value signifies an area of the cycle where the NMPC controller is using less energy than the baseline control. For this cycle, the main energy savings occurred during accelerations spent in LER and FER modes. The savings was achieved through a reduction in engine power during these events which was then compensated by an increase in electric motor power. While a short-term penalty is paid during this maneuver in the form of a reduction of SOC, which is shown in Figure 3-19,

that cost is later mitigated by bringing SOC back to the reference level during lower demand periods of operation. Long-term effects of this strategy are negligible as the reference SOC is maintained throughout the whole cycle.

$$\Delta Energy\ Consumed_{(k)} = Energy_{NMPC(k)} - Energy_{Baseline(k)} \qquad (3\text{-}26)$$
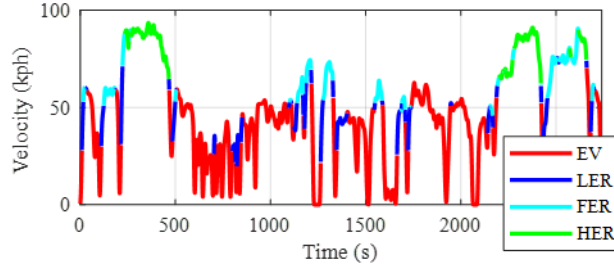


Figure 3-17. MTUDC Vehicle Velocity and Operating Mode.
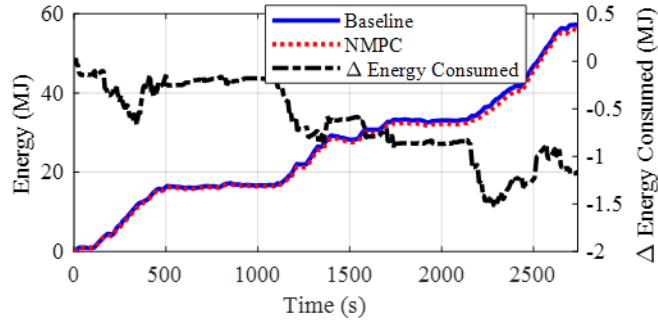


Figure 3-18. MTUDC Energy Consumption Comparison.
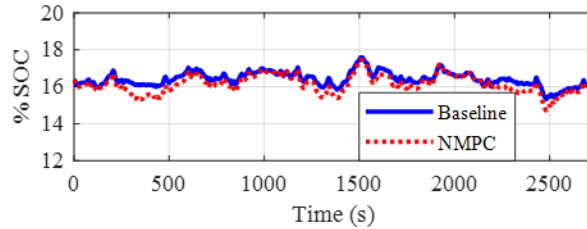


Figure 3-19. MTUDC SOC Comparison.

47

### 3.5.3 Real World Cycle Controller Performance

In order to further verify the performance of the NMPC PTC, simulation testing was expanded to two real-world cycles that have not been extensively tested like the standard cycles (UDDS, etc.) and the MTUDC. The purpose of this is to demonstrate that the controller is not "tuned' for those specific cycles. The first route, collected between MTU and Copper Harbor, MI, is a rural route driven at highway speeds with significant elevation and speed changes. The second route, collected in Ann Arbor, MI, is an urban route that consists of heavy traffic city speeds and high traffic urban freeway speeds. Both routes were driven by an MTU test vehicle. All vehicle performance data were logged in order to obtain a baseline set of control actions.

In both cases, a reduction in energy was realized. The reduction in energy occurred in the same situations as those in the MTUDC test, accelerations in LER and FER mode. As with the previous test cases, no major drop in SOC occurred over the duration of the drive cycle. It should be noted that the large SOC increase at time 4000 seconds is due to a ~150 m elevation decrease in which case the vehicle is regenerative braking for an extended period of time thus charging the battery. Details of this testing are provided in Table 3-3 and Figure 3-20 - Figure 3-22.

Table 3-3. Real World Cycle Energy Consumption

|  | Baseline | NMPC | Reduction |
|---|---|---|---|
| Copper Harbor to MTU | 126.015 MJ | 120.390 MJ | 3.9% |
| Ann Arbor Loop | 35.116 MJ | 34.105 MJ | 3.0% |
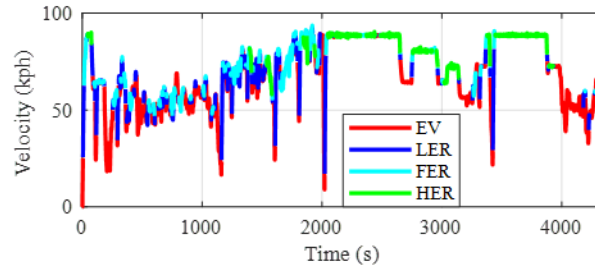
Figure 3-20. Copper Harbor to MTU Vehicle Velocity and Operating Mode.
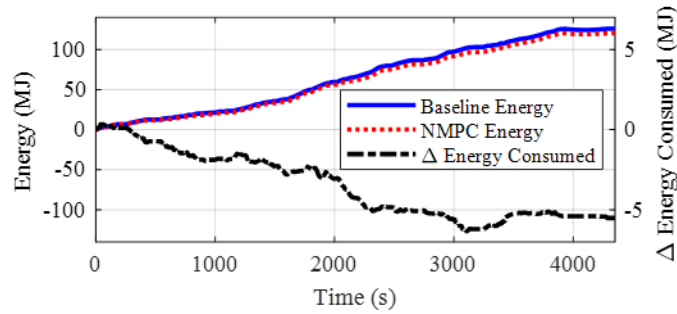


Figure 3-21. Copper Harbor to MTU Energy Consumption.
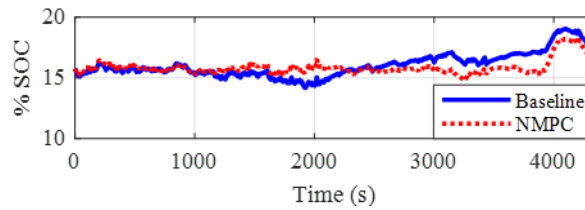


Figure 3-22. Copper Harbor to MTU SOC Comparison.

## 3.6 Real-Time Assessment

In this section, the testing conducted examined the real-time performance of the NMPC PTC. All testing in this section was completed in real-time during on-road tests by utilizing the NMPC PTC deployed onto the in-vehicle dSPACE MicroAutoBox. The engineer's station from which this testing is conducted is shown in Figure 3-23. This testing has two

purposes. Purpose 1 is to confirm that the energy savings benefits seen in simulation testing are presented when the controller is deployed in real-time. Purpose 2 is to demonstrate the ability of the NMPC PTC to run in real-time on an embedded controller that is integrated with hardware such as on-board sensors, the vehicle's CAN bus and control modules, and a cloud server that provides future road information.



Figure 3-23. In-vehicle engineer's station for conducting real-time tests of the NMPC PTC.

The analysis procedure for real time testing results is similar to that in simulation testing. The baseline vehicle and NMPC PTC control actions are passed through the MTU energy and SOC estimation tools in order to obtain energy consumption values. However, there are two key differences in this testing when compared to the completed simulation testing. Difference 1 is that the NMPC PTC is being run in real-time in the vehicle while the baseline control actions are being recorded. Difference 2 is that the NMPC PTC is taking inputs from multiple real-time sources. Vehicle speed, axle torque, and mode are read from the CAN bus at each time step of the controller. While the vehicle is capable of

communicating with a cloud server in order to obtain the required velocity reference profile, this testing did not utilize that feature and instead computed the reference profile locally on the MAB. This decision was made in this initial testing in order to focus solely on the NMPC PTC performance. The influence of cloud communication on NMPC PTC performance will be the subject of future testing. The reference velocity profile used for this testing was generated using an optimal velocity prediction algorithm developed as part of the MTU NEXTCAR project. This algorithm is presented in [57, 58]. Timing information for the test is provided in Table 3-4. The vehicle testing was conducted on the first eight km of the MTUDC. A shortened segment of the MTUDC was selected for in-vehicle testing in order to reduce the time requirements of on road testing. This section was chosen as it contains periods of operation in all powertrain modes at both city and highway speeds. The reference SOC for the NMPC PTC for this testing was set as the vehicle's current SOC at the start of the test. This value stays constant for the remainder of the test.

Table 3-4. Real-Time Test Parameters

| NMPC Controller Step Time | 0.2 sec |
|---|---|
| Prediction Horizon | 10 sec |

Energy savings achieved during real-time testing was within the range observed in simulation testing. An average savings of 1.1% across 10 tests was realized through the use of the NMPC controller when compared to the vehicle's baseline control. A summary of testing results and the distribution of energy savings are provided in Table 3-5 and Figure 3-24, respectively.

Table 3-5. MTUDC Real Time Energy Consumption

|  | Number of Cycles | Average Energy Savings | 95% CI |
|---|---|---|---|
| MTUDC (First 8 km) | 10 | 1.1% | (0.6%, 1.5%) |
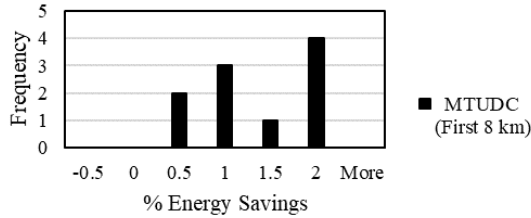


Figure 3-24. Real -time testing energy savings over the first 8 km of the MTUDC.

The following analysis more closely examines the energy savings from one of the 10 real-time tests conducted on the first 8 km of the MTUDC. This cycle, whose velocity and mode profile are presented in Figure 3-25, resulted in an energy savings of 1.3%. As was shown in the simulation testing, the primary sources of energy savings, shown in Figure 3-26, occur through the increased use of battery power during accelerations followed by a recovery in SOC during lower demand portions of the drive cycle. SOC over this cycle is shown in Figure 3-27.
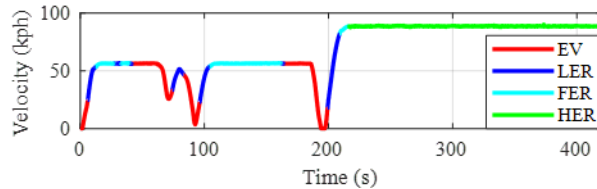


Figure 3-25. Real-time testing Velocity and Operating Mode over the first 8 km of the MTUDC.
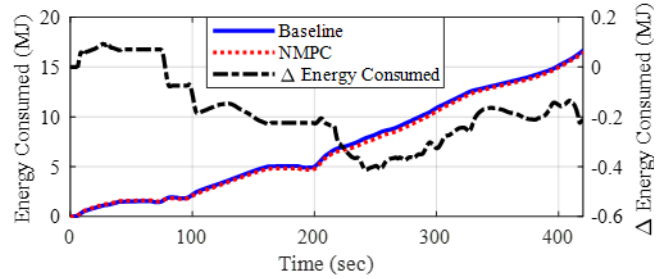
Figure 3-26. Real-time testing Vehicle Energy Consumption over the first 8 km of the MTUDC.
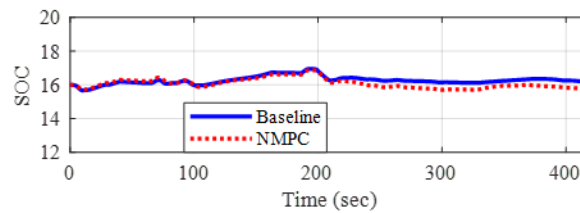


Figure 3-27. Real-time testing SOC over the first 8 km of the MTUDC.

Controller turnaround time, shown in Figure 3-28, differs between the operating modes of the vehicle due to the different number of control variables presented in each mode. The hybrid modes with 3 control variables, LER and HER, had turnaround times in the range of 90-110 ms. Due to the turnaround time exceeding 100 ms in certain instances, the update rate of the controller was slowed to 200 ms in order to avoid computation overruns. FER mode had a faster turnaround time in the range of 50-70 ms. The EV mode had a turnaround time in the range of 80-100 ms. These turnaround times are approaching those that would be required for supervisory control of an HEV thus demonstrating the real-time feasibility of the developed controller.
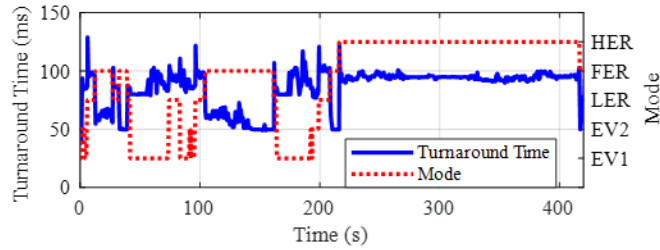
Figure 3-28. Real-time testing Turnaround Time over the first 8 km of the MTUDC.

In-vehicle testing demonstrated the energy savings capability of the NMPC PTC as well as the real-time capability of the controller. This demonstration of real-time NMPC used in conjunction with real-time communication is an important step in demonstrating the feasibility of real-time predictive optimal control methods for PHEVs.

## 3.7 Conclusion

This paper presents a real-time NMPC control algorithm for energy management in a connected multi-mode PHEV. The developed controller utilizes a reference of future vehicle speed and power demand in order to make more efficient energy management decisions. Extensive simulation testing has shown that the NMPC PTC provides an energy savings of 1 to 4% across multiple standard and non-standard drive cycles when compared to the vehicle's production baseline control. Furthermore, the developed controller was deployed and tested in a real-time control system where the energy savings observed in simulations was confirmed in a real-time application during on-road testing.

This work has demonstrated the feasibility of utilizing CAV and predictive control technologies to improve PHEV energy consumption at the powertrain control level.

54

Controller computation times observed during real-time testing show that the implementation of a predictive optimal energy management strategy in a production vehicle is feasible. The next step in demonstrating this production potential would be to utilize the NMPC PTC as the supervisory controller for the vehicle's powertrain in an in-vehicle or dynamometer test in order to demonstrate the controller's ability to control physical components. In addition, extensive testing of the NMPC PTC used in conjunction with cloud communication needs to be completed. Finally, as the developed NMPC PTC is designed to be one part of a larger PHEV CAV controls and optimization system, testing of the NMPC PTC with other components of the PHEV CAV controls and optimization system has occurred both in simulation and in real-time in-vehicle tests. Future work includes the continued testing of the NMPC PTC while integrated with the other pieces of the overall control system.

# 4 Integrated Predictive Powertrain Control for a Multi-Mode Plug-in Hybrid Electric Vehicle

In the ongoing push for a more energy efficient vehicle fleet, the multi-mode Plug-in Hybrid Electric Vehicle (PHEV) is an effective vehicle architecture for reducing vehicle energy consumption when paired with a proper energy management strategy. Due to the complexity of a multi-mode PHEV powertrain, the energy management strategy of said powertrain is a prime candidate for the application of optimal control methods. This paper presents a predictive control strategy for optimal mode selection and powertrain control for a multi-mode PHEV capable of real-time control. This method utilizes predictions of future vehicle behavior in order to plan an optimal path of vehicle powertrain modes that minimizes energy consumption. In addition, this paper also presents the integration of the developed optimal mode control strategy with an optimal powersplit strategy using Nonlinear Model Predictive Control (NMPC) to create a real-time Integrated Predictive Powertrain Controller (IPPC) responsible for all aspects of multi-mode PHEV powertrain supervisory control. The IPPC provides a real-time optimal solution to address the major challenge of a multi-mode HEV powertrain control: an integrated discrete and continuous optimization. Testing in simulation has shown the IPPC to be capable of reducing PHEV energy consumption by 4-10% across real-world and standard drive cycles. In addition, the presented IPPC was deployed onto a rapid prototyping embedded controller where on-road, real-time testing has shown the IPPC to be capable of real-time control while providing an energy reduction of 5%, thus confirming the energy savings observed in simulation.

## 4.1 Introduction

Over the past two decades, automotive manufacturers have turned vehicle electrification in order to reduce overall vehicle energy consumption and to meet emissions standards. Hybrid electric vehicles (HEVs) have been the most popular electrified option for manufacturers with single-mode hybrids being the most common design. Single mode hybrids, such as the Toyota Prius, are defined as having permanent arrangement of power delivery within the drivetrain. More recently, multi-mode hybrids, such as the Chevrolet Volt, were introduced to the market. Multi-mode hybrids make use of clutches within the drivetrain to change the arrangement of power delivery which allows more flexibility and options to propel the car in the most efficient way possible [65]. However, with this greater flexibility comes a larger control problem. While supervisory powertrain control of a single mode HEVs requires only a control decision regarding the powersplit among the engine and motor(s) be made, a multi-mode HEV requires that powertrain operating mode and powersplit both be controlled. The major challenge of a multi-mode HEV supervisory powertrain control is that a combination of discrete optimization (mode selection) and continuous optimization (power-split) is required.

An early research on optimal multi-mode HEV control was conducted on a GM 2-mode hybrid system. A partial instantaneous optimization controller was developed that uses rule-based logic to control engine ON/OFF decisions and SOC management while instantaneous optimization is used to determine the mode and operating points that provide the lowest fuel consumption [66]. More recently, work was conducted on the optimization

of multi-mode HEV design, including clutch arrangement and components sizing for minimum fuel consumption [67-74]. While the work in [67-74] did result in an optimal mode selection strategy, the method used is a form of exhaustive search that is not applicable to on-line control. Zhuang et al. [75] presents a map-based control strategy for a multi-mode HEV. Dynamic programming (DP) is used offline to determine an optimal mode selection and powersplit strategy over several drive cycles. The mode selection output of the DP algorithm is then used to generate a best mode selection map for each vehicle speed and torque demand that is suitable for use in online control. This mode selection map is then paired with an equivalent consumption minimization strategy (ECMS) controller for powersplit in order to create a complete powertrain controller. Zhuang et al. conducted a similar study in [76] where the ECMS controller was replaced a normalized efficiency maximum strategy that improves upon the fuel economy of the ECMS controller. Similarly, Wang et al. [11] uses ECMS to develop best mode and operating point maps for a given vehicle speed and torque that can then be used for online control. Anselma et al. [77] presents an online multi-mode HEV control strategy that utilizes the outputs of the offline optimal control methods presented in [72, 74] to train a neural network. The resulting trained neural network is capable of outputting a powertrain mode and powersplit in an online implementation. Finally, in [18], a DP-based receding horizon control method for HEV mode selection and powertrain control that uses a forward look ahead of vehicle speed in order to determine a best current operating point. However, this method was tested in simulation only and was not validated in real-time control.

58

While optimal control of multi-mode HEVs has been well studied, the real-time applications of these technologies are limited. In addition, the predictive real-time optimal control of multi-mode HEVs that is considerate of future road conditions such as elevation changes and stops has not been extensively studied. With the advancement of vehicle-to-vehicle (V2V) and vehicle-to-infrastructure (V2I) technologies, more and more real-time traffic and road information will be available to vehicles. This information can be used by powertrain controllers to provide superior mode selection and powersplit strategies [35, 78]. This paper presents an integrated predictive powertrain controller for a multi-mode PHEV in connected vehicle environment. The controller integrates with connected and automated vehicle (CAV) technologies, which provide short-term predictions of future vehicle velocity and road conditions over the prediction horizon. Two-layer control architecture is employed for this integrated powertrain controller: mode path planning and powersplit control. The upper layer is an optimal mode path planning algorithm that generates a drive unit mode path for a given prediction horizon in real-time. The optimal mode path planning algorithm is developed based on the discrete optimal planning technology. The lower layer of this integrated powertrain controller is a Nonlinear Model Predictive Control (NMPC) powersplit controller developed and vetted in [55] in order to create a comprehensive optimal controller for the multi-mode 2$^{nd}$ generation Chevrolet Volt powertrain.

This work was completed as part of the Michigan Technological University (MTU) NEXTCAR program which has a target reducing energy consumption of a PHEV by 20% through the use of CAV technologies [56]. This program aimed at all aspects of vehicle

dynamics and powertrain operation in order to discover areas where energy consumption can be reduced. Technologies developed include Eco Arrival and Departure Speed Harmonization [59], Optimal Velocity Profiling [57, 58], Charge Depleting/Charge Sustaining Optimization [43], and NMPC power split management [55].

The main contributions of this article are the following: (1) Develop an algorithm capable of using predictive information obtained through CAV technologies to optimize mode path planning for a given prediction horizon in a multi-mode PHEV. (2) Combine the developed Optimal Mode Path Planning algorithm with NMPC powersplit management in order to produce an integrated predictive powertrain controller (IPPC) that provides full supervisory control for a multi-mode PHEV. (3) Demonstrate the effectiveness of the IPPC in simulation and on-road testing and show the energy benefit over baseline vehicle control and NMPC powersplit control.

The chapter is organized in the following manner. Section 4.2 provides details of the Optimal Mode Path Planning Algorithm. Section 4.3 describes the automated weight factor selection strategy used in the Optimal Mode Path Planning Algorithm. Section 4.4 presents the integration of the Optimal Mode Path Planning Algorithm and the NMPC powertrain controller developed in [55]. Finally, Section 4.5 presents the resulting energy improvements of the IPPC in both simulation and on-road testing.

## 4.2 Optimal Mode Path Planning Algorithm

The objective of the Optimal Mode Path Planning algorithm is to utilize a prediction of vehicle state, which includes future vehicle speed and torque demand, in order to plan a best trajectory of drive unit operating mode over the next $N$ seconds. Planning this trajectory of future modes allows for the best possible mode command to be issued at the current time step. By repeating this process at each execution step of the controller, a near optimal mode selection strategy can be followed for the entire drive cycle. The Optimal Mode Path Planning algorithm is based upon the forward value iteration for discrete optimal planning with a fixed length method presented by Lavelle in [79].

### 4.2.1 Algorithm Overview

Equation (4-1) represents the problem definition of the Optimal Mode Path Planning algorithm. The system state $X$ is defined as the battery $SOC$ as well as the current operating mode, namely EV, LER, FER, and HER, and is shown in (4-2). The control variable $U$, represented in (4-3), is the operating mode of the vehicle to be issued as a command. The disturbance vector $V$ is comprised of the predicted future velocity of the vehicle and expected road grade and is shown in (4-4).

$$\dot{X} = f(X, U, V) \tag{4-1}$$

$$X = \begin{bmatrix} SOC \\ mode \end{bmatrix} \tag{4-2}$$

$$U = [mode] \tag{4-3}$$

$$V = \begin{bmatrix} v_{Profile} \\ \theta_{Grade} \end{bmatrix} \tag{4-4}$$

The change in system state, $\dot{SOC}$, is given in (4-5). It is a function of the assumed constant

battery parameters $V_{OC}$, the open ciruit voltage, $R_{Battery}$, the internal resistance, and

$Q_{Battery}$, the total battery capacity, as well as battery power as shown in (4-7). It should

be noted that battery parameters are assumed constant in this paper. The effects of changing

battery parameters have been studied in other works such as [29]. $P_{Battery}$, as well as the

fuel consumption term $m_f$ as shown in (4-8), are a function of the control and disturbance

vectors. The values for these variables are determined offline as a result of the computed

optimal operating point for a given mode, velocity, and torque request combination using

the methods presented in [11]. The disturbance vector variable $v_{Profile}$ is the predicted

future velocity of the vehicle. This profile is produced by an optimal velocity prediction

tool developed as part of the MTU NEXTCAR program. Details of this tool can be found

in [56-58].

$$\dot{SOC}_{(k)} = \frac{\sqrt{V_{OC}^2 - 4P_{Battery(k)}R_{Battery}} - V_{OC}}{2Q_{Battery}R_{Battery}} \tag{4-5}$$

$$T_{Out,Profile} = \frac{R_{Tire}}{FDR} * \begin{pmatrix} ma_{Profile} + F_0 + F_1 * v_{Profile} \\ +F_2 * v_{Profile}^2 + mgsin(\theta_{Grade}) \end{pmatrix} \tag{4-6}$$

$$P_{Battery(k)} = f(Mode_{(k)}, v_{Profile(k)}, T_{Out,Profile(k)}) \tag{4-7}$$

$$m_{f(k)} = f(Mode_{(k)}, v_{Profile(k)}, T_{Out,Profile(k)}) \tag{4-8}$$

$$a_{Profile} = \frac{v_{Profile(k+1)} - v_{Profile(k)}}{\Delta t} \tag{4-9}$$

The cost function, shown in (4-10), is comprised of two types of cost. The first is the cost incurred by residing in a specific mode in a given time step. This includes terms for the fuel consumed during each time step, $m_{f,(k)}$, and a term penalizing deviation in the actual SOC from the reference SOC, $\left(SOC_{Reference} - SOC_{(k)}\right)$. The second type of cost is that incurred by transitioning from one mode to another, the *mode shift penalty* term. Shown in (4-11), this term includes the kinetic energy change in rotating components due to a mode shift, the electrical energy required by the electric hydraulic pump to execute the shift, and, in the case of a shift that requires an engine start, the additional fuel required to start the engine. This term serves two purposes. Purpose 1 is to prevent energy intensive mode transitions. Purpose 2 is to prevent frequent mode shifts that would result in poor perceived drive quality by the driver. The hydraulic pump and engine-on penalties, defined in (4-12) and (4-13), are functions of the current time step control variable, $Mode_{(k)}$, and the previous time step's control variable, $Mode_{(k-1)}$. The component speeds used in the kinetic energy calculations are defined in (4-14)-(4-16).

$$cost = \sum_{k=1}^{N} \binom{\alpha * m_{f,(k)} + \beta\left(SOC_{Reference} - SOC_{(k)}\right)}{+\gamma * mode\ shift\ penalty_{(k)}} \tag{4-10}$$

$$
\begin{aligned}
&mode\ shift\ penalty \\
&= \begin{pmatrix}
\left|0.5 \cdot I_{MA} \cdot \left(\omega_{MA,(k)}^2 - \omega_{MA,(k-1)}^2\right)\right| + \\
\left|0.5 \cdot I_{MB} \cdot \left(\omega_{MB,(k)}^2 - \omega_{MB,(k-1)}^2\right)\right| + \\
\left|0.5 \cdot I_{Engine} \cdot \left(\omega_{Engine,(k)}^2 - \omega_{Engine,(k-1)}^2\right)\right| + \\
m_{f,Engine\ On} + Energy_{pump}
\end{pmatrix}
\end{aligned} \tag{4-11}
$$

63

$$m_{f,\,Engine\,On(k)} = f\big(Mode_{(k)}, Mode_{(k-1)}\big) \tag{4-12}$$

$$Energy_{pump(k)} = f\big(Mode_{(k)}, Mode_{(k-1)}\big) \tag{4-13}$$

$$\omega_{MA(k)} = f\big(Mode_{(k)}, v_{Profile(k)}, T_{Out,Profile(k)}\big) \tag{4-14}$$

$$\omega_{MB(k)} = f\big(Mode_{(k)}, v_{Profile(k)}, T_{Out,Profile(k)}\big) \tag{4-15}$$

$$\omega_{Engine(k)} = f\big(Mode_{(k)}, v_{Profile(k)}, T_{Out,Profile(k)}\big) \tag{4-16}$$

### 4.2.2 Algorithm Details

The optimal mode path planning algorithm is shown in Figure 4-1. The problem is defined with the following terms. $k$ represents the time step in the prediction horizon. Let $n$ be the possible mode options, $M$, at time step $T_k$. Let $p$ be the possible mode options at time step $T_{k-1}$. Let $C_{n,k}$ be the cumulative cost of traveling from $M_0$ at $T_0$ to $M_n$ at time step $T_k$. $H_{n,k}$, shown in (4-17), is the cost of residing in $M_n$ at time step $T_k$. $J_{n,p,k}$, shown in (4-18), is the cost of going from $M_p$ at time step $T_{k-1}$ to $M_n$ at time step $T_k$. $P_{n,k}$ is the mode at time step $T_{k-1}$ that gives the path with least cost $C_{n,k}$ as shown in (4-19).

$$H_{n,k} = \alpha * m_{f,(k)} + \beta * \big(SOC_{Reference} - SOC_{(k)}\big) \tag{4-17}$$

$$J_{n,p,k} = \gamma * mode\ shift\ penalty_k \tag{4-18}$$

$$C_{n,k} = \min_{p \in \left\{ \substack{M_0, if\ k=1 \\ 1:n, if\ k \neq 1} \right\}} \big(C_{p,k-1} + H_{n,k} + J_{n,p,k}\big) \tag{4-19}$$
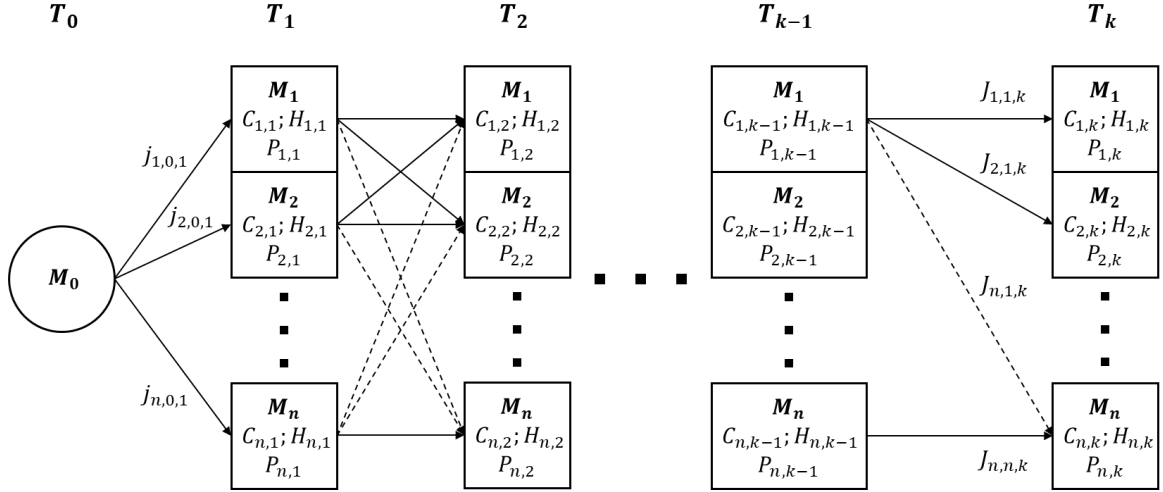
Figure 4-1: Mode selection process for a problem with $n$ modes and $k$ timesteps.

For an example of the calculation process, equations (4-20)-(4-25) show the calculation process for time step $T_k$ for a problem with $n$ modes. At timestep $T_k$, the cumulative cost for each mode $M_{1:n}$ is evaluated for each potential path from time $T_{k-1}$ to time $T_k$ as shown in (4-20), (4-22), and (4-24). The mode at time $T_{k-1}$ that resulted in the minimum cumulative cost at time $T_k$ is then stored as $P_{n,k}$ in order to track the path of minimum cost as shown in (4-21), (4-23) and (4-25). This process is repeated for each timestep $T_1:T_N$. The result of this process will be a set of cumulative costs $C_{1:n,N}$, the minimum of which is the lowest path cost for the problem.

$$C_{1,k} = \min\{(C_{1,k-1} + J_{1,1,k} + H_{1,k}), (C_{2,k-1} + J_{1,2,k} + H_{1,k}), \cdots,$$
$$(C_{n,k-1} + J_{1,n,k} + H_{1,k})\} \tag{4-20}$$

$$P_{1,k} = \begin{cases} 1, if\ (C_{1,k-1} + J_{1,1,k} + H_{1,k})\ is\ the\ least\ cost \\ 2\ if\ (C_{2,k-1} + J_{1,2,k} + H_{1,k})\ is\ the\ least\ cost \\ \qquad \cdots \cdots \cdots \\ n\ if\ (C_{n,k-1} + J_{1,n,k} + H_{1,k})\ is\ the\ least\ cost \end{cases} \tag{4-21}$$

$$C_{2,k} = \min\{(C_{1,k-1} + J_{2,1,k} + H_{2,k}), (C_{2,k-1} + J_{2,2,k} + H_{2,k}), \cdots, \\ (C_{n,k-1} + J_{2,n,k} + H_{2,k})\} \tag{4-22}$$

$$P_{2,k} = \begin{cases} 1, if\ (C_{1,k-1} + J_{2,1,k} + H_{2,k})\ is\ the\ least\ cost \\ 2\ if\ (C_{2,k-1} + J_{2,2,k} + H_{2,k})\ is\ the\ least\ cost \\ \quad\quad \dots\dots\dots \\ n\ if\ (C_{n,k-1} + J_{2,n,k} + H_{2,k})\ is\ the\ least\ cost \end{cases} \tag{4-23}$$

$$C_{n,k} = \min\{(C_{1,k-1} + J_{n,1,k} + H_{n,k}), (C_{2,k-1} + J_{n,2,k} + H_{n,k}), \cdots, \\ (C_{n,k-1} + J_{n,n,k} + H_{n,k})\} \tag{4-24}$$

$$P_{n,k} = \begin{cases} 1, if\ (C_{1,k-1} + J_{n,1,k} + H_{n,k})\ is\ the\ least\ cost \\ 2\ if\ (C_{2,k-1} + J_{n,2,k} + H_{n,k})\ is\ the\ least\ cost \\ \quad\quad \dots\dots\dots \\ n\ if\ (C_{n,k-1} + J_{n,n,k} + H_{n,k})\ is\ the\ least\ cost \end{cases} \tag{4-25}$$

### 4.2.3  Algorithm Application

The following sections details how the algorithm described in 4.2.2 is specifically applied to mode path planning for the Chevrolet Volt. The Volt has 5 distinct operating modes; however, the NMPC powertrain controller outlined in [55] treats 1-EV and 2-EV as one mode and determines the best powersplit between the two motors. Therefore, the number of modes, $n$, considered in the Optimal Mode Path Planning algorithm is four: EV, LER, FER, and HER (mode 1, 2, 3, and 4). An example of an optimal mode path for the Volt is shown in Figure 4-2.
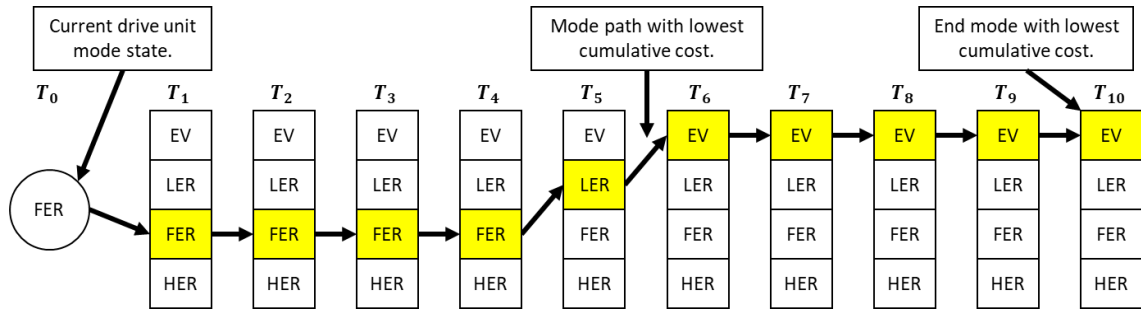
Figure 4-2: Optimal mode path example with a starting state of FER mode and an end state of EV mode.

Several physical limitations of the Volt drive unit must be considered in the formulation of the Optimal Mode Path Planning algorithm. Mode shifting on the Volt is relatively slow process as mode shifts take on the seconds scale to complete. Because of this, the prediction horizon is discretized into time steps with a length of one second. Time steps of a shorter duration would not be appropriate to consider as the drive unit cannot physically shift that quickly. Another physical limitation that must be accounted for in the problem formulation involves what are and what are not allowable shifts. Due to the design of the Volt drive unit, only direct shifts that require the actuation of one clutch between consecutive modes are possible. For example, EV→LER, FG→HER, or FG→LER are direct shifts. However, EV→HER, FG→EV, or LER→HER would all be indirect shifts. Because of this, only

legal shift paths are considered. For example, if the cost $C_{HER,k}$ is being computed, only paths $J_{HER,FER,k}$ and $J_{HER,HER,k}$ will be evaluated.

## 4.3 Automated Weight Factor Selection

Crucial to the performance of any optimization problem with multiple cost function terms is the weighting of the terms in the cost function [80]. Methods for the selection of weight factors often involve some form of manual tuning that produces a suitable output. However, relying on a single set of tuned values can result in cases where the chosen weight factors do not lead to an optimal solution. For this reason, it was desired to use a method that automatically selects and updates weighting factors based on the current state of the system.

The weighting process is started by introducing normalization terms. As all terms in the cost function are in a unit of energy, it was desired to convert all terms to a common unit of energy. In order to accomplish this, it was chosen to leave the fuel consumption term in its base units of grams of fuel consumed and normalize the SOC and mode sift penalty terms to equivalent grams of fuel consumed. These normalized terms are presented in equations (4-26) and (4-27) where $\lambda$ is the normalizing factor, $Q_{Battery}$ is the total capacity of the battery in $kWh$, $N$ is the number of prediction horizon steps, and $BSFC_{Min}$ is the minimum BSFC point of the engine in $\frac{grams}{kWh}$, the most efficient operating point to use the engine to replenish the charge used from the battery. Multiplying $\lambda_{SOC}$ by the percentage the current prediction horizon step's SOC is below the reference SOC results in the grams

of fuel required to raise the SOC back to the reference SOC level. This quantity is then divided by the number of time steps in the prediction horizon in order to determine the amount of fuel required to return SOC to the reference level at the end of the prediction horizon. Multiplying the energy required to execute a mode shift, the $mode\ shift\ penalty$, by $\lambda_{mode\ shift\ penalty}$ results in the equivalent grams of fuel required to execute the shift. Applying these normalizing factors places all three cost function terms in directly comparable units. This assists in the application of appropriate weighting terms.

$$\lambda_{SOC} = \frac{Q_{Battery} * BSFC_{Min}}{N} \tag{4-26}$$

$$\lambda_{mode\ shift\ penalty} = BSFC_{Min} * mode\ shift\ penalty_{(k)} \tag{4-27}$$

The objective function goal of maintaining a reference SOC level is accomplished through penalizing control actions that lead to deviations below the reference SOC set point. In order to achieve this, the SOC tracking term is weighted using a progressive term that imposes a stricter penalty the further the predicted SOC deviates from the reference SOC level. This is accomplished through the use of the exponential function where the operand is the current time step's predicted SOC below the reference SOC level. This function is shown in equation (4-28).

$$\beta_{(k)} = e^{(SOC_{Reference} - SOC_{(k)})} * \lambda_{SOC} \tag{4-28}$$

The purpose of the mode shift penalty term is to prevent energy intensive mode transitions while also preventing frequent mode shifts that would result in poor perceived drive quality

69

by the driver. Developing a weighting factor for this term was focused on eliminating frequent mode shifts as energy intensive mode shifts are avoided by normalizing the energy consumed to execute the mode shift to equivalent grams of fuel. However, what this does not cover is low required energy mode shift where the potential of frequent back and forth mode switching exists. To counter this potential behavior, an exponential weight factor has been introduced where the operand is the number of mode changes that occurred in the previous prediction horizon or the $mode\ shift\ count$. This ensures that if a high number of mode changes were predicted in the previous controller step, the mode shift weight for the current step is increased to eliminate this behavior. The formula for this term is given in equation (4-29). It should be noted that if the power demand remains negative for the entirety of the prediction horizon, the value this weight is set to 1 so as to not discourage shifts to EV mode.

$$\gamma = e^{mode\ shift\ count} * \lambda_{mode\ shift\ penalty} \tag{4-29}$$

## 4.4 Integrated Multi-Mode PHEV Powertrain Control

### 4.4.1 Summary of NMPC Controller

An NMPC powertrain controller (PTC) was developed for the 2$^{nd}$ generation Chevrolet Volt PHEV. This controller utilizes predictions of future vehicle velocity and torque demand, provided by the MTU-developed optimal velocity profiling algorithm [57, 58], to optimize drive unit powersplit and battery SOC management. Depending on the operating mode commanded, the NMPC powertrain controller will command one or both motor

torques, engine torque, and engine speed [55]. A simplified representation of the NMPC powertrain controller is shown in Figure 4-3.
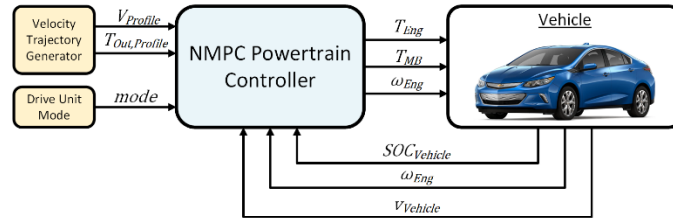


Figure 4-3: NMPC Powertrain Controller Architecture for LER and HER modes.

As tested in [55], the NMPC PTC received its commanded mode input from the stock vehicle controller in the form of logged vehicle testing data in the case of simulations or from CAN feedback to the dSPACE MicroAutoBox in the case of on-road, in-vehicle testing. Simulation testing showed that this controller reduced energy consumption from 1-4% when compared to the vehicle's stock control across 32 drive cycles. In-vehicle, real-time testing confirmed the energy reduction shown in simulation by demonstrating a 1% energy reduction over 10 drive cycles while maintaining controller turnaround times between 50-100 ms.

### 4.4.2 Integrated Predictive Powertrain Controller

As outlined in [55, 56], the Optimal Mode Path Planning Algorithm and NMPC powertrain controller are the two MTU NEXTCAR-developed technologies that are designed to provide optimal powertrain control using a short, seconds length horizon prediction of future vehicle operating condition. While capable of being implemented without the other, these two technologies were designed to be implemented as one integrated predictive

powertrain controller. Their integration is diagrammed in Figure 4-4. At each controller execution step, both the Optimal Mode Path Planning algorithm and the NMPC powertrain controller receive predictions of future vehicle speed and torque demand from the MTU-developed optimal velocity profiling algorithm [57, 58]. In addition, both controllers receive feedback of the current vehicle states, including current vehicle speed and battery SOC. The Optimal Mode Path Planning Algorithm uses this information to compute an optimal drive unit mode trajectory for the prediction horizon. This information is provided to the NMPC powertrain controller which computes an optimal powersplit strategy for the prediction horizon. Once both the optimal mode and optimal powersplit are computed, the next time step mode and powersplit is issued as a command and the process repeats itself at the next controller execution step.
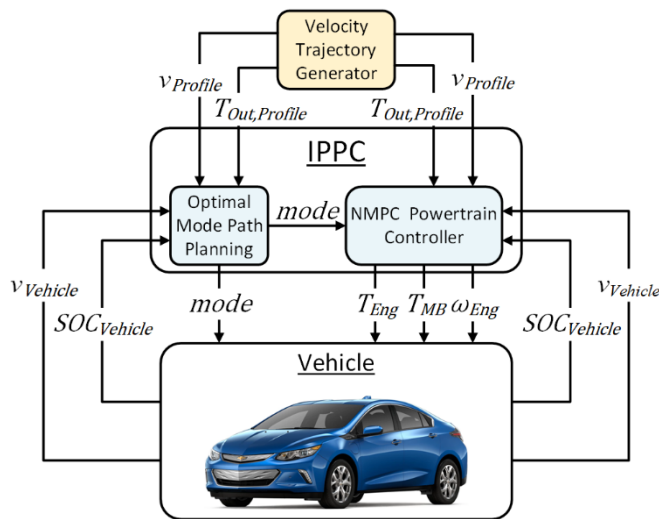
Figure 4-4: IPPC architecture including both NMPC powertrain control and Optimal Mode Path Planning.

## 4.5 Performance Assessment of IPPC

The integrated predictive powertrain controller has undergone extensive testing both in simulations and on-road, in-vehicle testing. The logged drive cycles tested in simulation in [55] with only the NMPC powertrain controller were re-tested in this work using the full integrated predictive powertrain controller. The main reason for using these same drive cycles is to directly show the added benefit of integrating the Optimal Mode Path Planning algorithm with the NMPC powertrain controller. In addition to the completed simulation testing, on-road real-time testing was completed in order to confirm the energy savings demonstrated in simulation and to show the real-time feasibility of the integrated predictive powertrain controller.

### 4.5.1 Simulation Assessment

Simulations of the integrated powertrain controller were conducted using a Simulink implementation of the IPPC and an MTU NEXTCAR developed model of the Volt. These simulations were conducted over 28 different drive cycles. Three of the drive cycles tested were the standard EPA cycles; the US06, the UDDS, and the HWFET. 22 of the cycles were logged on the Michigan Technological University Drive Cycle, or MTUDC. The MTUDC is a real-world drive cycle located in the Houghton/Hancock, MI area. Developed as part of the MTU NEXTCAR program, this cycle was designed to incorporate elements of all three EPA cycles in order to provide a comprehensive test of vehicle performance.

Full details of the MTUDC can be found in [51]. The final three cycles tested are real-world cycles logged by MTU. These three cycles consist of a rural highway route collected between Copper Harbor, MI and the MTU campus in Houghton, MI, a mixed urban and freeway route collected in the Ann Arbor, MI area, and a mixed urban and highway cycle collected at the American Center for Mobility (ACM) vehicle testing facility in Ypsilanti, MI.

The following paragraph details the method used to analyze the energy consumption of both the baseline vehicle and IPPC control actions. All baseline energy consumption values reported in this study are a function of vehicle speed and axle torque as well as vehicle control actions, such as mode, engine torque, and engine speed, recorded during either on-road or dynamometer testing. This logged data is then processed through the MTU energy calculator and SOC prediction tools, shown in (3-8), in order to obtain the final baseline energy consumption and SOC values. Energy assessment of the IPPC is conducted in the following manner as shown in Figure 4-5. The vehicle velocity and axle torque recorded by the baseline vehicle are provided as inputs to the Integrated Predictive Powertrain Controller. Internal to the IPPC, the Optimal Mode Path Planning algorithm uses these inputs in addition to feedback from the SOC predictor for the current SOC level and the previously commanded mode in order to determine an optimal path of modes for the prediction horizon. The first mode in this path is then issued as a command to the NMPC Powertrain Controller. The NMPC powertrain controller uses this mode command, velocity and axle torque inputs, and the current SOC level from the SOC predictor to compute an optimal powersplit command. This powersplit and mode command is then

issued by the IPPC to the MTU energy calculator and SOC predictor tools whose outputs can directly be compared to the baseline values. Finally, in order to provide an accurate energy savings value using the IPPC, the final energy savings value is adjusted to account for any end of cycle SOC values using (4-30) and (4-31).

$$Energy\ Savings = \left(\frac{Energy_{Baseline} - Energy_{IPPC} + Energy_{\Delta SOC}}{Energy_{Baseline}}\right) \qquad (4\text{-}30)$$

$$Energy_{\Delta SOC} = \left(SOC_{End,IPPC} - SOC_{End,Baseline}\right) * Q_{Battery} \qquad (4\text{-}31)$$
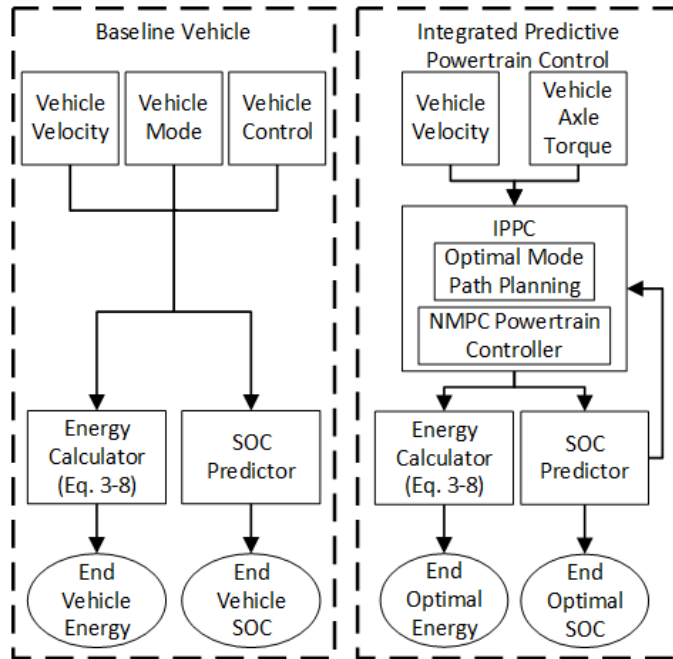


Figure 4-5: Evaluation process for determining the energy consumed of the baseline vehicle and integrated predictive powertrain controller.

### 4.5.1.1   Standard Drive Cycles

Simulation testing of the EPA standard drive cycles demonstrated that the use of the integrated predictive powertrain control offers significant energy improvements over both the baseline vehicle control and powersplit optimization only. It should be noted that the baseline energy consumption for the standard cycles was collected by Argonne National Laboratory (ANL) during their assessment of the 2nd generation Chevrolet Volt and provided to the MTU NEXTCAR team by ANL. As shown in Table 4-1, the integrated predictive powertrain controller provides, depending on the cycle, a 4-10% reduction in energy consumption relative to the vehicle's baseline control. In addition to the savings seen relative to baseline vehicle control, savings have also been demonstrated using the IPPC relative to just using NMPC powertrain control as presented in [55]. The addition of the Optimal Mode Path Planning algorithm provided a 4%, 4%, and 5% energy savings increase in the US06, UDDS, and HWFET, respectively. Production vehicles have been calibrated well for standard drive cycles. However, dyno calibration does not consider a prediction of the upcoming velocity profile. That may be the reason that mode path planning can provide a good amount of energy saving.

Table 4-1: Standard drive cycle energy savings distribution using Integrated Predictive Powertrain Control.

| Cycle | Baseline | Integrated Predictive Powertrain Control | Energy Savings |
|---|---|---|---|
|  |  |  |  |

| | | | |
|---|---|---|---|
| US06 | 23.289 MJ | 22.016 MJ | 3.7% |
| UDDS | 16.952 MJ | 15.401 MJ | 9.8% |
| HWFET | 22.423 MJ | 20.963 MJ | 5.7% |

Figure 4-6 - Figure 4-9 present the areas where the IPPC provides an energy consumption reduction in the HWFET. Figure 4-6 and Figure 4-7 show the powertrain mode over the drive cycle for both baseline vehicle control and optimal mode selection, respectively. Figure 4-8 shows the energy consumption for both baseline vehicle control and the IPPC as well as the cumulative difference in energy consumption between the baseline and IPPC controllers as defined in (4-32). It can be observed from these three figures that the IPPC provides the most benefit in drive cycle conditions where a reduction in power demand can be predicted such as the decelerations at the 200 and 600 second marks. The IPPC is able to recognize this power demand drop and turn off the engine which results in an overall energy savings. This occurs while maintaining SOC within 0.5% of the baseline SOC as shown in Figure 4-9.

$$\Delta Energy\ Consumed(k) = Energy_{IPPC}(k) - Energy_{Baseline}(k) \qquad (4\text{-}32)$$
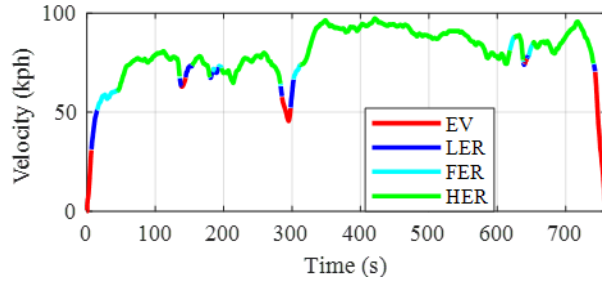
Figure 4-6: HWFET Vehicle Velocity and Baseline Operating Mode.
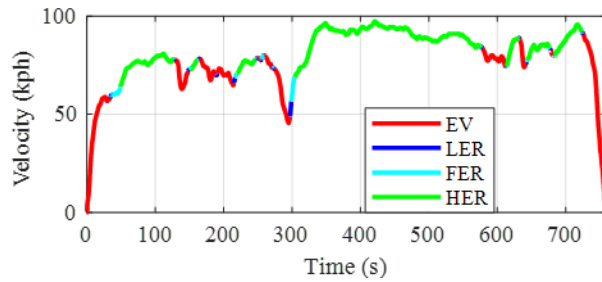


Figure 4-7: HWFET Vehicle Velocity and Optimal Operating Mode.
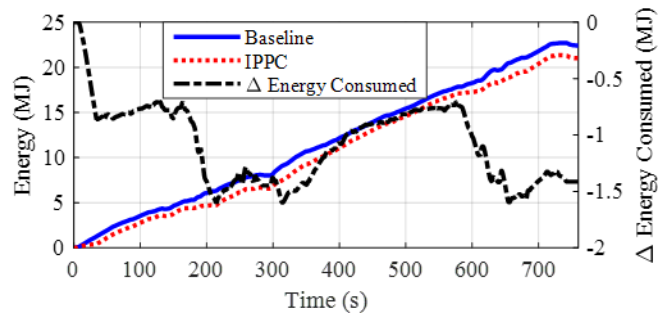


Figure 4-8: HWFET Baseline vs. IPPC Energy Consumption Comparison.
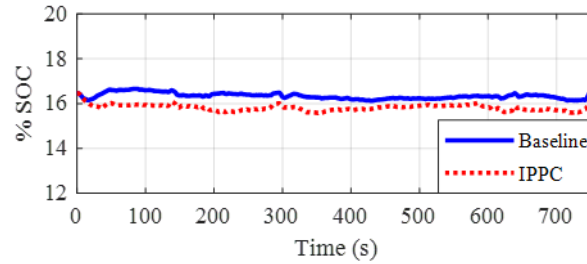
Figure 4-9: HWFET Baseline vs. IPPC SOC Comparison.

### 4.5.1.2   MTU Drive Cycle

The integrated predictive powertrain control was evaluated on 22 velocity profiles recorded by MTU test vehicles on the MTUDC which is shown in Figure 3-15. Of the 22 cycles, 12 were logged in the counterclockwise, or forward, direction and 10 were recorded in the clockwise, or reverse direction which is abbreviated as the reverse MTUDC or RMTUDC. This large number of simulations was conducted in order to quantify the distribution of energy savings that will occur due to the variations in velocity profile that appear when a particular drive route is driven multiple times. Outlined in Table 4-2, this testing showed that use of the IPPC resulted in an average savings of 5% in the forward direction and an average of 6% savings in the reverse direction relative to baseline vehicle control. This also represents an additional 4% energy savings in the forward and reverse directions  when compared to using just the NMPC powertrain controller presented in [55]. The distribution of this savings relative to the baseline vehicle control is shown in Figure 4-10.

79

Table 4-2: MTUDC Energy Savings Using Integrated Predictive Powertrain Control.

|  | Number of Cycles | Average Energy Savings | 95% Confidence Interval |
|---|---|---|---|
| MTUDC | 12 | 4.8% | (3.5%, 6.0%) |
| RMTUDC | 10 | 5.7% | (4.6%, 6.8%) |
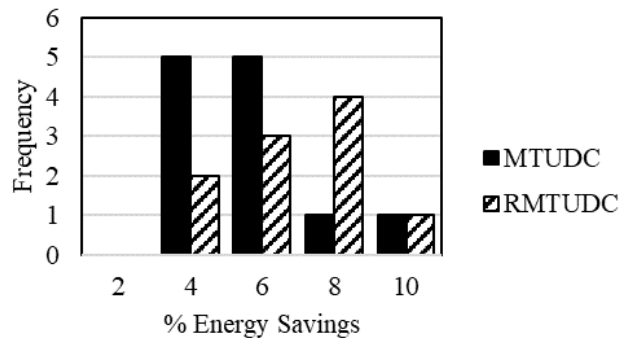


Figure 4-10: MTUDC energy savings distribution using Integrated Predictive Powertrain Control.

Figure 4-11 - Figure 4-15 present the areas where the IPPC provides an energy consumption reduction. Figure 4-11 and Figure 4-12 show the powertrain mode selected by the stock vehicle controller and the Optimal Mode Path Planning algorithm, respectively. Figure 4-13 shows the energy consumption of both the baseline vehicle and the IPPC controller as well as the delta energy consumed between the two controllers. What Figure 4-13 shows in conjunction with Figure 4-14, the elevation profile of the RMTUDC, is that the energy reductions occur during areas with significant elevation change such as

80

those between 0-500 seconds and 1000-2000 seconds. This is due to the ability of the IPPC to utilize predictions of future power demands to optimize the current control actions. For example, the knowledge of an extended period of downhill road grade between time 0-500 seconds allows the IPPC to make the decision to turn the engine off knowing that power demand will be low enough that engine use is unnecessary. This is all accomplished with no detriment to battery SOC as a consistent SOC level is able to be maintained through the whole cycle as shown in Figure 4-15.
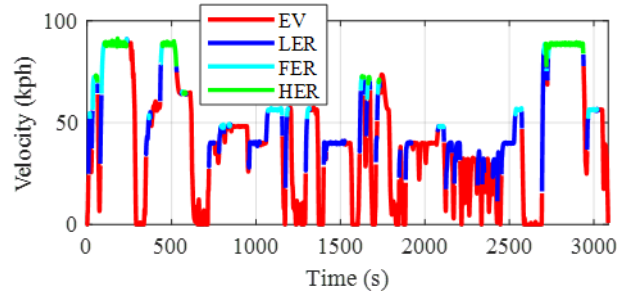


Figure 4-11: RMTUDC Vehicle Velocity and Baseline Operating Mode.
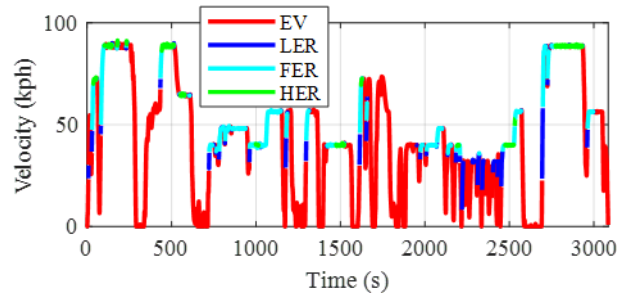


Figure 4-12: RMTUDC IPPC Velocity and Optimal Operating Mode.
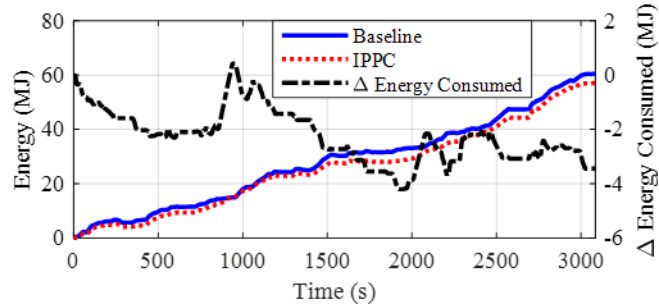
Figure 4-13: RMTUDC Baseline vs. IPPC Energy Consumption Comparison.
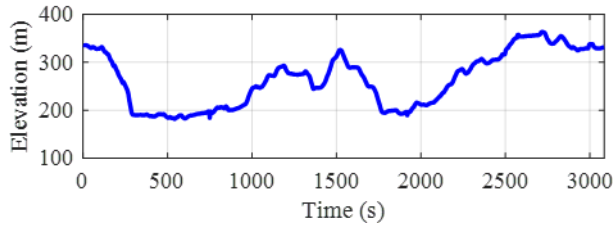


Figure 4-14: RMTUDC Elevation Profile.
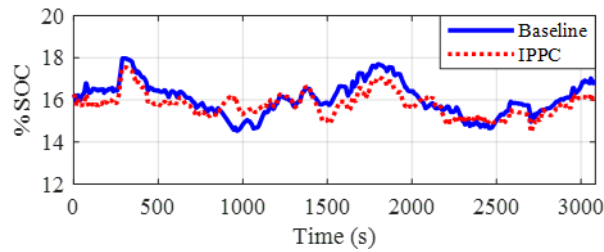


Figure 4-15: RMTUDC Baseline vs. IPPC SOC Comparison.

### 4.5.1.3   *Additional Real-World Drive Cycles*

In addition to the assessment of the IPPC over the standardized drive cycles and the MTUDC, the IPPC was evaluated over additional three real-world drive cycles. The first of the three cycles was logged by MTU on a rural route starting in Copper Harbor, MI and ending at the MTU campus in Houghton, MI as shown in Figure 4-16. This route contains

two distinctive scenarios designed to test the IPPC. The first scenario occurs between kilometers 0-25 of the drive cycle. This part of the route features repeated tight curves and small elevation changes that cause frequent changes in vehicle speed and power demand. The second distinct scenario of this route is highway speed driving with large elevation changes and occurs between kilometers 25-80. The second of the three cycles was logged by MTU in the Ann Arbor, MI area and is shown in Figure 4-17. This cycle proceeds through urban roads with heavy traffic frequent starts and stops and then finishes on a section of urban freeway. The last of the three cycles was collected by MTU at the American Center for Mobility (ACM) Smart City Test Center. Shown in Figure 4-18, the ACM route includes both urban boulevard sections with frequent starts and stops as well as high speed urban arterial sections of road.
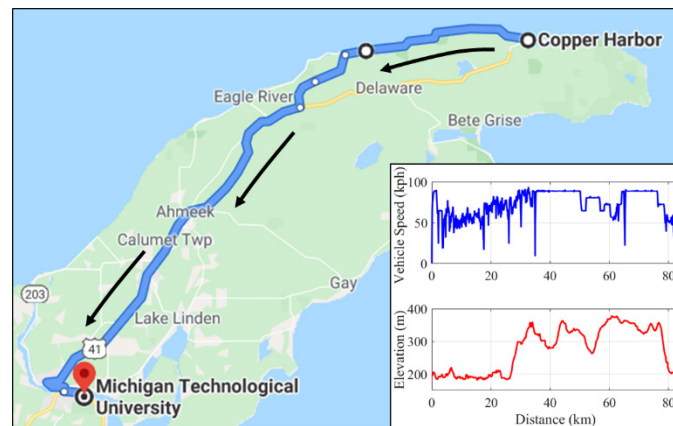


Figure 4-16: Copper Harbor to MTU route with velocity and elevation profiles versus drive cycle distance.
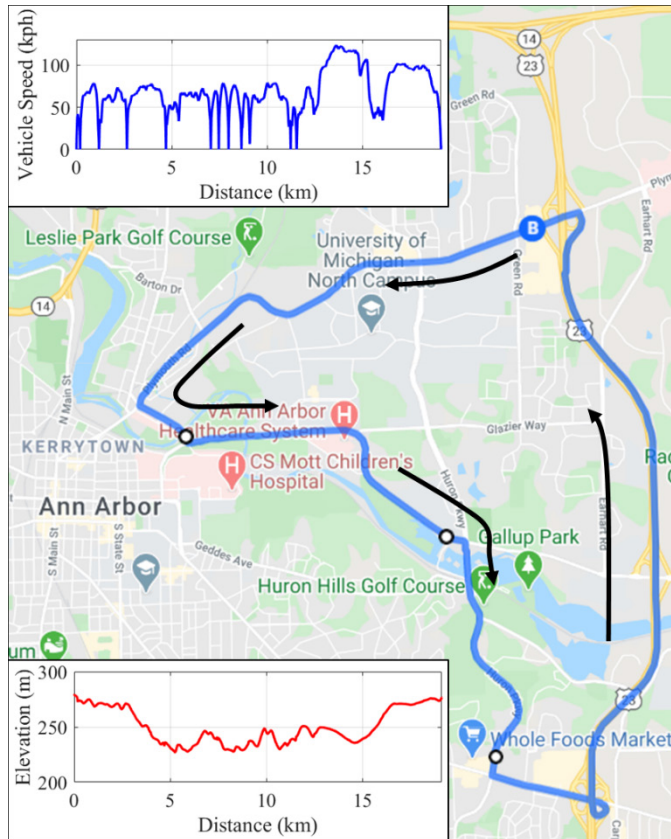
Figure 4-17: Ann Arbor Loop route with velocity and elevation profiles versus drive cycle distance.
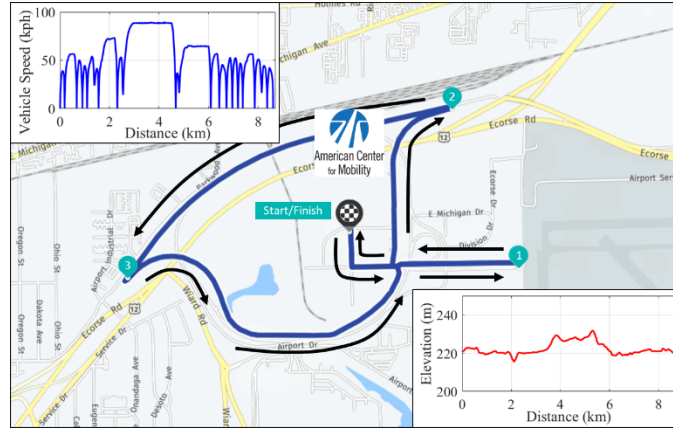
Figure 4-18: ACM Loop route with velocity and elevation profiles versus drive cycle distance.

In all three test scenarios, the IPPC provided an energy savings benefit over the baseline control of the vehicle. A 5.1% energy savings was observed on both the Copper Harbor to MTU and Ann Arbor Loop routes while a 2.9% reduction in energy consumption was observed on the ACM Loop. Full details are provided in Table 4-3. In the case of the Copper Harbor to MTU and Ann Arbor routes, utilizing the IPPC provided an additional 1.2% and 2.1% energy savings, respectively, when compared to using only NMPC powersplit control as presented in [55].

Table 4-3: Real World Drive Cycle Energy Savings Using Integrated Powertrain Control.

| Cycle | Baseline | Integrated Predictive Powertrain Control | Energy Savings |
|---|---|---|---|
| | | | |

| | | | |
|---|---|---|---|
| Copper Harbor to MTU | 126.015 MJ | 118.953 | 5.1% |
| Ann Arbor Loop | 35.116 MJ | 34.362 MJ | 5.1% |
| ACM Loop | 36.855 MJ | 36.325 MJ | 2.9% |

There are several specific areas of each drive cycle where the majority of the energy savings occurred. For example, in the case of the Copper Harbor to MTU route, 4% of the total 5% energy savings occurred in the first 2000 seconds of the drive route where the tight road curves and very frequent small elevation changes make for a transient velocity and torque demand profile. This 2000 seconds corresponds to the first 35 km of the drive cycle as shown in Figure 4-16. The predictive capability of the IPPC is able to better handle this scenario than stock controller by avoiding unnecessary engine starts and mode shifts thus producing an energy savings, as shown in Figure 4-19 - Figure 4-21. This is all accomplished while maintaining a consistent SOC level as shown in Figure 4-22.
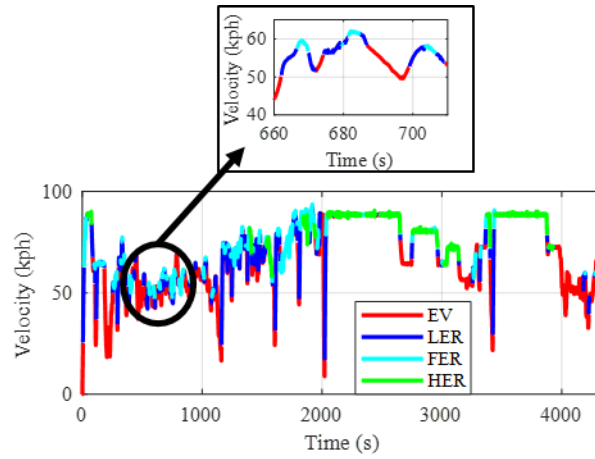
Figure 4-19: Copper Harbor to MTU Vehicle Velocity and Baseline Operating Mode.
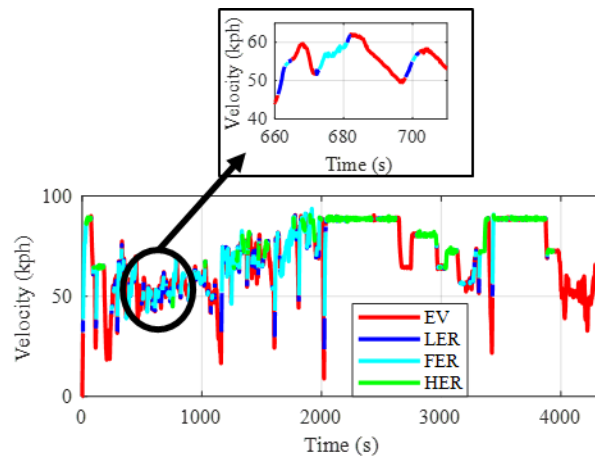


Figure 4-20: Copper Harbor to MTU Vehicle Velocity and IPPC Operating Mode.
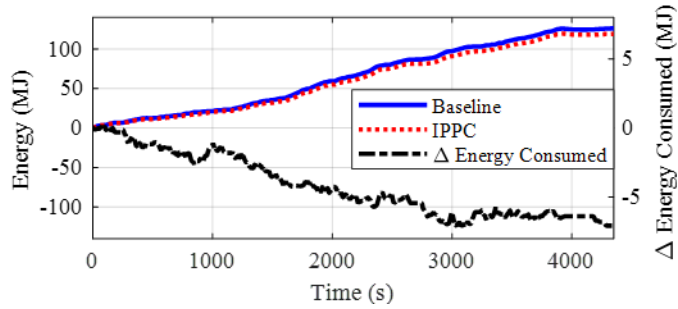
Figure 4-21: Copper Harbor to MTU Baseline vs. IPPC Energy Consumption
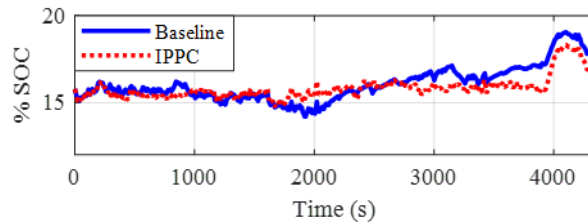
Comparison.



Figure 4-22: Copper Harbor to MTU Baseline vs. IPPC SOC Comparison. (SOC spike at

time 4000 seconds is due to an extended downhill section of road where regenerative

braking is in use).

### 4.5.2 Real-time Performance Assessment

An important aspect of the presented IPPC is the capability of the controller to run in real-time. To demonstrate this capability, the IPPC was tested on-road in an instrumented Chevrolet Volt. Shown in Figure 4-23, the MTU Chevrolet Volt instrumentation package consists of a multitude of sensors and communication devices. Sensors include forward facing LiDAR, GPS, voltage and current sensors, temperature sensors, and accelerometers. Also installed in the vehicle is a dedicated short-range communication (DSRC) device used

88

for vehicle-to-infrastructure (V2I) communication with traffic signals. A dSPACE MicroAutoBox (MAB) II prototyping ECU integrates the installed sensors and communication devices as well as interfaces with the vehicle's CAN bus and powertrain control modules for the purposes of logging real-time vehicle behavior as well for the use of real-time CAN signals as inputs to MTU-developed control algorithms. For further details on the MTU Chevrolet Volt instrumentation package, papers [51, 55] provide supplemental detail on the instrumentation system.



Figure 4-23: MTU Chevrolet Volt In-Vehicle Instrumentation Package.

The testing procedure is as follows. The IPPC is integrated into the test vehicle Simulink model where the controllers are interfaced with the test vehicle sensors, communication devices, and CAN bus. This model is then compiled into executable code and uploaded to the MAB II through dSPACE ControlDesk. Once on the MAB II, the IPPC is run parallel to the stock vehicle control during on-road testing. For energy consumption analysis, a similar process to that used for simulation assessment is used. The MTU energy estimation

tool is integrated onto the MAB II. In real-time, both the vehicle and IPPC control actions are fed into the energy estimation tool to provide a real-time look of the energy consumption of both controllers.

Real-time assessment of the IPPC was conducted on the first 8 km of the MTUDC. This section of the MTUDC was chosen as it has both a slow speed section with multiple stops and starts as well as a highway section with elevation change. In addition, all powertrain modes are utilized over this testing route. As the IPPC requires a prediction of future vehicle behavior, the MTU optimal velocity profiling algorithm was used to generate an optimal velocity profile for the test route. This profile was then used as the future reference input to the IPPC. Several important parameters of the test are included in Table 4-4.

Table 4-4: Real-time testing parameters.

| Parameter | Value |
|---|---|
| Prediction Horizon Length | 10 sec |
| Optimal Mode Path Planning Step Time | 1 sec |
| NMPC Powertrain Control Step Time | 0.2 sec |

Ten on-road tests of the IPPC were conducted. An average energy savings of 4.8% was achieved through the use of the IPPC. Using the IPPC adds an additional ~4% of energy savings when compared to using just the NMPC powertrain controller as was tested in [55]. As was the case with simulation testing, this energy savings value does account for any

differences in end SOC between the vehicle and IPPC by using equations (4-30) and (4-31).

Table 4-5 provides a testing results summary while a distribution of energy savings from

the 10 tests is presented in Figure 4-24.

Table 4-5: IPPC real-time testing energy savings.

|  | Number of Cycles | Average Energy Savings | 95% Confidence Interval |
|---|---|---|---|
| MTUDC (First 8 km) | 10 | 4.8% | (4.0%, 5.7%) |
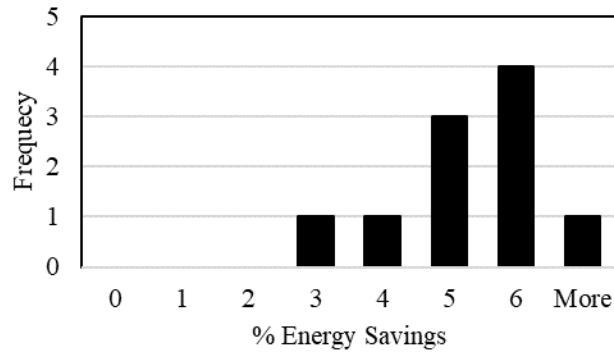


Figure 4-24: IPPC real-time testing energy savings distribution.

Energy savings, shown in Figure 4-25, are realized at several points along the drive cycle.

For example, at time 70, the IPPC is able to recognize the upcoming required deceleration

due to a stop sign. The IPPC, shown in Figure 4-27, is able to avoid the engine start that

the vehicle performs, shown in Figure 4-26, and thus save energy without an SOC impact.

Another area of energy savings occurs a time ~350 seconds. The road at this point

transitions into and extended segment of a slight downhill grade which results in a low

torque demand. The IPPC is able to recognize this low power demand for the near future, recognize that no major SOC penalty will be paid by turning off the engine, as shown in Figure 4-28, and transition to EV mode in order to save fuel.
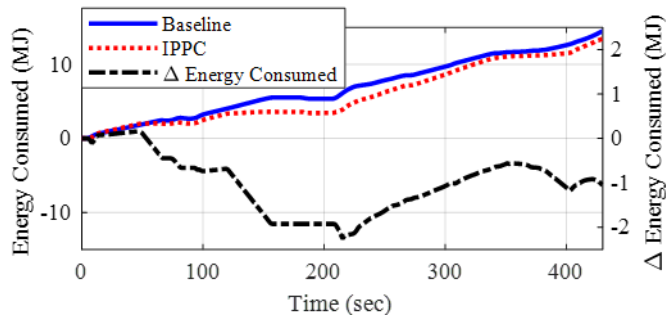


Figure 4-25: Real-time testing energy consumption comparison.
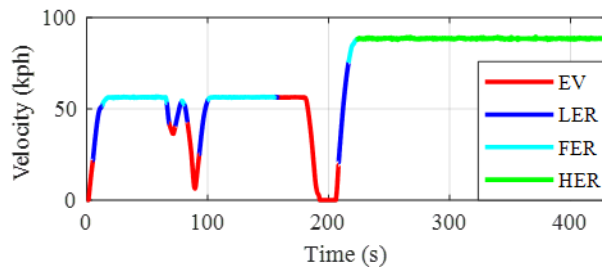


Figure 4-26: Real-time testing velocity and baseline mode.
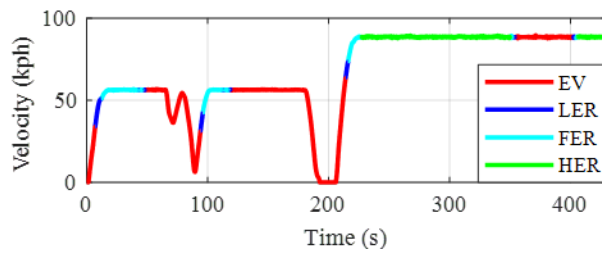


Figure 4-27: Real-time testing velocity and IPPC powertrain mode.
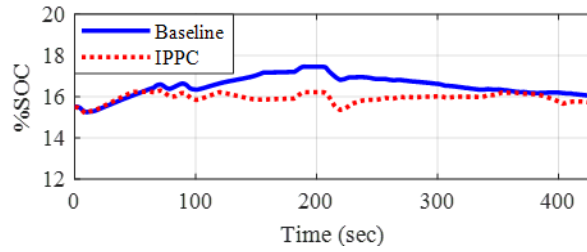
Figure 4-28: IPPC real-time testing SOC comparison.

A key metric of real-time controller performance is the computation requirements of the controller. The turnaround time of the NMPC powertrain control portion of the IPPC was already examined in [55], the computation time requirement of the Optimal Mode Path Planning (OMPP) algorithm needed to be assessed. Shown in Figure 4-29, the Optimal Mode Path Planning algorithm has an average turnaround time of ~15 ms. This is well below the one second controller step time of the OMPP making the OMPP suitable for real-time control.
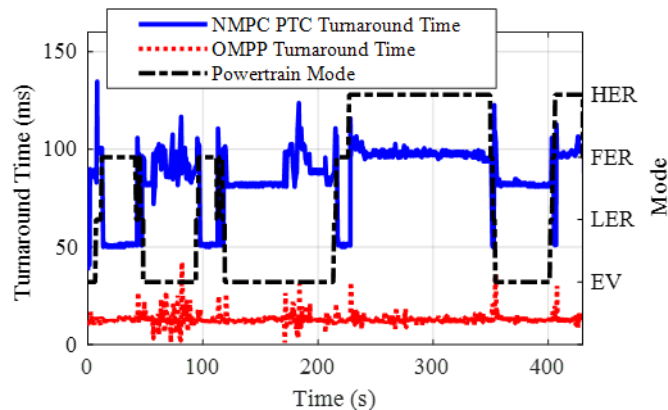


Figure 4-29: IPPC real-time testing turnaround time separated into NMPC powertrain control (NMPC PTC) and Optimal Mode Path Planning components.

## 4.6　Conclusion

This paper presents a real-time predictive control strategy for a comprehensive control of a multi-mode PHEV powertrain. An algorithm for optimal powertrain mode selection has been detailed that uses a prediction of future vehicle behavior to plan a best path of mode to minimize vehicle energy consumption. This algorithm was then integrated with an existing method that utilizes NMPC for powertrain powersplit management in order to create an Integrated Predictive Powertrain Controller. This integrated controller was thoroughly tested in both simulation and real-time environments. Simulation testing revealed that the presented controller can provide an 4-10% energy savings in standard drive cycles and a 3-7% energy savings over non-standard, real-world drive cycles. Real time testing of the IPPC was completed on an in-vehicle installed rapid prototyping ECU. On-road testing showed that the presented controller provides an energy savings of 4-6% over baseline vehicle control while achieving computational turnaround times suitable for real-time control. The next steps in the development of the proposed IPPC involve the full integration of the controller with the physical vehicle drive unit. While the IPPC has been tested on real-time controller hardware, the control output was not used to physically control the drive unit. Full integration of the IPPC with physical hardware would allow for a physical demonstration of the energy savings the IPPC has been analytically shown to provide in this paper.

# 5  Controller Performance Analysis

This chapter aims to expand the analysis of the performance of the NMPC Powertrain Controller presented in Chapter 3 and the Integrated Predictive Powertrain Controller presented in Chapter 4. Due to the page limits of the journal papers, analysis of the controller performance was limited. This chapter will examine the control decisions that were made by the NMPC PTC and IPPC that lead to the energy savings benefits they provide.

## 5.1  NMPC PTC Powersplit Analysis

This section will examine the powersplit decisions made by the NMPC PTC within each of the hybrid powertrain modes. Used for example is a section from one of the 20 forward direction MTUDC's presented in Chapter 3. Specifically, it is the first ~500 seconds of the recorded MTUDC presented in Figure 3-17. This section of the MTUDC was chosen for closer examination as all modes of the vehicle are used over the course of the cycle. Figure 5-1 shows velocity profile from the first ~500 seconds of the MTUDC along with the accompanying powertrain mode. Figure 5-2 presents the energy consumption of both the baseline vehicle and the NMPC PTC. Figure 5-3 gives the powersplit between the engine and motors of the baseline vehicle over the drive cycle segment while Figure 5-4 presents the powersplit between the engine and electric motors from the NMPC PTC. Finally, Figure 5-5 shows the SOC profile over this drive cycle segment from both the baseline vehicle and the NMPC PTC.

95
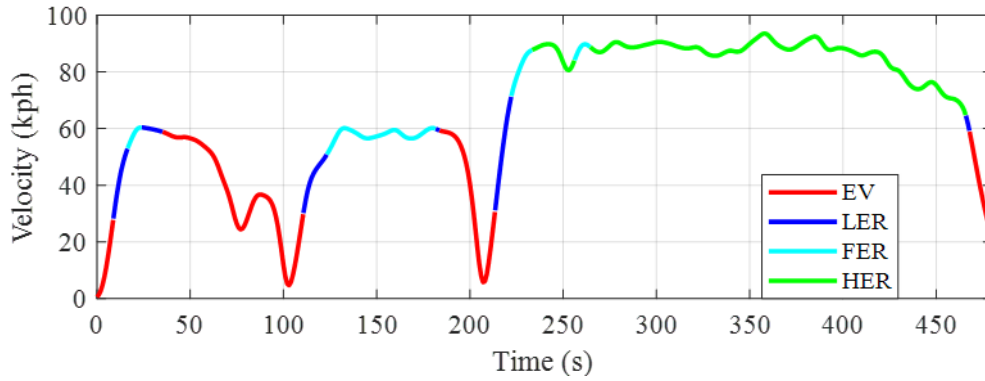
Figure 5-1: MTUDC Vehicle Velocity and Operating Mode.
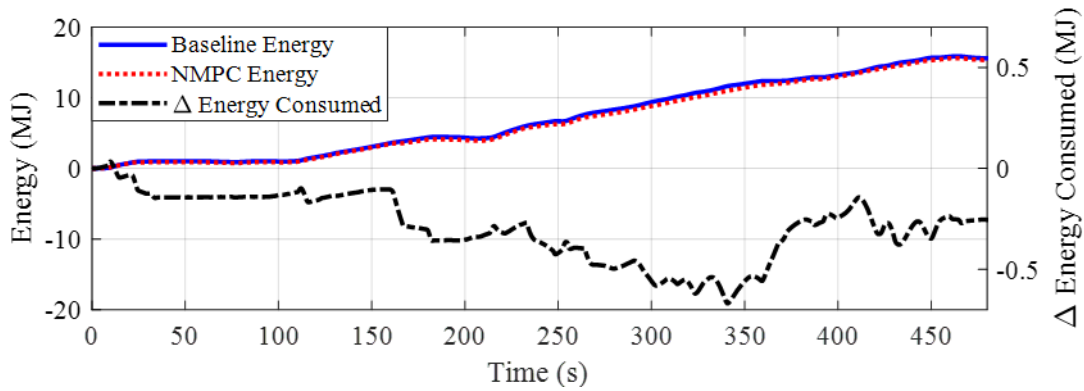


Figure 5-2: MTUDC Energy Consumption Comparison.
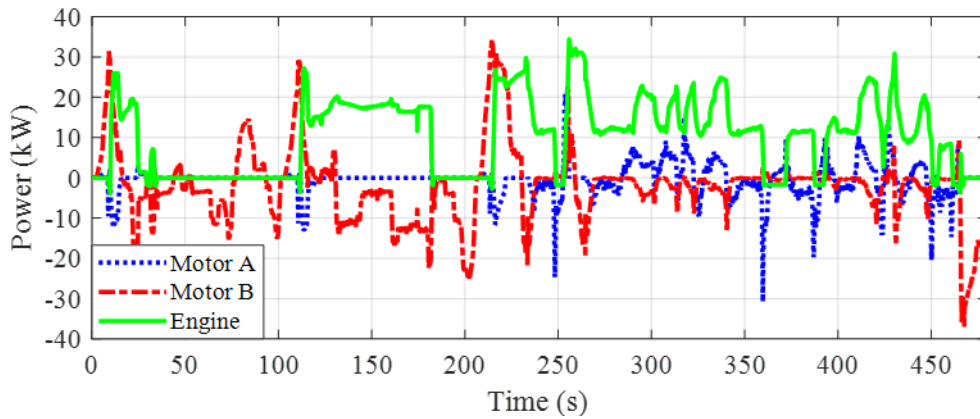


Figure 5-3: MTUDC Baseline Vehicle Powersplit.
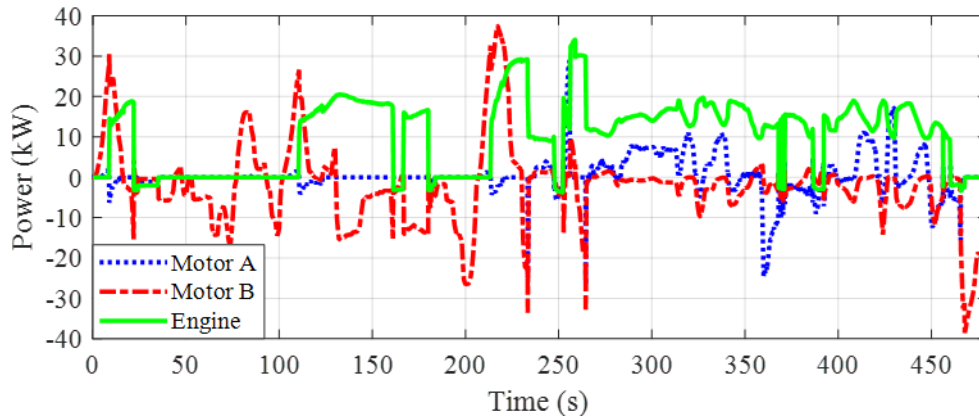
Figure 5-4: MTUDC NMPC PTC Powersplit.
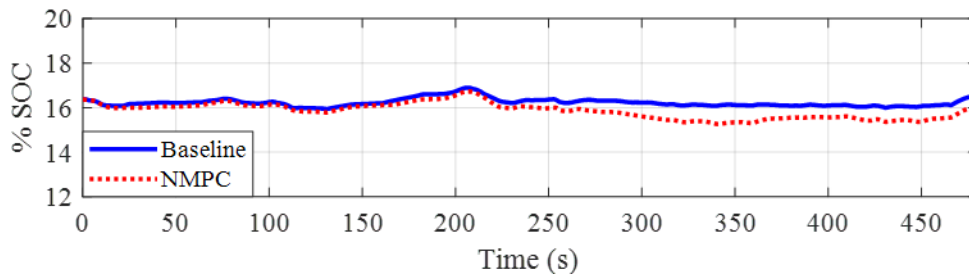


Figure 5-5: MTUDC SOC Comparison.

The first mode examined will be LER. As previously described, this mode is an input powersplit design and is utilized during high torque, low speed events such as vehicle launch. In this particular example, LER mode is utilized for propulsion three times during the three vehicle launches contained in this example at approximately times 10, 110 and 210 as can be seen in Figure 5-1. It was stated in Section 3.5.2 that the main place energy savings occur using the NMPC PTC is during these acceleration events due to an increase in electrical power usage and a decrease in engine power usage. By examining Figure 5-3 and Figure 5-4, one can see that the NMPC uses a lower power request from engine and increases the e-motor power request. This leads to a small overall energy savings in each

97

case that over the course of a drive cycle can add up to a non-insignificant savings. Due to the short duration of these events, there is minimal impact to SOC as can be seen in Figure 5-5.

The next mode examined will be FER, a parallel hybrid mode used during acceleration events and mid vehicle speeds. During periods of relatively steady state operation in FER mode, the powersplit decisions made by the baseline vehicle and the NMPC controller are largely similar. This is due to the limited optimization opportunity presented in the FER mode. Because engine speed is directly couple to the wheels and Motor A being grounded, the only variables to control are engine torque and Motor B torque. While there theoretically is an opportunity to optimize between these two variables, practically, a large optimization opportunity does not exist. This is due to there typically being a most efficient engine torque at which to operate at the vehicle-speed-constrained engine speed. This leads to very similar powersplit decisions between the baseline vehicle and the NMPC controller as can be observed in Figure 5-3 and Figure 5-4.

The final powersplit examined is that in HER mode. This is the mode that provides the most flexibility in operating point selection due to its compound power split design. However, because this mode of operation is used in low-torque demand, high speed operation like highway driving where vehicles are rather efficient at operating, the energy savings opportunities are limited. This being said, the HER implementation of the NMPC PTC does use a slightly different operating strategy than that of the baseline controller. For example, the NMPC PTC maintains a narrower window of engine power operation when

compared to the baseline control; however, the mean engine power output over the segment remains roughly equivalent as can be observed in Figure 5-3 and Figure 5-4. The end result for HER operation over this segment is an equivalent energy consumption when using baseline control and NMPC control even with accounting for the slight difference in end SOC.

## 5.2   OMPP Mode Selection Analysis

This section will examine the mode selections the OMPP algorithm makes with a specific examination of how well the modes chosen along a prediction horizon align with the eventual commanded mode. This is done in order to show that predicted future modes are accurately influencing the current commanded mode. The cycle studied in this section will be the Copper Harbor to MTU cycle that was examined in Section 4.5.1.3. This was chosen for examination due to the variation in vehicle speed and elevation that presents conditions ideal for the OMPP to improve upon the mode selection decisions made by the vehicle. Figure 5-6 provides the velocity and mode profile of the baseline vehicle for a selected segment of the Copper Harbor to MTU cycle. Figure 5-7 gives the velocity and mode profile of the IPPC for the selected segment. The elevation profile of the selected segment is shown Figure 5-8. Finally, Table 5-1 presents the mode prediction made by the OMPP at several time points located within the selected segment.
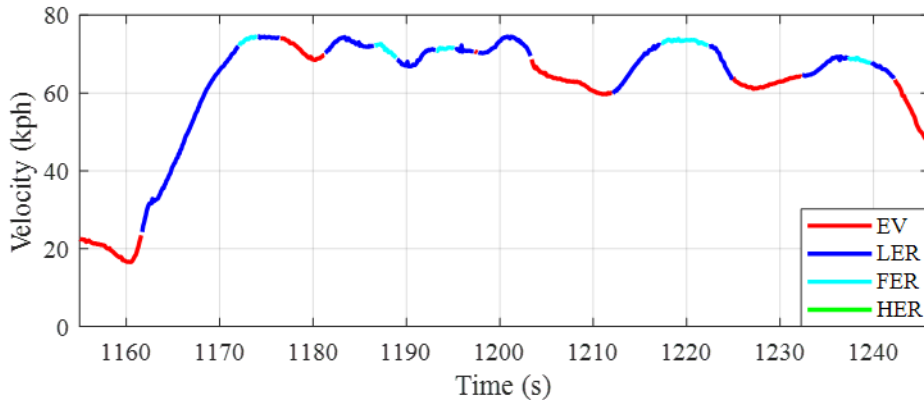
Figure 5-6: Copper Harbor to MTU Vehicle Velocity and Baseline Operating Mode.
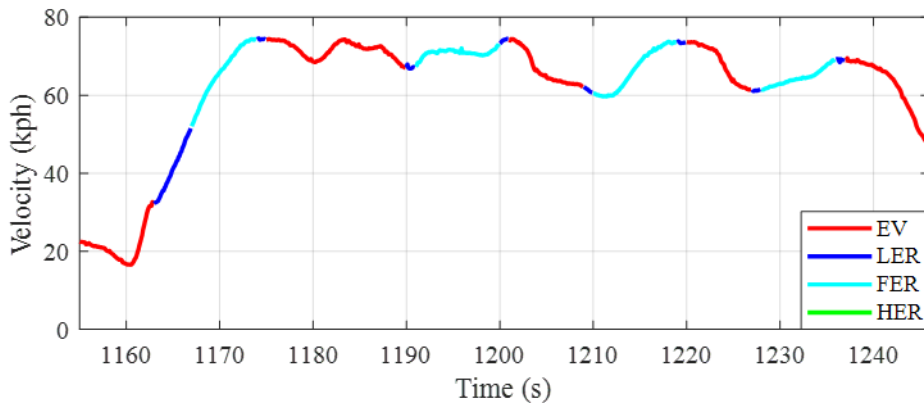


Figure 5-7: Copper Harbor to MTU Vehicle Velocity and IPPC Operating Mode.
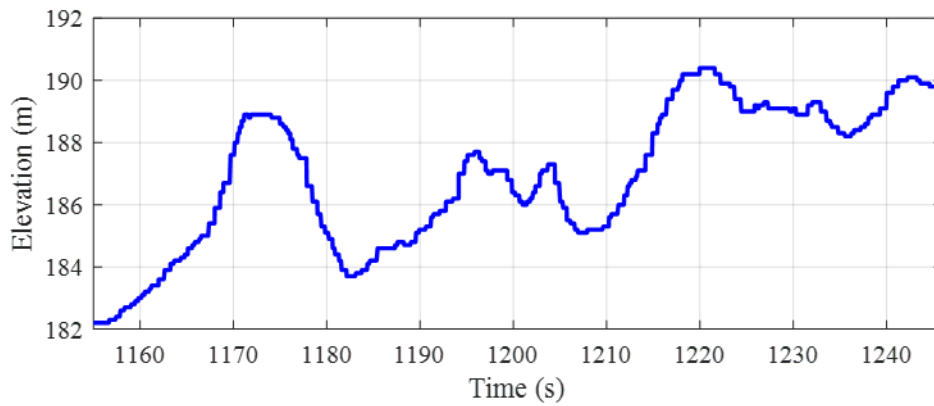


Figure 5-8: Copper Harbor to MTU Elevation Profile.

100

Table 5-1: Copper Harbor to MTU Mode Selection Predictions.

| Time N | N | N+1 | N+2 | N+3 | N+4 | N+5 | N+6 | N+7 | N+8 | N+9 |
|--------|-----|-----|-----|-----|-----|-----|-----|-----|-----|-----|
| 1170 | FER | FER | FER | FER | LER | EV | EV | EV | EV | EV |
| 1185 | EV | EV | EV | EV | EV | LER | FER | FER | FER | FER |
| 1195 | FER | FER | FER | FER | FER | LER | EV | EV | EV | EV |
| 1220 | EV | EV | EV | EV | EV | EV | LER | FER | FER | FER |

Table 5-1 provides the optimal mode predictions for several selected time points. The mode listed at time N is the command issued by the controller. The modes listed from times N+1 to N+9 are the modes predicted at time N for the remainder of the prediction horizon. The purpose of this example is to show that the control action predictions made by the OMPP algorithm properly account for changes in driving conditions, such as velocity or elevation changes, that are observed within the prediction horizon.

The first example examined occurs at time 1170. At this time, the vehicle is performing an acceleration and is in a current state of FER mode. The OMPP algorithm recognizes that the vehicle will be accelerating for the next several seconds and therefore, FER mode is chosen as the commanded mode and predicted as the best for the first four seconds of the prediction horizon. It is at this point in the prediction horizon, time 1174, that the OMPP algorithm recognizes that the vehicle speed levels off and begins to decrease as shown in Figure 5-7. In addition, it is at this point that elevation begins to decrease, shown in Figure 5-8. These two factors lead to a decreased power demand which the OMPP recognizes and predicts a shift to LER at time 1174 and EV mode for the remainder of the prediction

horizon. This particular prediction ends up mirroring the actual control actions issued as can be observed in Figure 5-7. This is largely due to the continuation of the downhill road grade, something that is captured within the prediction horizon of subsequent control steps. This may not have been the case if, for example, a power demand increase, due to a vehicle speed or elevation increase, came within the view of subsequent prediction horizons. In this case, the modes predicted at 1170 for the next 10 seconds may not have matched the mode command at 1178 if an increased power demand began at time 1181. However, with sufficient prediction horizon length, this issue can be avoided.

Three more mode selection predictions made at times 1185, 1195, and 1220 in the drive cycle. While these will not be examined in-depth like the predictions made at time 1170, these other three examples follow a similar pattern. In each case, some event, either a speed or elevation change, occurs in the middle of the prediction horizon that provides the possibility for a mode change. Each time, the OMPP responds by predicting a mode change in response to this event. In all three cases the modes predicted by the OMPP end up mirroring the eventual commanded mode. These four examples demonstrate an important point about the OMPP algorithm. The OMPP algorithm does in fact respond to disturbances that occur within the prediction horizon such as an elevation or speed change. This ability to predict control actions that respond to these events leads to the issuance of control actions at the current control step that, over the course of a drive cycle, reduce overall vehicle energy consumption.

## 5.3  OMPP Automated Weight Factor Selection Performance

Presented in Chapter 4.3 is a method for the automatic selection of the weighting factors used in the Optimal Mode Path Planning Algorithm cost function. This section will examine the performance and implementation benefits of the automated selection process when compared to the manual selection of weighting factor. The simulation results, presented in Chapter 4, of the IPPC controller that utilize the automated weight factor selection process are compared against simulation results of the same drive cycles that utilize manually tuned weighting factors for the OMPP cost function.

The simulation and analysis process of the IPPC controller using the manually tuned OMPP cost function is identical to that as presented in Section 4.5.1 with the only change being the use of manually tuned weighting factors for the OMPP cost function. Simulations of the IPPC were conducted using the Simulink implementation of the IPPC, with manual OMPP weighting, and the MTU NEXTCAR developed model of the Volt. The simulations were conducted over the 28 different drive cycles examined in Section 4.5.1, which include a mix of standard drive cycles, MTU developed drive cycles, and real-world drive cycles. In order to determine energy consumption of the baseline of the IPPC control actions, the control actions of each are fed through the MTU energy consumption and SOC prediction tools in order to find the final SOC and energy consumption values. Energy savings are then computed using (5-1) and (5-2) in order to account for any end of cycle SOC differences between the baseline and IPPC results.

$$Energy\ Savings = \left(\frac{Energy_{Baseline} - Energy_{IPPC} + Energy_{\Delta SOC}}{Energy_{Baseline}}\right) \quad (5\text{-}1)$$

$$Energy_{\Delta SOC} = \left(SOC_{End,IPPC} - SOC_{End,Baseline}\right) * Q_{Battery} \quad (5\text{-}2)$$

As with the automated weight procedure, the manual weighting procedure utilizes normalizing terms to convert the SOC and mode shift penalty terms to equivalent grams of fuel consumed. These terms, $\lambda_{SOC}$ and $\lambda_{mode\ shift\ penalty}$, are defined in equations (4-26) and (4-27). In order to highlight the cycle to cycle adaptability of the automatic tuning method when compared to the manual method, the same values of $\beta$ and $\gamma$ were utilized for all drive cycles. The values used for $\beta$ and $\gamma$ were determined through a manual search process using the forward MTUDC cycle and were selected based on the values that maximize energy savings while maintaining SOC levels.

Energy savings results for the manual weight factor and automatic weight factor selection for the OMPP algorithm are presented in Table 5-2. The use of the automated weight factor selection procedure offers equivalent to improved performance when it comes to energy savings. The main reason for this is the adaptability of the weight factor terms to the drive cycle. For example, in the case of the MTUDC, there is no energy savings benefit offered by using the automated method. This is because the manual weight factors were tuned using this cycle resulting in the maximum possible energy savings. However, when other driving cycles are encountered, the manually selected weight factors are no longer optimal as is the case in RMTUDC. These scenarios will be broken down in detail for the $\beta$ and $\gamma$ terms in Sections 5.3.1 and 5.3.2.

Table 5-2: Manual vs. Automatic OMPP Cost Function Weight Factor Selection

| Cycle | Manual Weight Factor Energy Savings | Automated Weighting Factor Energy Savings | Improvement |
|---|---|---|---|
| US06 | -0.3% | 3.7% | 4.0% |
| UDDS | 9.2% | 9.8% | 0.6% |
| HWFET | 1.2% | 5.7% | 4.5% |
| MTUDC (12 Cycle Average) | 4.9% | 4.8% | -0.1% |
| RMTUDC (10 Cycle Average) | 4.5% | 5.7% | 1.2% |
| Copper Harbor to MTU | 3.7% | 5.1% | 1.4% |
| Ann Arbor Loop | 4.8% | 5.1% | 0.3% |
| ACM Loop | 3.7% | 2.9% | -0.8% |

### 5.3.1 SOC Weight Factor Analysis

Presented in Figure 5-9 through Figure 5-12 is a comparison between the use of the manually tuned SOC weight factor and the automatically tuned SOC weight factor over

the forward direction MTUDC, the cycle used for the manual tuning of the SOC weight factor. Note that a single cycle is examined in these figures and that the MTUDC energy values in Table 5-2 are an average of all MTUDC cycles tested. One can observe in Figure 5-9 and Figure 5-10 that the resulting mode selected by the OMPP is largely identical between the manual and automatically weight cost functions. As a result of this, the subsequent SOC trajectory over the course of the drive cycle for the two weight factor methods is near identical, as shown in Figure 5-11. Figure 5-12 shows the change of the SOC weight factor, $\beta$, over the course of the drive cycle while Figure 5-13 gives the energy consumption of the two methods over the cycle. From this drive cycle, one could conclude that, despite the automatically weighted value of $\beta$ adjusting itself to the current SOC, the automatically weighted term has limited impact when compared to the manually weighted term as the SOC trajectory, shown in Figure 5-11, remain largely the same for the two methods for this particular drive cycle. However, the next drive cycle examined will show situation where the automatically weighted SOC term does provide benefit for SOC maintenance.

Figure 5-9: MTUDC Vehicle Velocity and Optimal Operating Mode with Manual Weighting ($\alpha = 1, \beta = 2.5, \gamma = 2$).



Figure 5-10: MTUDC Vehicle Velocity and Optimal Operating Mode with Automatic Weighting.
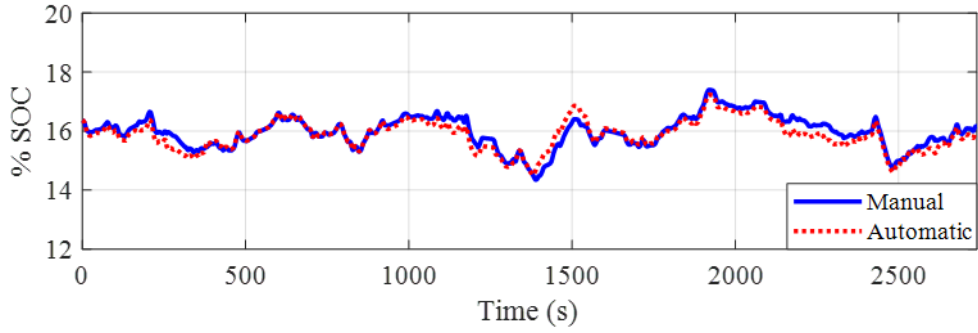
Figure 5-11: MTUDC SOC Comparison Between Manual and Automatic Weighting.
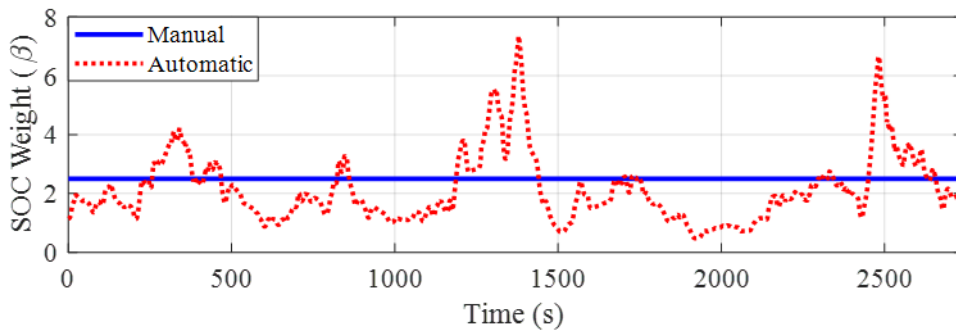


Figure 5-12: MTUDC SOC Weighting Factor Comparison Between Manual and Automatic Weighting.
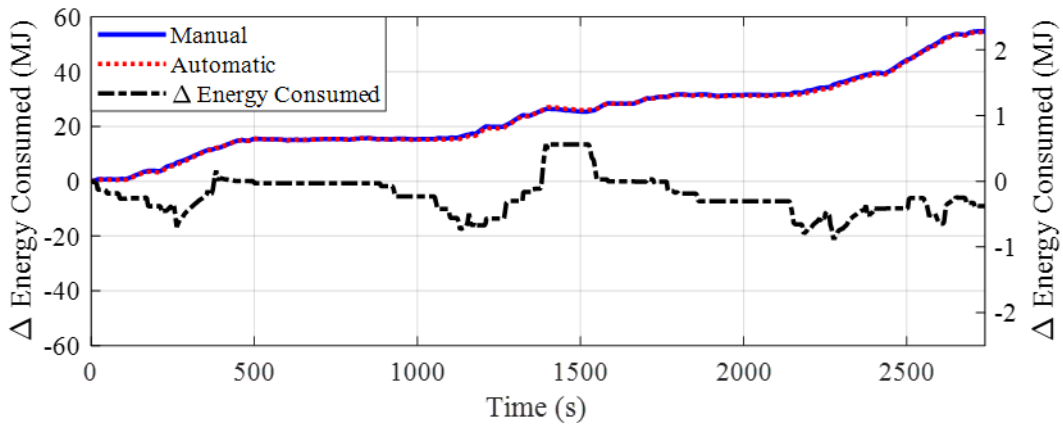


Figure 5-13: MTUDC Energy Consumption for Manual and Automatic Weighting.

108

The next cycle examined is the reverse MTUDC or RMTUDC. The performance of the OMPP will be examined when using the manually weighted SOC cost term and the automatically weighted term. Note that a single cycle is examined in these figures and that the MTUDC energy values in Table 5-2 are an average of all MTUDC cycles tested. Figure 5-14 and Figure 5-15 shown the velocity and mode selection profiles for the manually weighted and automatically weighted cost functions, respectively. Once again, as in the case with the forward MTUDC example, the modes selected for the RMTUDC remain largely the same for both weighting methods with one critical exception. From time 2200-2500, an uphill start/stop section of the drive cycle, the manually weighted controller responds by solely commanding EV mode which leads to a 2% drop in SOC as shown in Figure 5-16. This represents a significant amount of SOC depletion for the particular vehicle under study especially in the battery depleted charge-sustaining under which the vehicle is operating. In contrast, the automatically weighted controller increases the SOC weight over this section of the drive cycle as shown in Figure 5-17. This results in the selection of LER and FER hybrid modes during this portion of the drive cycle which act to maintain an acceptable SOC level. In terms of energy consumption, the energy saved during this section of the drive cycle by the manually weighted controller by not using the engine is cancelled out due to the extra fuel spent in the subsequent section of the drive cycle in order to recover the SOC level to normal operating levels.

Figure 5-14: RMTUDC Vehicle Velocity and Optimal Operating Mode with Manual Weighting ($\alpha = 1, \beta = 2.5, \gamma = 2$).



Figure 5-15: RMTUDC Vehicle Velocity and Optimal Operating Mode with Automatic Weighting.
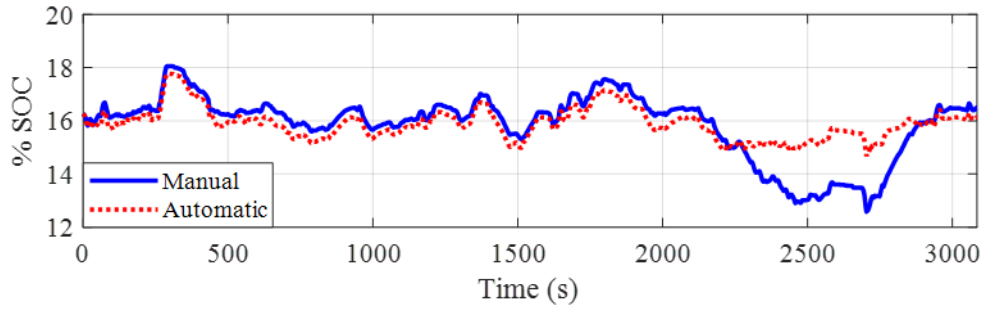
Figure 5-16: RMTUDC SOC Comparison Between Manual and Automatic Weighting.
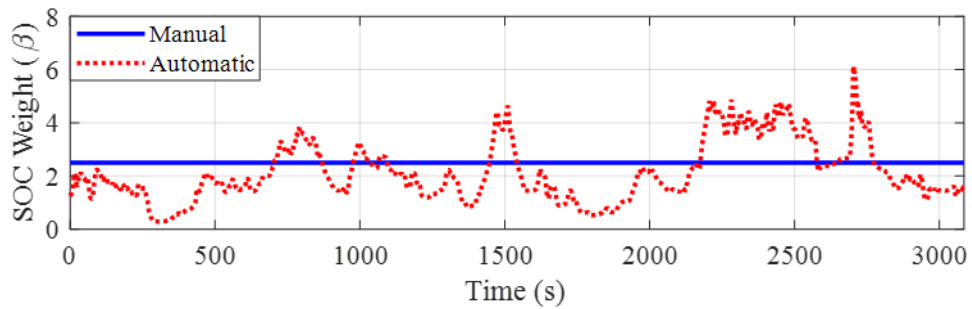


Figure 5-17: RMTUDC SOC Weighting Factor Comparison Between Manual and Automatic Weighting.
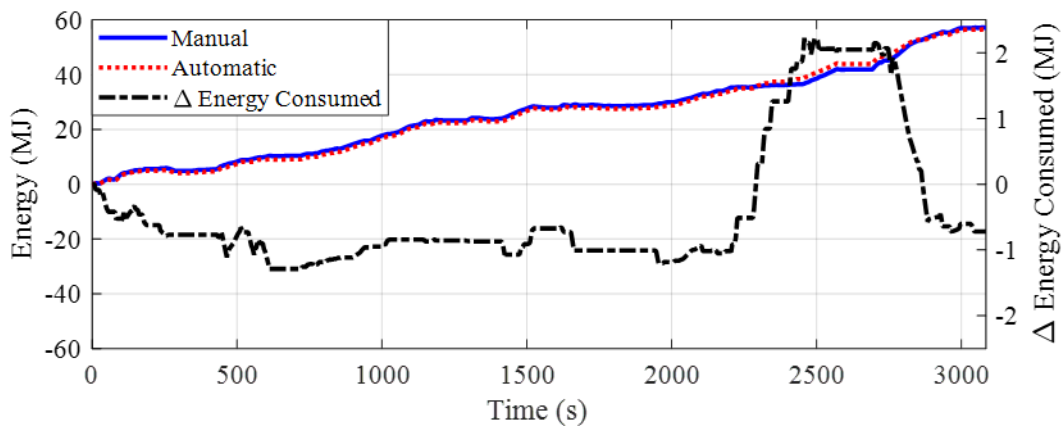


Figure 5-18: RMTUDC Energy Consumption for Manual and Automatic Weighting.

### 5.3.2 Mode Shifting Weight Factor Analysis

The impact of the mode shifting weight factor will be examined using a situation from the MTU drive cycle. Presented in Figure 5-19 through Figure 5-23 is a comparison between the use of the manually tuned mode shift weight factor and the automatically tuned mode shift weight factor over the forward direction MTUDC. Specifically, the portion of the drive cycle from time 2670 to 2770 will be examined. As can be seen in Figure 5-21, the manually weighted controller commands frequent mode shifts. This is a result of the different modes of the vehicle having similar residing costs in this particular driving scenario. The manually weighted controller's decision to change mode at each controller execution step, such as between time 2710 and 2720, is not practical as the drive unit cannot physically perform the changes this quickly. The automatically weighted controller, shown in Figure 5-22, eliminates this rapid shifting behavior and produces a much more reasonable shift strategy that is practical for the physical vehicle to perform. Shown in Figure 5-23, the automated weight factor increases in value in response to an increasing amount of predicted mode shifts. As a result, this rapid shifting behavior observed in the use of the manually weighted controller is eliminated and practical mode shift strategy is produced.
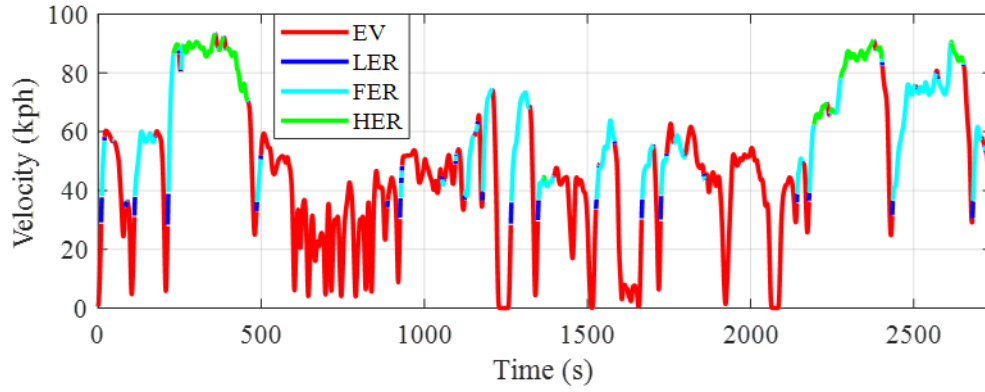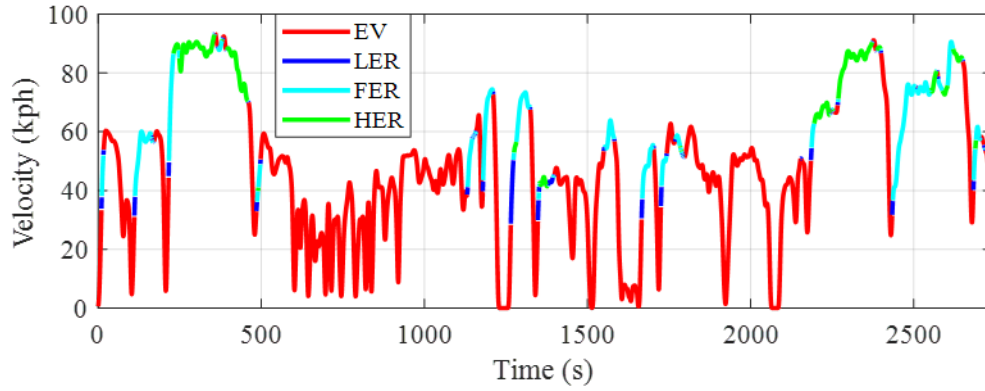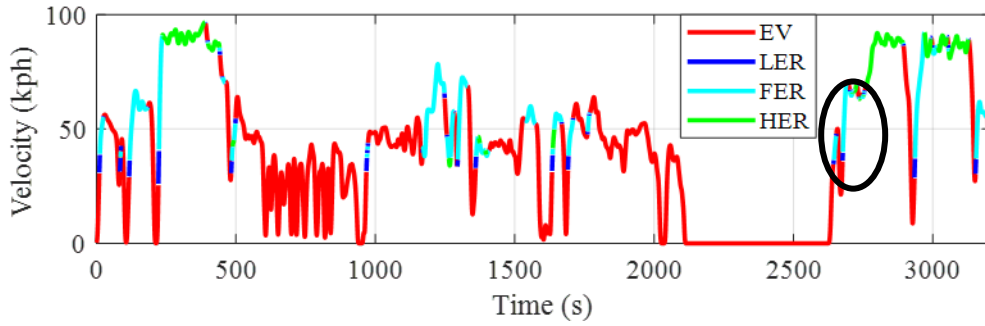
Figure 5-19: MTUDC Vehicle Velocity and Optimal Operating Mode with Manual Weighting ($\alpha = 1, \beta = 2.5, \gamma = 2$).
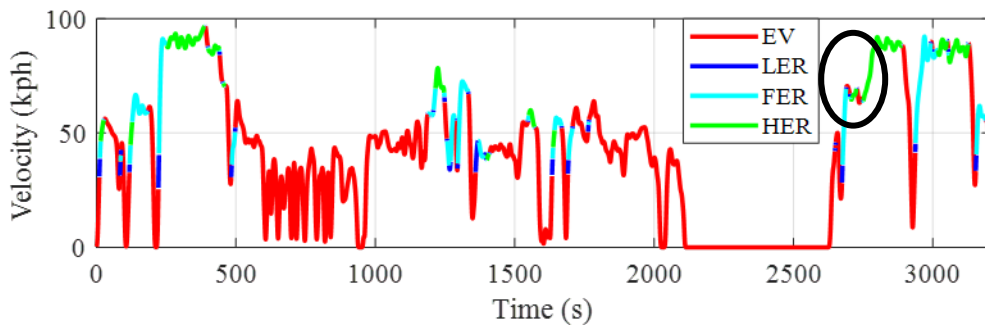


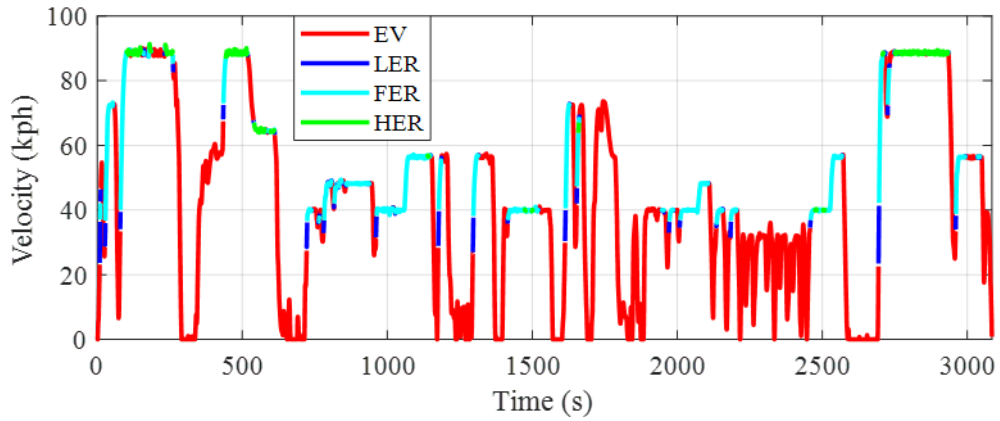Figure 5-20: MTUDC Vehicle Velocity and Optimal Operating Mode with Automatic Weighting.
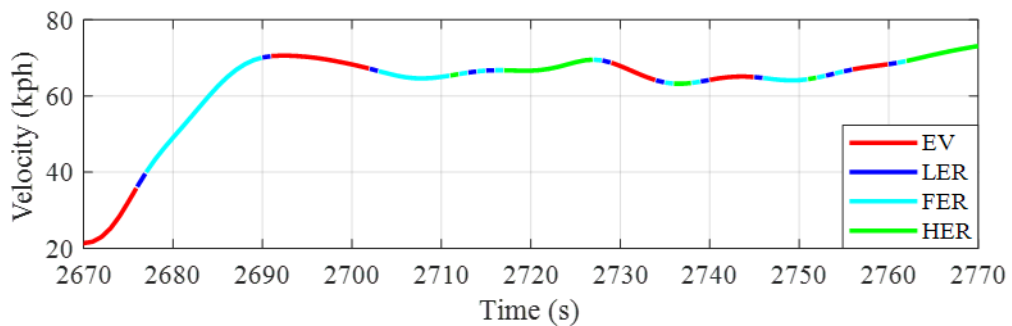


Figure 5-21: MTUDC Vehicle Velocity and Optimal Operating Mode with Manual Weighting ($\alpha = 1, \beta = 2.5, \gamma = 2$).

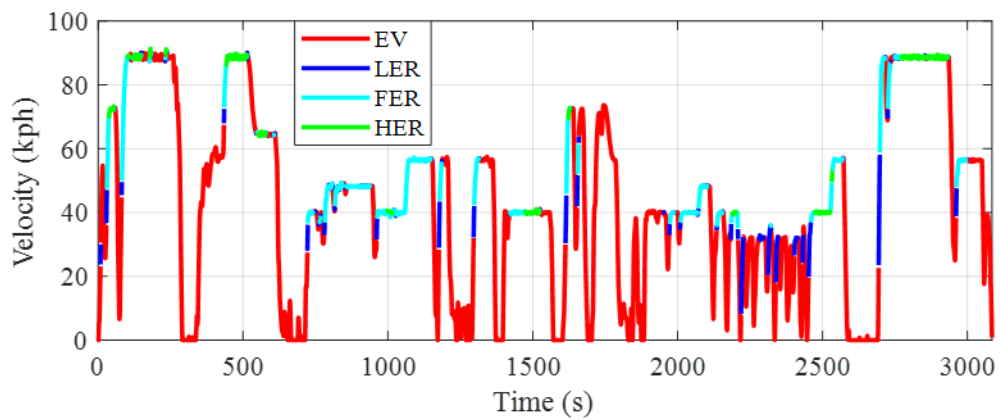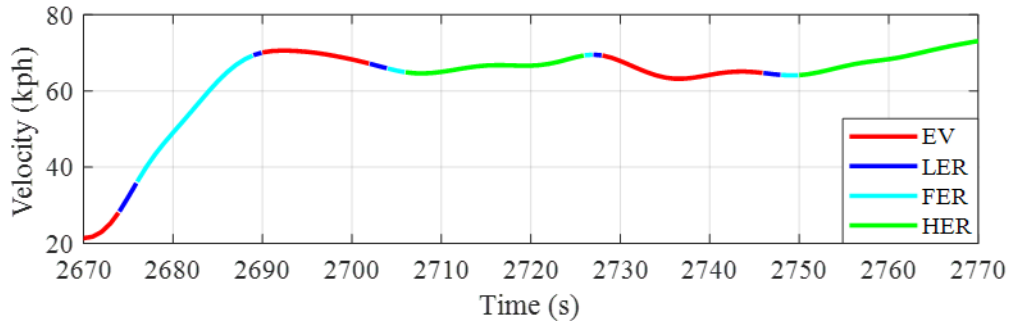Figure 5-22: MTUDC Vehicle Velocity and Optimal Operating Mode with Automatic Weighting.
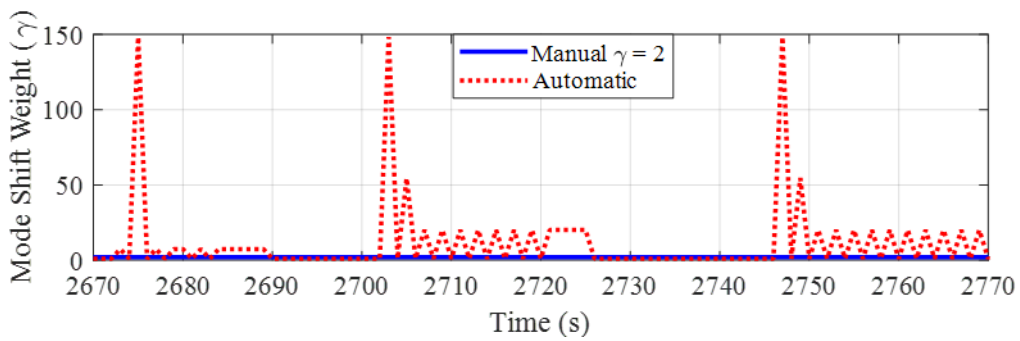


Figure 5-23: MTUDC Mode Shifting Weighting Factor Comparison Between Manual and Automatic Weighting.

114

# 6 Predictive Control Application Across xEV Powertrain Architectures

So far, this dissertation has been focused on predictive powertrain control technologies specifically for one vehicle platform, the 2nd generation Chevrolet Volt. However, while tested on one specific vehicle platform, the predictive powertrain control methods presented in this dissertation are not valid only for this one vehicle. This chapter will discuss how the predictive powertrain control methods presented in this dissertation could be applied to other vehicle platforms in order to show that this research has future relevance.

The multi-mode design of the 2nd generation Chevrolet Volt utilized three separate hybrid architectures. Included in the Volt drive unit are an input powersplit hybrid mode, a parallel hybrid mode, and a compound powersplit mode. Because predictive controllers were developed for each of these three modes, the conclusions drawn for this vehicle can be extrapolated to other vehicle platforms, both single-mode or multi-mode, that utilize one of the architectures that are present in the Volt. This chapter will highlight cases where the controllers developed in this work could apply to other platforms in order to highlight that this work is not constrained to one vehicle platform and has potential future applications.

## 6.1   NMPC PTC Application to Other Vehicle Platforms

Multiple different vehicle platforms utilizing a powersplit hybrid architecture are available on the market today. One such example is the Toyota Hybrid System (THS), the underlying architecture of popular vehicle models such as the Prius [81]. Variations of the THS underpins an array of models available from Toyota in the US market [81-83]. A second example is the eFlite dedicated hybrid transmission utilized in the FCA Chrysler Pacifica Hybrid. Two implementations of THS II and the Pacifica will be briefly discussed in order to convey how the IPPC controller presented in this dissertation could apply to different vehicle platforms. The first implementation examined will be the front-wheel drive (FWD)version utilized in vehicles such as the Prius and Camry and the eFlite used in the Pacifica. The second implementation studied will be the all-wheel drive (AWD) version utilized in vehicle such as the RAV4 Hybrid and the Highlander Hybrid.

While independent designs, the THS and the eFlite utilize a similar architecture. The FWD implementation of the THS as well as the eFlite is shown in Figure 6-1. The generator is connected to the sun gear of the planetary gearset. The engine is connected to the planet carrier. Some implementations of the THS connect the engine to the planet carrier through a one-way clutch in order to enable dual motor operation when in EV only operation. The main traction motor is connected to the ring gear through a parallel shaft reduction gear. Finally, the output of the system is connected to the ring gear [83, 84].
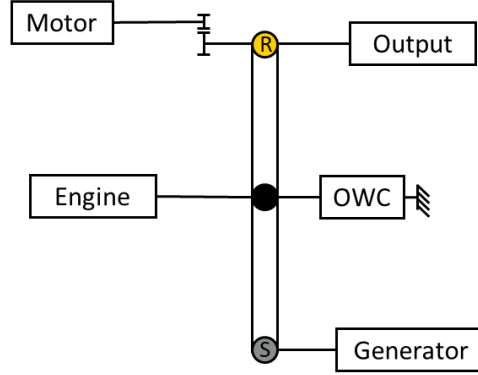
Figure 6-1: Toyota Hybrid System and FCA eFlite Architecture.

As the THS and eFlite are a power split architecture similar to the LER mode in the $2^{nd}$ generation Chevrolet Volt, a control implementation of the NMPC PTC similar to that used for LER mode can be used. The governing torque and speed equations of the eFlite and THS are given in equation (6-1). Upon review of these equations, it can be seen that the same control vector used for the LER mode in the Volt can be applied to the eFlite and THS. By controlling engine speed, engine torque, and traction motor torque, the torque split between the engine and motor can be optimized as well as the engine operating point. The control vector is shown in equation (6-2).

$$\begin{cases} T_{Out} = \left(\frac{R}{R+S}\right) * T_{Engine} + GR_{Motor} * T_{Motor} \\ T_{Generator} = \left(\frac{S}{R}\right) * T_{Out} \\ \omega_{Generator} = \left(\frac{R+S}{S}\right) * \omega_{Engine} + \left(\frac{R}{S}\right) * \omega_{Out} \\ \omega_{Front\ Motor} = GR_{Motor} * \omega_{Out} \end{cases} \quad (6\text{-}1)$$

$$U = \begin{bmatrix} \omega_{Engine} \\ T_{Engine} \\ T_{Motor,Front} \end{bmatrix} \quad (6\text{-}2)$$

117

The AWD implementation of the THS utilizes the same front axle drive unit, with model specific alterations, as the FWD implementation of the THS. However, an additional e-motor is added to the rear axle for AWD capability [82]. The layout of this architecture is shown in Figure 6-2.
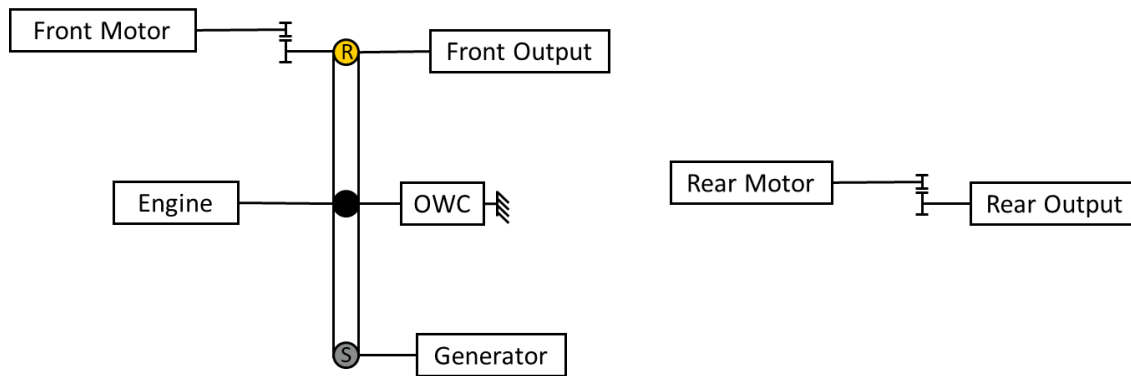


Figure 6-2: Toyota Hybrid System AWD Architecture.

This additional motor slightly alters the NMPC PTC implementation. The governing torque and speed equations, given in equation (6-3), remain largely unchanged with the only modification being the addition of the rear motor into the computation of total output torque. Because of the addition of the extra motor, the control vector needs modification as well. Shown in equation (6-4), rear motor torque needs to be added to the control vector. The addition of rear motor torque as a control variable provides even further opportunity to optimize the torque split of the powertrain for minimal energy consumption. Furthermore, the potential exists to utilize the NMPC PTC not only for energy consumption considerations, but also for drivability management of the vehicle. The addition of a motor to the rear axle, completely independent of the front axle, provides a mechanism to impact

vehicle handling through powertrain control. By including predicted vehicle behavior and future road conditions in the determination of a torque split, the possibility exists to adapt the torque split of the vehicle proactively rather than reactively in order to maximize traction and stability.

$$\begin{cases} T_{Out} = \left(\dfrac{R}{R+S}\right) * T_{Engine} + GR_{Front\ Motor} * T_{Front\ Motor} \\ \qquad\qquad + GR_{Rear\ Motor} * T_{Rear\ Motor} \\ \qquad T_{Generator} = \left(\dfrac{S}{R}\right) * T_{Out} \\ \quad \omega_{Generator} = \left(\dfrac{R+S}{S}\right) * \omega_{Engine} + \left(\dfrac{R}{S}\right) * \omega_{Out} \\ \qquad \omega_{Front\ Motor} = GR_{Front\ Motor} * \omega_{Out} \\ \qquad \omega_{Rear\ Motor} = GR_{Rear\ Motor} * \omega_{Out} \end{cases} \qquad (6\text{-}3)$$

$$U_{AWD} = \begin{bmatrix} \omega_{Engine} \\ T_{Engine} \\ T_{Front\ Motor} \\ T_{Rear\ Motor} \end{bmatrix} \qquad (6\text{-}4)$$

## 6.2 Optimal Mode Path Planning Applications to Other Vehicle Platforms

Section 6.1 highlighted how the NMPC PTC is not limited to just the 2nd generation Volt platform and can be utilized for other hybrid architectures. This section will examine how the Optimal Mode Path Planning algorithm also has use cases outside of the Volt platform. The obvious use case for applying the optimal mode path planning algorithm is other multi-mode HEVs and PHEVs. For example, the Honda Clarity, introduced in for MY 2018, is a PHEV that utilizes three distinct powertrain operating modes. These include an EV only mode, a parallel hybrid mode, and series hybrid mode. Switching between modes is accomplished through the use of a clutch placed between the engine and output [85]. The

methodology and implementation of the OMPP used for the Volt could easily be adapted to the Clarity platform. The same problem formulation would be able to be used. The only modifications required would be the creating of optimal operating point maps specific to the Clarity as well as modifying the mode shift penalty term to correlate with this vehicle platform.
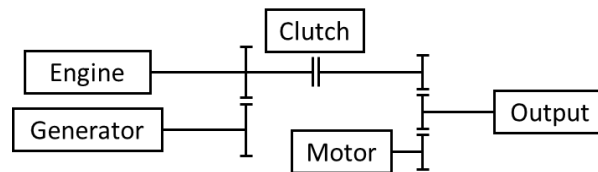


Figure 6-3: Honda Clarity Powertrain Architecture.

As previously stated, the obvious use case for the OMPP algorithm is other multi-mode hybrid platforms such as the Honda Clarity. However, the number of multi-mode hybrid vehicle platforms in production is limited when compared to single mode hybrids. This does not mean that there is limited application for the OMPP. In Chapter 4, it was discovered during the analysis of the OMPP that the majority of the energy savings benefit of the OMPP algorithm occurs by strategically utilizing EV mode when an extended segment of low power demand is detected in the prediction horizon thus allowing the vehicle to turn off its engine with no to minimal SOC depletion. Therefore, it is reasonable to conclude that the OMPP can provide an energy savings benefit to any HEV that is capable of extended electric only operation. This includes both multi-hybrid-mode and single-hybrid-mode PHEVs. This greatly expands the amount of use cases for the OMPP algorithm as there are significant number of PHEVs currently for sale in the US as well as

planned by auto manufactures. For example, Toyota produces two PHEVs, the Prius Prime and RAV4 Prime [86]. FCA currently produces the Pacifica PHEV [87] and is introducing the Jeep Wrangler 4Xe for MY 2021 [88]. Ford Motor Company offers the Lincoln Aviator with a PHEV architecture and is introducing the Corsair PHEV for MY 2021 [89]. Honda currently produces the Clarity PHEV [90], and finally, Subaru introduced their Crosstrek PHEV for MY 2019 [91]. This is only a partial list of all the PHEVs available or planned and is limited to the US market. However, even this partial list demonstrates that there is a significant presence of PHEVs in the automotive market. Therefore, ample opportunity to apply the OMPP algorithms to other vehicle platforms.

# 7 Conclusions and Future Work

## 7.1 Conclusions

This dissertation presents the development, implementation, and evaluation of real-time predictive control methods for a connected multi-mode PHEV. Two controllers were presented. A lower-level NMPC-based controller was developed for powersplit management, while an upper-level path planning-based mode selection controller was developed for optimal mode selection.

The NMPC predictive powertrain controller was developed for power-split management in a connected multi-mode PHEV. This controller utilizes a forecast of future vehicle state, such as vehicle speed and torque demand, in order to optimize torque and powersplit decision at the current control instant. The proposed controller was tested extensively across numerous standardized and real-world drive cycles where it was found that the NMPC powertrain controller utilizes less energy than the baseline vehicle control. Additionally, the NMPC powertrain controller was deployed onto a rapid-prototyping embedded controller for real-time, in-vehicle testing. These on-roads tests confirmed the energy savings observed in simulation testing as well as demonstrated the presented controller was capable of computation speeds required for real-time powertrain supervisory control.

The optimal mode path planning algorithm was presented for optimal mode selection of a multi-mode PHEV for reduced energy consumption. Once again using forecasts of future

vehicle state, such as vehicle speed and torque demand, the optimal mode path planning algorithm determines a path of best mode for minimal energy consumption over the predicted vehicle trajectory in order to issue an optimal mode command. This optimal mode selection controller was then integrated with the NMPC powertrain controller in order to create an Integrated Predictive Powertrain Controller responsible for full supervisory control of a multi-mode PHEV powertrain. This combined powersplit and mode selection controller was assessed in simulation testing over standard and real-world drive cycles in order to determine the energy savings provided by the controller. This testing revealed that the IPPC was able to provide an additional energy savings relative to baseline control when compared to using only the NMPC powersplit controller. The IPPC was deployed on an in-vehicle installed rapid prototyping ECU and evaluated with on-road testing. This testing confirmed the energy savings results observed in simulation testing while achieving computational turnaround times suitable for real-time control.

Finally, the applicability of the two controllers developed in this research to other vehicle platforms was examined. Because the multi-mode PHEV used as a research platform combines several hybrid architectures (an input powersplit hybrid mode, a parallel hybrid mode, and a compound powersplit mode) into one platform, the controllers presented in this research are valid for multiple hybrid architectures. Therefore, a number of HEV and PHEV vehicle platforms were presented, and how the controllers developed as a part of this research could be applied to these other platforms was discussed.

## 7.2 Future Work

Three main areas in which future work should be continued on the research presented in this dissertation. The three areas are the expansion of the controller to other vehicle platforms, the integration of the developed controllers with a physical powertrain, and finally, the full integration of the developed controllers with a robust communication system.

The first area of future work, implementing the developed predictive powertrain controllers on other vehicle platforms, is an important task for several reasons. First, the production of the $2^{nd}$ generation Chevrolet Volt ended in 2019 with no replacement planned. This means that, while the current vehicle platform can be used for development and testing, the controller needs to be implemented on other vehicle platforms in order to have applicability to future production vehicles. As discussed in Chapter 6, this should be a straightforward task as there are a number of other vehicle platforms to which the IPPC controller could easily be adapted.

The second area of future work is concerned with further development of the controller. This dissertation validated the energy savings benefits of the developed controllers in simulation. In addition, the real-time capability of the controllers and energy savings when ran in real-time was demonstrated. However, the real-time testing of the controllers did not involve the physical control of the powertrain. In order to fully validate the real-time capability and practicality of the developed controller, testing would need to occur with physical powertrain components. As this level of testing and integration requires

significant resources and proprietary knowledge of the vehicle, it would be best performed by or in close association with the manufacturer of the vehicle platform on which this testing would be performed.

The final area of future work involves the full integration of the IPPC controller with a robust CAV system. The main focus of this dissertation was to demonstrate the energy savings that can be achieved with a predictive powertrain that utilizes predictions of future vehicle behavior that are obtained through CAV technologies. While the controllers were integrated with a simple real-time communication system, it was not in the scope of this work to integrate the developed controllers with a robust CAV system that can reliably provide future vehicle behavior predictions. In order to fully validate the predictive powertrain control concept, focus should be placed on this integration.

# 8 Reference List

[1]     M. Taiebat, A. L. Brown, H. R. Safford, S. Qu, and M. Xu, "A Review on Energy, Environmental, and Sustainability Implications of Connected and Automated Vehicles," *Environmental Science & Technology,* vol. 52, no. 20, pp. 11449-11465, 2018, doi: 10.1021/acs.est.8b00127.

[2]     Y. Zhou, A. Ravey, and M.-C. Péra, "A survey on driving prediction techniques for predictive energy management of plug-in hybrid electric vehicles," *Journal of Power Sources,* vol. 412, pp. 480-495, 2019, doi: https://doi.org/10.1016/j.jpowsour.2018.11.085.

[3]     J. Guanetti, Y. Kim, and F. Borrelli, "Control of connected and automated vehicles: State of the art and future challenges," *Annual Reviews in Control,* vol. 45, pp. 18-40, 2018, doi: 10.1016/j.arcontrol.2018.04.011.

[4]     C. M. Martinez, X. Hu, D. Cao, E. Velenis, B. Gao, and M. Wellers, "Energy Management in Plug-in Hybrid Electric Vehicles: Recent Progress and a Connected Vehicles Perspective," *IEEE Transactions on Vehicular Technology,* vol. 66, no. 6, pp. 4534-4549, 2017, doi: 10.1109/TVT.2016.2582721.

[5]     L. Serrao, S. Onori, and G. Rizzoni, "A Comparative Analysis of Energy Management Strategies for Hybrid Electric Vehicles," *Journal of Dynamic Systems, Measurement, and Control,* vol. 133, no. 3, 2011, doi: 10.1115/1.4003267.

[6]     A. Sciarretta and L. Guzzella, "Control of hybrid electric vehicles," *IEEE Control Systems Magazine,* vol. 27, no. 2, pp. 60-70, 2007, doi: 10.1109/MCS.2007.338280.

[7]     A. Biswas and A. Emadi, "Energy Management Systems for Electrified Powertrains: State-of-the-Art Review and Future Trends," *IEEE Transactions on Vehicular Technology,* vol. 68, no. 7, pp. 6453-6467, 2019, doi: 10.1109/TVT.2019.2914457.

[8]     N. Jalil, N. A. Kheir, and M. Salman, "A rule-based energy management strategy for a series hybrid vehicle," in *Proceedings of the 1997 American Control Conference (Cat. No.97CH36041)*, 1997, vol. 1, pp. 689-693 vol.1, doi: 10.1109/ACC.1997.611889.

[9]     Y. Yuan, W. Zhou, and L. Shi, "An Investigation on the Control Strategies and Fuel Economy of a Novel Plug-In Hybrid Electric Vehicle System," *IEEE Transactions on Vehicular Technology,* vol. 68, no. 6, pp. 5271-5280, 2019, doi: 10.1109/TVT.2019.2910273.

[10]    G. Paganelli, S. Delprat, T. M. Guerra, J. Rimaux, and J. J. Santin, "Equivalent consumption minimization strategy for parallel hybrid powertrains," in *Vehicular Technology Conference. IEEE 55th Vehicular Technology Conference. VTC Spring 2002 (Cat. No.02CH37367)*, 2002, vol. 4, pp. 2076-2081 vol.4, doi: 10.1109/VTC.2002.1002989.

[11]    H. Wang, K. Sacheva, J. Tripp, B. Chen, D. Robinette, and M. Shahbakhti, "Optimal Map-Based Mode Selection and Powertrain Control for a Multi-Mode Plug-in Hybrid Electric Vehicle," in *2018 14th IEEE/ASME International Conference on Mechatronic and Embedded Systems and Applications (MESA)*, 2018, pp. 1-6, doi: 10.1109/MESA.2018.8449157.

[12]    A. Rezaei, J. B. Burl, and B. Zhou, "Estimation of the ECMS Equivalent Factor Bounds for Hybrid Electric Vehicles," *IEEE Transactions on Control Systems Technology,* vol. 26, no. 6, pp. 2198-2205, 2018, doi: 10.1109/TCST.2017.2740836.

[13]    C. Musardo, G. Rizzoni, Y. Guezennec, and B. Staccia, "A-ECMS: An Adaptive Algorithm for Hybrid Electric Vehicle Energy Management," *European Journal of Control,* vol. 11, no. 4, pp. 509-524, 2005, doi: 10.3166/ejc.11.509-524.

[14]    L. Johannesson, M. Asbogard, and B. Egardt, "Assessing the Potential of Predictive Control for Hybrid Vehicle Powertrains Using Stochastic Dynamic Programming," *IEEE Transactions on Intelligent Transportation Systems,* vol. 8, no. 1, pp. 71-83, 2007, doi: 10.1109/TITS.2006.884887.

[15]    R. M. Patil, Z. Filipi, and H. K. Fathy, "Comparison of Supervisory Control Strategies for Series Plug-In Hybrid Electric Vehicle Powertrains Through Dynamic Programming," *IEEE Transactions on Control Systems Technology,* vol. 22, no. 2, pp. 502-509, 2014, doi: 10.1109/TCST.2013.2257778.

[16]    N. Denis, M. R. Dubois, J. P. F. Trovão, and A. Desrochers, "Power Split Strategy Optimization of a Plug-in Parallel Hybrid Electric Vehicle," *IEEE Transactions on Vehicular Technology,* vol. 67, no. 1, pp. 315-326, 2018, doi: 10.1109/TVT.2017.2756049.

[17]    D. Pei and M. J. Leamy, "Dynamic Programming-Informed Equivalent Cost Minimization Control Strategies for Hybrid-Electric Vehicles," *Journal of Dynamic Systems, Measurement, and Control,* vol. 135, no. 5, 2013, doi: 10.1115/1.4024788.

[18]    H. Wang, J. Oncken, and B. Chen, "Receding Horizon Control for Mode Selection and Powertrain Control of a Multi-mode Hybrid Electric Vehicle," in *2019 IEEE 90th Vehicular Technology Conference (VTC2019-Fall)*, 2019, pp. 1-5, doi: 10.1109/VTCFall.2019.8891382.

[19]    J. Liu, Y. Chen, J. Zhan, and F. Shang, "Heuristic Dynamic Programming Based Online Energy Management Strategy for Plug-In Hybrid Electric Vehicles," *IEEE Transactions on Vehicular Technology,* vol. 68, no. 5, pp. 4479-4493, 2019, doi: 10.1109/TVT.2019.2903119.

[20]    J. Liu, Y. Chen, J. Zhan, and F. Shang, "An On-Line Energy Management Strategy Based on Trip Condition Prediction for Commuter Plug-In Hybrid Electric Vehicles," *IEEE Transactions on Vehicular Technology,* vol. 67, no. 5, pp. 3767-3781, 2018, doi: 10.1109/TVT.2018.2815764.

[21]    Y. Huang, H. Wang, A. Khajepour, H. He, and J. Ji, "Model predictive control power management strategies for HEVs: A review," *Journal of Power Sources,* vol. 341, pp. 91-106, 2017, doi: 10.1016/j.jpowsour.2016.11.106.

[22]    G. Ripaccioli, A. Bemporad, F. Assadian, C. Dextreit, S. Di Cairano, and I. V. Kolmanovsky, "Hybrid Modeling, Identification, and Predictive Control: An Application to Hybrid Electric Vehicle Energy Management," Berlin, Heidelberg, 2009: *Springer Berlin Heidelberg*, in Hybrid Systems: Computation and Control, pp. 321-335.

[23]    G. Ripaccioli, D. Bernardini, S. D. Cairano, A. Bemporad, and I. V. Kolmanovsky, "A stochastic model predictive control approach for series hybrid electric vehicle power management," in *Proceedings of the 2010 American Control Conference*, 2010, pp. 5844-5849, doi: 10.1109/ACC.2010.5530504.

[24]    F. Yan, J. Wang, and K. Huang, "Hybrid Electric Vehicle Model Predictive Control Torque-Split Strategy Incorporating Engine Transient Characteristics," *IEEE Transactions on Vehicular Technology,* vol. 61, no. 6, pp. 2458-2467, 2012, doi: 10.1109/TVT.2012.2197767.

[25]    M. Bidarvatan and M. Shahbakhti, "Analysis and Control of Torque Split in Hybrid Electric Vehicles by Incorporating Powertrain Dynamics," *Journal of Dynamic Systems, Measurement, and Control,* vol. 140, no. 11, pp. 111009-111009-11, 2018, doi: 10.1115/1.4040219.

[26]    X. Zeng and J. Wang, "A Parallel Hybrid Electric Vehicle Energy Management Strategy Using Stochastic Model Predictive Control With Road Grade Preview," *IEEE Transactions on Control Systems Technology,* vol. 23, no. 6, pp. 2416-2423, 2015, doi: 10.1109/TCST.2015.2409235.

[27]    H. Borhan, A. Vahidi, A. M. Phillips, M. L. Kuang, I. V. Kolmanovsky, and S. D. Cairano, "MPC-Based Energy Management of a Power-Split Hybrid Electric Vehicle," *IEEE Transactions on Control Systems Technology,* vol. 20, no. 3, pp. 593-603, 2012, doi: 10.1109/TCST.2011.2134852.

[28]   M. Cheng, L. Feng, and B. Chen, "Nonlinear Model Predictive Control of a Power-Split Hybrid Electric Vehicle with Electrochemical Battery Model," 2017, SAE Technical Paper 2017-01-1252, 2017, doi: 10.4271/2017-01-1252.

[29]   M. Cheng and B. Chen, "Nonlinear Model Predictive Control of a Power-Split Hybrid Electric Vehicle With Consideration of Battery Aging," *Journal of Dynamic Systems, Measurement, and Control,* vol. 141, no. 8, pp. 081008-081008-9, 2019, doi: 10.1115/1.4042954.

[30]   J. Zhang and T. Shen, "Real-Time Fuel Economy Optimization With Nonlinear MPC for PHEVs," *IEEE Transactions on Control Systems Technology,* vol. 24, no. 6, pp. 2167-2175, 2016, doi: 10.1109/TCST.2016.2517130.

[31]   A. Bemporad, D. Bernardini, M. Livshiz, and B. Pattipati, "Supervisory Model Predictive Control of a Powertrain with a Continuously Variable Transmission," 2018, SAE Technical Paper 2018-01-0860, doi: 10.4271/2018-01-0860.

[32]   K. Moran, B. Foley, U. Fastenrath, and J. Raimo, "Digital Maps, Connectivity and Electric Vehicles - Enhancing the EV/PHEV Ownership Experience," 2010, SAE Technical Paper 2010-01-2316, 2010, doi: 10.4271/2010-01-2316.

[33]   P. Michel, D. Karbowski, and A. Rousseau, "Impact of Connectivity and Automation on Vehicle Energy Use," 2016, SAE Technical Paper 2016-01-0152, 2016, doi: 10.4271/2016-01-0152.

[34]   H. Arian, "Eco-Routing of Plug-In Hybrid Electric Vehicles in Transportation Networks," in *21st International Conference on Intelligent Transportation Systems*, Maui, Hawaii, USA, 2018, pp. 1508-1513, doi: 10.1109/ITSC.2018.8569982.

[35]   A. Vahidi and A. Sciarretta, "Energy saving potentials of connected and automated vehicles," *Transportation Research Part C: Emerging Technologies,* vol. 95, pp. 822-843, 2018, doi: 10.1016/j.trc.2018.09.001.

[36]   N. Wikström, A. F. Parrilla, S. J. Jones, and A. Grauers, "Energy-Efficient Cooperative Adaptive Cruise Control with Receding Horizon of Traffic, Route Topology, and Traffic Light Information," *SAE International Journal of Connected and Automated Vehicles,* vol. 2, no. 2, pp. 87-98, 2019, doi: 10.4271/12-02-02-0006.

[37]   J. Heinovski and F. Dressler, "Platoon Formation: Optimized Car to Platoon Assignment Strategies and Protocols," in *2018 IEEE Vehicular Networking Conference (VNC)*, 2018, pp. 1-8, doi: 10.1109/VNC.2018.8628396.

[38]   S. D. Cairano, D. Bernardini, A. Bemporad, and I. V. Kolmanovsky, "Stochastic MPC With Learning for Driver-Predictive Vehicle Control and its Application to

HEV Energy Management," *IEEE Transactions on Control Systems Technology,* vol. 22, no. 3, pp. 1018-1031, 2014, doi: 10.1109/TCST.2013.2272179.

[39]    D. Baker, Z. D. Asher, and T. Bradley, "V2V Communication Based Real-World Velocity Predictions for Improved HEV Fuel Economy," 2018, SAE Technical Paper 2018-01-1000, 2018, doi: 2018-01-1000.

[40]    D. R. Varnhagen, "Electronic Horizon: A Map as a Sensor and Predictive Control," 2017: *SAE International*, doi: 10.4271/2017-01-1945.

[41]    P. Olin *et al.*, "Reducing Fuel Consumption by Using Information from Connected and Automated Vehicle Modules to Optimize Propulsion System Control," 2019, SAE Technical Paper 10.4271/2019-01-1213, 2019, doi: 10.4271/2019-01-1213.

[42]    J. Hu, Y. Shao, Z. Sun, and J. Bared, "Integrated vehicle and powertrain optimization for passenger vehicles with vehicle-infrastructure communication," *Transportation Research Part C: Emerging Technologies,* vol. 79, pp. 85-102, 2017, doi: https://doi.org/10.1016/j.trc.2017.03.010.

[43]    N. Rama, H. Wang, J. Orlando, D. Robinette, and B. Chen, "Route-Optimized Energy Management of Connected and Automated Multi-Mode Plug-In Hybrid Electric Vehicle Using Dynamic Programming," SAE Technical Paper 2019-01-1209, 2019, doi: 10.4271/2019-01-1209.

[44]    J. Platt, N. Moehle, J. D. Fox, and W. Dally, "Optimal Operation of a Plug-In Hybrid Vehicle," *IEEE Transactions on Vehicular Technology,* vol. 67, no. 11, pp. 10366-10377, 2018, doi: 10.1109/TVT.2018.2866801.

[45]    M. Anwar, M. Hayes, A. Tata, M. Teimorzadeh, and T. Achatz, "Power Dense and Robust Traction Power Inverter for the Second-Generation Chevrolet Volt Extended-Range EV," *SAE International Journal of Alternative Powertrains,* vol. 4, no. 1, pp. 145-152, 2015, doi: 10.4271/2015-01-1201.

[46]    D. Cesiel and C. Zhu, "Next Generation "Voltec" Charging System," SAE Technical Paper 2016-01-1229, 2016, doi: 10.4271/2016-01-1229.

[47]    B. M. Conlon *et al.*, "The Next Generation "Voltec" Extended Range EV Propulsion System," *SAE International Journal of Alternative Powertrains,* vol. 4, no. 2, pp. 248-259, 2015, doi: 10.4271/2015-01-1152.

[48]    J. Jocsak, D. White, C. Armand, and R. S. Davis, "Development of the Combustion System for General Motors' High-Efficiency Range Extender Ecotec Small Gas Engine," *SAE International Journal of Engines,* vol. 8, no. 4, pp. 1587-1601, 2015, doi: 10.4271/2015-01-1272.

[49]     S. Jurkovic, K. Rahman, N. Patel, and P. Savagian, "Next Generation Voltec Electric Machines; Design and Optimization for Performance and Rare-Earth Mitigation," *SAE International Journal of Alternative Powertrains,* vol. 4, no. 2, pp. 336-342, 2015, doi: 10.4271/2015-01-1208.

[50]     N. Kim, S. Choi, J. Jeong, R. Vijayagopal, K. Stutenberg, and A. Rousseau, "Vehicle Level Control Analysis for Voltec Powertrain," *World Electric Vehicle Journal,* vol. 9, no. 2, p. 29, 2018, doi: 10.3390/wevj9020029.

[51]     D. Robinette *et al.*, "PHEV Real World Driving Cycle Energy and Fuel and Consumption Reduction Potential for Connected and Automated Vehicles," SAE Technical Paper 2019-01-0307, 2019, doi: 10.4271/2019-01-0307.

[52]     H. L. Benford and M. B. Leising, "The Lever Analogy: A New Tool in Transmission Analysis," 1981, SAE Technical Paper 810102, 1981, doi: 10.4271/810102.

[53]     R. Yadav, "Modeling and Analysis of Energy Consumption in Chevrolet Volt Gen II Hybrid Electric Vehicle," M.S. thesis, Dept. Mech. Eng.-Eng. Mech., Michigan Technological Univ., Houghton, MI, USA, 2018.

[54]     N. Rama and D. Robinette, "Computationally Efficient Reduced-Order Powertrain Model of a Multi-Mode Plug-In Hybrid Electric Vehicle for Connected and Automated Vehicles," SAE Technical Paper 2019-01-1210, 2019, doi: 10.4271/2019-01-1210.

[55]     J. E. Oncken and B. Chen, "Real-Time Model Predictive Powertrain Control for a Connected Plug-In Hybrid Electric Vehicle," *IEEE Transactions on Vehicular Technology,* vol. 69, no. 8, pp. 8420 - 8432, 2020, doi: 10.1109/TVT.2020.3000471.

[56]     J. Oncken *et al.*, "A Connected Controls and Optimization System for Vehicle Dynamics and Powertrain Operation on a Light-Duty Plug-In Multi-Mode Hybrid Electric Vehicle," SAE Technical Paper 2020-01-0591, 2020, doi: 10.4271/2020-01-0591.

[57]     B. Barik, P. K. Bhat, J. Oncken, B. Chen, J. Orlando, and D. Robinette, "Optimal velocity prediction for fuel economy improvement of connected vehicles," *IET Intelligent Transport Systems,* vol. 12, no. 10, pp. 1329-1335, 2018, doi: 10.1049/iet-its.2018.5110.

[58]     P. K. Bhat, J. Oncken, R. Yadav, B. Chen, M. Shahbakhti, and D. Robinette, "Generation of Optimal Velocity Trajectory for Real-Time Predictive Control of a Multi-Mode PHEV," in *2019 IEEE 90th Vehicular Technology Conference (VTC2019-Fall)*, 2019, pp. 1-5, doi: 10.1109/VTCFall.2019.8891569.

[59]   C. Morgan, D. Robinette, P. Santhosh, and J. Bloom-Edmonds, "Utilization of Vehicle Connectivity for Improved Energy Consumption of a Speed Harmonized Cohort of Vehicles," SAE Technical Paper 2020-01-0587, 2020, doi: 10.4271/2020-01-0587.

[60]   A. N. Duhon, K. S. Sevel, S. A. Tarnowsky, and P. J. Savagian, "Chevrolet Volt Electric Utilization," 2015, SAE Technical Paper 2015-01-1164, 2015, doi: 10.4271/2015-01-1164.

[61]   A. Cordoba-Arenas, S. Onori, and G. Rizzoni, "A control-oriented lithium-ion battery pack model for plug-in hybrid electric vehicle cycle-life studies and system design with consideration of health management," *Journal of Power Sources,* vol. 279, pp. 791-808, 2015, doi: 10.1016/j.jpowsour.2014.12.048.

[62]   R. Quirynen, M. Vukov, M. Zanon, and M. Diehl, "Autogenerating microsecond solvers for nonlinear MPC: A tutorial using ACADO integrators," *Optimal Control Applications and Methods,* vol. 36, no. 5, pp. 685-704, 2015, doi: 10.1002/oca.2152.

[63]   B. Houska, H. J. Ferreau, and M. Diehl, "ACADO toolkit—An open-source framework for automatic control and dynamic optimization," *Optimal Control Applications and Methods,* vol. 32, no. 3, pp. 298-312, 2011, doi: doi:10.1002/oca.939.

[64]   B. Houska, H. J. Ferreau, and M. Diehl, "An auto-generated real-time iteration algorithm for nonlinear MPC in the microsecond range," *Automatica,* vol. 47, no. 10, pp. 2279-2285, 2011, doi: 10.1016/j.automatica.2011.08.020.

[65]   W. Zhuang *et al.*, "A survey of powertrain configuration studies on hybrid electric vehicles," *Applied Energy,* vol. 262, 2020, doi: 10.1016/j.apenergy.2020.114553.

[66]   D. Karbowski, J. Kwon, N. Kim, and A. Rousseau, "Instantaneously Optimized Controller for a Multimode Hybrid Electric Vehicle," SAE Technical Paper 2010-01-0816, 2010, doi: 10.4271/2010-01-0816.

[67]   X. Zhang, C. Li, D. Kum, and H. Peng, "Prius + and Volt - : Configuration Analysis of Power-Split Hybrid Vehicles With a Single Planetary Gear," *IEEE Transactions on Vehicular Technology,* vol. 61, no. 8, pp. 3544-3552, 2012, doi: 10.1109/TVT.2012.2208210.

[68]   X. Zhang, S. Eben Li, H. Peng, and J. Sun, "Efficient Exhaustive Search of Power-Split Hybrid Powertrains With Multiple Planetary Gears and Clutches," *Journal of Dynamic Systems, Measurement, and Control,* vol. 137, no. 12, 2015, doi: 10.1115/1.4031533.

[69]     X. Zhang, H. Peng, and J. Sun, "A Near-Optimal Power Management Strategy for Rapid Component Sizing of Multimode Power Split Hybrid Vehicles," *IEEE Transactions on Control Systems Technology,* vol. 23, no. 2, pp. 609-618, 2015, doi: 10.1109/TCST.2014.2335060.

[70]     W. Zhuang, X. Zhang, Y. Ding, L. Wang, and X. Hu, "Comparison of multi-mode hybrid powertrains with multiple planetary gears," *Applied Energy,* vol. 178, pp. 624-632, 2016, doi: 10.1016/j.apenergy.2016.06.111.

[71]     W. Zhuang, X. Zhang, H. Peng, and L. Wang, "Rapid Configuration Design of Multiple-Planetary-Gear Power-Split Hybrid Powertrain via Mode Combination," *IEEE/ASME Transactions on Mechatronics,* vol. 21, no. 6, pp. 2924-2934, 2016, doi: 10.1109/TMECH.2016.2575359.

[72]     P. G. Anselma, Y. Huo, E. Amin, J. Roeleveld, A. Emadi, and G. Belingardi, "Mode-shifting Minimization in a Power Management Strategy for Rapid Component Sizing of Multimode Power Split Hybrid Vehicles," SAE Technical Paper 2018-01-1018, 2018, doi: 10.4271/2018-01-1018.

[73]     G. Buccoliero, P. G. Anselma, S. A. Bonab, G. Belingardi, and A. Emadi, "A New Energy Management Strategy for Multimode Power Split Hybrid Electric Vehicles," *IEEE Transactions on Vehicular Technology,* pp. 1-1, 2019, doi: 10.1109/TVT.2019.2950033.

[74]     P. G. Anselma, Y. Huo, J. Roeleveld, A. Emadi, and G. Belingardi, "Rapid optimal design of a multimode power split hybrid electric vehicle transmission," *Proceedings of the Institution of Mechanical Engineers, Part D: Journal of Automobile Engineering,* vol. 233, no. 3, pp. 740-762, 2019, doi: 10.1177/0954407017750789.

[75]     W. Zhuang, X. Zhang, D. Li, L. Wang, and G. Yin, "Mode shift map design and integrated energy management control of a multi-mode hybrid electric vehicle," *Applied Energy,* vol. 204, pp. 476-488, 2017, doi: 10.1016/j.apenergy.2017.07.059.

[76]     W. Zhuang, X. Zhang, G. Yin, H. Peng, and L. Wang, "Mode Shift Schedule and Control Strategy Design of Multimode Hybrid Powertrain," *IEEE Transactions on Control Systems Technology,* pp. 1-12, 2019, doi: 10.1109/TCST.2019.2895799.

[77]     P. G. Anselma, Y. Huo, J. Roeleveld, G. Belingardi, and A. Emadi, "Integration of On-Line Control in Optimal Design of Multimode Power-Split Hybrid Electric Vehicle Powertrains," *IEEE Transactions on Vehicular Technology,* vol. 68, no. 4, pp. 3436-3445, 2019, doi: 10.1109/TVT.2019.2901901.

[78] S. Wang and X. Lin, "Eco-driving control of connected and automated hybrid vehicles in mixed driving scenarios," *Applied Energy,* vol. 271, 2020, doi: 10.1016/j.apenergy.2020.115233.

[79] S. M. LaValle, "Discrete Planning," in *Plannning Algorithms*: Cambridge University Press, 2006.

[80] P. Wang, H. Zhu, M. Wilamowska-Korsak, Z. Bi, and L. Li, "Determination of Weights for Multiobjective Decision Making or Machine Learning," *IEEE Systems Journal,* vol. 8, no. 1, pp. 63-72, 2014, doi: 10.1109/JSYST.2013.2265663.

[81] S. Fushiki, "The New Generation Front Wheel Drive Hybrid System," *SAE International Journal of Alternative Powertrains,* vol. 5, no. 1, 2016, doi: 10.4271/2016-01-1167.

[82] T. Kanayama, E. Yanagida, S. Kano, B. Geller, Y. Nakao, and M. Fukao, "Development of New Hybrid System for Mid-Size SUV," 2020, SAE Technical Paper 2020-01-0842, 2020, doi: 10.4271/2020-01-0842.

[83] S. Ichikawa *et al.*, "Development of New Plug-In Hybrid System for Compact-Class Vehicle," *SAE International Journal of Alternative Powertrains,* vol. 6, no. 1, pp. 95-102, 2017, doi: 10.4271/2017-01-1163.

[84] M. Pittel and D. Martin, "eFlite Dedicated Hybrid Transmission for Chrysler Pacifica," 2018, SAE Technical Paper 2018-01-0396, 2018, doi: 10.4271/2018-01-0396.

[85] T. Yamagishi and T. Ishikura, "Development of Electric Powertrain for CLARITY PLUG-IN HYBRID," *SAE International Journal of Alternative Powertrains,* vol. 7, no. 3, pp. 323-333, 2018, doi: 10.4271/2018-01-0415.

[86] "New Cars, Trucks, SUVs & Hybrids: Toyota Official Site." Toyota Motor Sales, U.S.A., Inc. https://www.toyota.com/ (accessed November 02, 2020).

[87] "Chrysler Vehicles." FCA USA LLC. https://www.chrysler.com/ (accessed November 02, 2020).

[88] "Jeep Wrangler 4Xe." FCA USA LLC. https://www.jeep.com/wrangler-4xe.html (accessed Novemeber 02, 2020).

[89] "Lincoln Hybrid Electric Vehicles." Ford Motor Company. https://www.lincoln.com/hybrid-electric-vehicles/?gnav=header-vehicles-phevlp (accessed November 02, 2020).

[90] "Honda Automobiles." American Honda Motor Co. https://automobiles.honda.com/ (accessed November 02, 2020).

[91] "Subaru Cars, Sedans, SUVs: Subaru of America." Subaru of America, Inc. https://www.subaru.com/index.html (accessed November 02, 2020).

# A    Copyright Documentation

## A.1    IEEE Copyright documentation for Chapter 3

Copyright Clearance Center    *RightsLink®*    🏠 Home    ❓ Help    ✉ Email Support    👤 Sign in    👤 Create Account

**IEEE** Requesting permission to reuse content from an IEEE publication

**Real-Time Model Predictive Powertrain Control for a Connected Plug-In Hybrid Electric Vehicle**

Author: Joseph Eugene Oncken

Publication: Vehicular Technology, IEEE Transactions on

Publisher: IEEE

Date: Dec 31, 1969

*Copyright © 1969, IEEE*

### Thesis / Dissertation Reuse

The IEEE does not require individuals working on a thesis to obtain a formal reuse license, however, you may print out this statement to be used as a permission grant:

*Requirements to be followed when using any portion (e.g., figure, graph, table, or textual material) of an IEEE copyrighted paper in a thesis:*

1) In the case of textual material (e.g., using short quotes or referring to the work within these papers) users must give full credit to the original source (author, paper, publication) followed by the IEEE copyright line © 2011 IEEE.
2) In the case of illustrations or tabular material, we require that the copyright line © [Year of original publication] IEEE appear prominently with each reprinted figure and/or table.
3) If a substantial portion of the original paper is to be used, and if you are not the senior author, also obtain the senior author's approval.

*Requirements to be followed when using an entire IEEE copyrighted paper in a thesis:*

1) The following IEEE copyright/ credit notice should be placed prominently in the references: © [year of original publication] IEEE. Reprinted, with permission, from [author names, paper title, IEEE publication title, and month/year of publication]
2) Only the accepted version of an IEEE copyrighted paper can be used when posting the paper or your thesis on-line.
3) In placing the thesis on the author's university website, please display the following message in a prominent place on the website: In reference to IEEE copyrighted material which is used with permission in this thesis, the IEEE does not endorse any of [university/educational entity's name goes here]'s products or services. Internal or personal use of this material is permitted. If interested in reprinting/republishing IEEE copyrighted material for advertising or promotional purposes or for creating new collective works for resale or redistribution, please go to http://www.ieee.org/publications_standards/publications/rights/rights_link.html to learn how to obtain a License from RightsLink.

If applicable, University Microfilms and/or ProQuest Library, or the Archives of Canada may supply single copies of the dissertation.

BACK                                                                        CLOSE WINDOW

136